DISPLACEMENT DEMAND EFFECTS IN VULNERABLE REINFORCED CONCRETE COLUMNS

BY

Charles Woods

Submitted to the graduate degree program in Civil Engineering
and to the Graduate Faculty of the University of Kansas
in partial fulfillment of the requirements for the degree of
Master of Science.

_____
Dr. Adolfo Matamoros, Chairman

Committee Members: _____
Dr. JoAnn Browning

_____
Dr. David Darwin

Date Defended: _____

The Thesis Committee for Charles Woods certifies
that this is the approved Version of the following thesis:

DISPLACEMENT DEMAND EFFECTS IN VULNERABLE REINFORCED CONCRETE COLUMNS

_____
Dr. Adolfo Matamoros, Chairman

Committee Members: _____
Dr. JoAnn Browning

_____
Dr. David Darwin

Date Approved: _____

ABSTRACT

The purpose of this study was to analyze the response of two full-scale reinforced concrete columns undergoing cyclic lateral loads. Specifically, columns were detailed to be similar to actual columns found in buildings constructed before 1970, under much less stringent seismic design requirements than today. Columns were constructed at the Structural Testing Laboratory at the University of Kansas and were instrumented and tested at the University of Minnesota NEES-MAST facility. Column cross sectional area was maintained constant between the two tests as well as material properties. Longitudinal and transverse reinforcement ratios, axial load ratio, and loading protocol were varied between tests. A constant axial compressive load was applied to both columns while being subjected to lateral deformations with increasing amplitude, until both lateral and axial load capacities were lost. Post-failure measurements were obtained to study the residual strength of the columns. Results show that all four of the aforementioned parameters affected column response. Data collected from this experiment are used to improve our understanding about the effect of displacement history and longitudinal reinforcement ratio on the drift ratio at axial failure of reinforced concrete columns.

ACKNOWLEDGEMENTS

I would like to extend my appreciation to the National Science Foundation for providing monetary support under award 0618804, which established the project through the Pacific Earthquake Engineering Research Center (PEER).

My advisor and professor, Dr. Adolfo B. Matamoros, provided intellectual insight, encouragement, and support. Thank you Dr. Matamoros for giving me the opportunity to be part of this project. I would also like to thank Dr. JoAnn Browning for her support and for the opportunity to be a graduate teaching assistant.

The staff at the University of Minnesota NEES-MAST Laboratory provided a tremendous amount of assistance. I would like to thank Paul Bergson, Carol Shield, Angela Kingsley, Jonathan Messier, and Drew Daugherty for their technical support and expertise throughout the instrumentation and testing phases of the project.

I would also like to thank those at the University of Kansas whose help was invaluable to this project. Lisa Matchulat contributed experience and knowledge that helped keep the project running smoothly. I would like to thank Jim Weaver at the Structural Testing Laboratory for his patience and guidance. The undergraduate research assistants ensured instrumentation ran without incidence—thank you to all of you who helped.

Many thanks to my wife, Caryn, who provided more encouragement, patience, and support than I can acknowledge.

TABLE OF CONTENTS

LIST OF FIGURES

LIST OF TABLES

CHAPTER 1: BACKGROUND AND PREVIOUS RESEARCH

1.1 Introduction

Understanding the behavior of reinforced concrete columns constructed prior to the implementation of modern seismic codes is of fundamental importance in order to estimate the losses and societal impacts of major earthquakes in urban environments. Post earthquake investigations have shown that some pre-1970s columns suffer sudden shear failures leading to an immediate loss of axial load carrying capacity and local collapse. Although the risk posed by such columns is well understood, the research community is still investigating the effects of various configuration parameters on the ability of columns to sustain axial load after suffering severe damage. Unfortunately, few full-scale columns with details similar to columns in service have been tested to the point of axial failure. For this reason, a very limited experimental base exists that can be used to develop and calibrate models to simulate the behavior of columns after suffering loss of lateral load capacity. There is a great need to expand the existing data set in order to improve our ability to estimate the potential for human and material losses posed by older reinforced concrete buildings.

1.2 Background and Previous Research

1.2.1 Failure Mechanisms

Classifying into categories according to failure mode is of paramount importance for establishing adequate modeling parameters and damage acceptance criteria. This process is described in detail in standards for seismic rehabilitation of

structures such as FEMA 356 and ASCE 41. Buildings in which axial failure is not likely to happen may be severely damaged but do not pose as high a threat to human life. Reconnaissance observations made after seismic events have shown that some reinforced concrete columns have failed suddenly and without warning (Elwood 2003). These particular columns are of most concern to the engineering community, and the implementation of damage mitigation measures should be a priority to prevent future catastrophic failures.

Existing failure models for columns can be used to analyze the effect of several factors including column geometry, longitudinal reinforcement ratio, axial load ratio, transverse reinforcement ratio, and lateral load demand can be analyzed on the type of failure mode most likely to occur for a particular column. For example, columns having light amounts of transverse reinforcement and high axial load have been shown to be particularly vulnerable to sudden shear failures while simultaneously losing axial load carrying capacity (Matamoros et al., 2008).

Shear, flexural-shear, and flexural failures are three behavior categories used to describe failure patterns for columns subjected to lateral load reversals (Matamoros, 2006). A similar classification is implemented in ASCE 41, although in that case columns are classified into three similar but broader categories i, ii, and iii. Shear failures in columns are characterized by a sudden, unrestrained inclined crack that often results in the loss of the axial load capacity in the column simultaneously or shortly after the loss of lateral load capacity. The sudden nature of the appearance of the inclined crack and unrestrained growth are the prevailing reasons why this failure

mode is precluded in modern codes. Figure 1.1 shows a schematic representation of the failure envelopes for reinforced concrete columns that experience flexural-shear failure when subjected to lateral load reversals (Matamoros 2006).

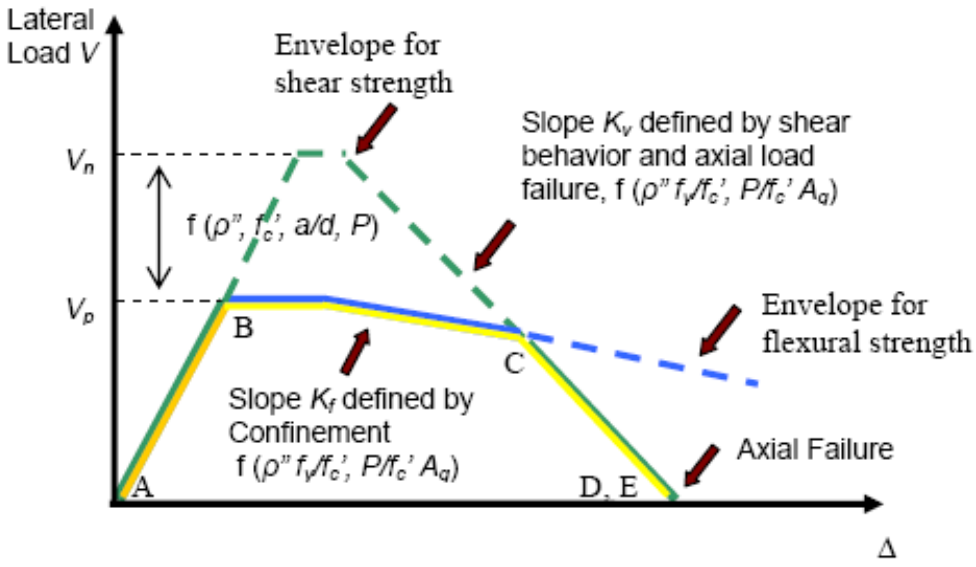

Figure 1.1: Idealized failure envelopes for reinforced concrete columns subjected to lateral load reversals.

For columns without splices, Matamoros (2006) used a simple framework to describe the load deflection response of columns that experience shear failure when subjected to load reversals. This framework is consistent with the definitions of forced-controlled and deformation-controlled elements used in FEMA 356 and ASCE 41. Columns controlled by shear capacity, or shear-critical columns, are defined as those in which lateral deformation demand results in the shear capacity of the column being exceeded prior to the lateral load at which the longitudinal reinforcement yields, V_p. Based on test data, Matamoros (2006) suggested that the shear strength for

undamaged columns be calculated in a simple manner by using ACI equation 11-4. The plastic shear demand for columns subjected to double curvature, is calculated from equilibrium:

$$V_p = \frac{2M_p}{h_{col}} \tag{1}$$

For columns with an initial shear capacity larger than the plastic shear demand, the failure envelope is initially controlled by the flexural strength of the column (Matamoros 2006). Loss of lateral load capacity occurs when damage causes the shear strength to become less than the flexural capacity (Fig. 1.1). The third category of columns, not evaluated in this experimental study, corresponds to columns in which the shear strength in the damaged state never drops below the flexural strength. These types of columns are designated as flexure-controlled columns and a typical envelope is shown in Fig. 1.2. P-Δ effects and buckling of the longitudinal reinforcement in elements with very low axial loads dominate the failure mode for these columns and behavior is such that ample warning is provided by very visible damage before loss of axial load capacity.

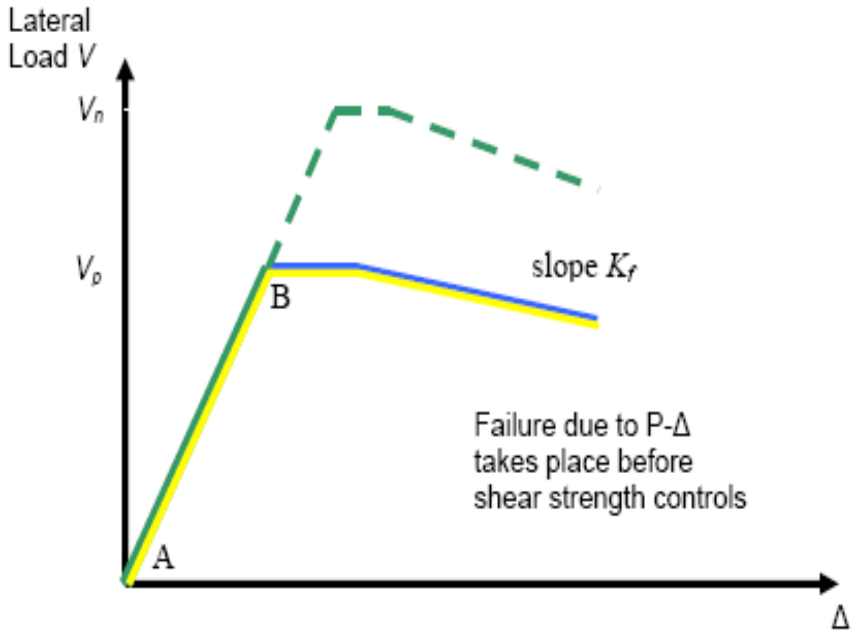

Figure 1.2: Flexural failure envelope for reinforced concrete columns

1.2.2 Axial Load Ratio Effect on Failure Mode

Columns tested by Matchulat (2009), Sezen (2000), and Lynn (2001) have shown that the axial load ratio largely affects the load deflection response and the mode of failure. These test results show that columns with larger axial load ratios, with all other properties held constant, result in lower drift ratio at axial failure.

Figures 1.4 and 1.5 show the load-displacement relationship for specimens 1 and 2 tested by Matchulat (2009). The axial load demand of $0.50A_g f'c$ and $0.35A_g f'c$ for specimens 1 and 2 respectively was the chief difference between the two.

Specimen 2 reached a larger lateral deformation before experiencing simultaneous loss of lateral and axial load carrying capacities than specimen 1.

Tests by Matchulat (2009), Lynn (2001), and Sezen (2000) showed that columns subjected to higher axial load ratios were more likely to experience sudden, brittle failures than columns subjected to lower axial load ratios. Research performed by Sezen (2000) studied variations in behavior between columns with the same detailing and flexural capacities but varying axial load ratio. The results indicated that the column with the lower axial load ratio experienced flexural yielding prior to the loss of axial load carrying capacity, while the column with the larger axial load ratio experienced a sudden, simultaneous failure of both lateral load and axial load capacities. The column with the lower axial load ratio was able to maintain axial load capacity after experiencing shear failure, even after the lateral load capacity had been reduced to zero.

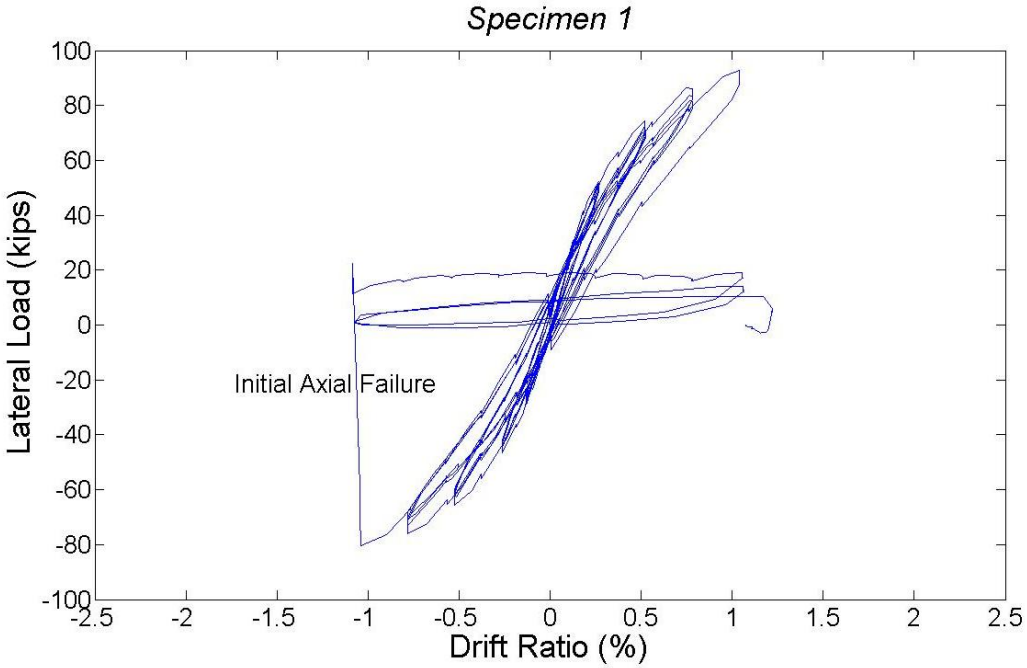

Figure 1.3: Lateral load-deflection response for $0.50A_g f'c$ axial load level.

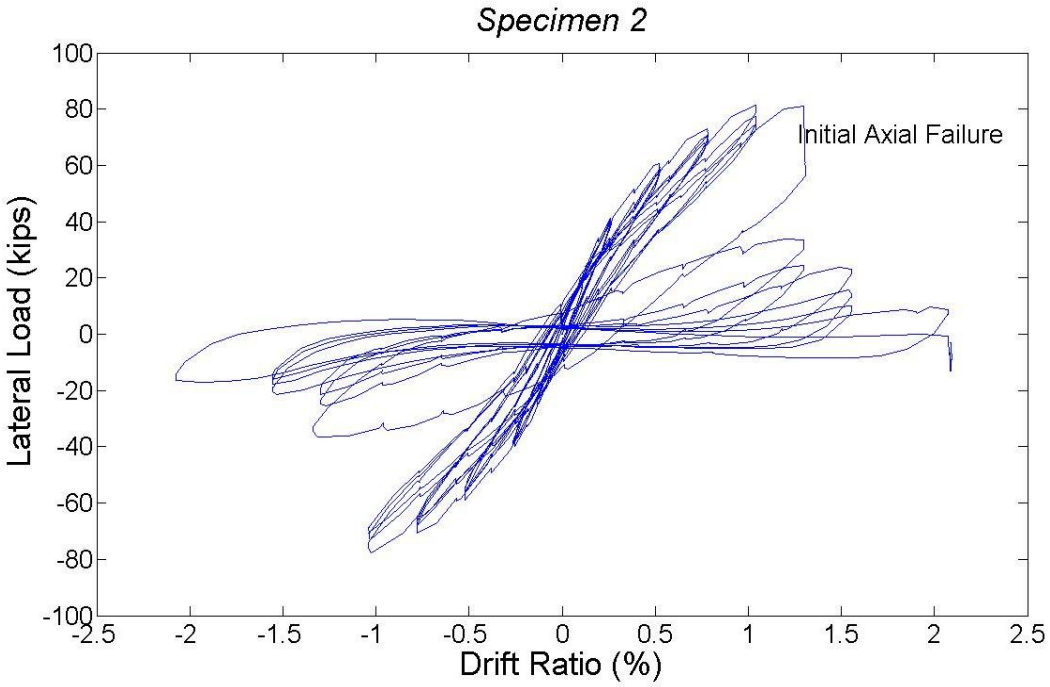

Figure 1.4: Lateral load-deflection response for $0.35A_g f'c$ axial load level.

1.2.3 Effect of Load Protocol on Drift Capacity

Although no comprehensive studies were found on the effect of loading protocol on the drift ratio at axial failure of columns, there are several studies that investigate the effect of load protocol on the drift ratio at loss of lateral load capacity.

A large number of column studies have been conducted using two or three cycles at each displacement level. Comparisons between the Northridge, CA to Nisqually, WA earthquakes have shown, that while the magnitudes of both earthquakes were relatively equal, the difference between the hypocenters played a significant role in the load effects experienced between the two locations. The Northridge earthquake had a hypocenter depth of 11 miles, while the Nisqually earthquake had a hypocenter depth of 33 miles. Furthermore, the Northridge earthquake originated on a shallow and brittle crust rather than an oceanic slab like that of the Nisqually earthquake. The Northridge earthquake lasted between 10 to 20 seconds while the Nisqually earthquake lasted nearly 40 seconds (Southern California Earthquake Center, 2007).

Although the magnitude of the two earthquakes was nearly equal, other factors, such as the number and amplitude of force cycles, explain the significant differences in the damage found on structural elements in the effected zones. These observed differences in the damage show that detailing is not the only factor that plays an important role in structural performance and that the characteristics of the ground motion also can have a very important effect, giving causation to studying the

effects that variations of the lateral loading displacement protocol have on structural performance.

Tests conducted by Sezen (2000) evaluated the effect of monotonic and cyclic lateral loading protocols. Sezen (2000) tested two similar specimens with an axial load ratio of 0.15 and varied the displacement protocol between the control and the second specimen. Sezen found that near failure the specimen tested under monotonic loading did not experience the significant increase in deformations related to shear observed in the column subjected to multiple cycles. Additionally, the specimen tested under monotonic loading reached an ultimate lateral deformation (deformation at loss of lateral load capacity) of 3.33 inches versus 2.97 inches recorded for the specimen subjected to cyclic loading, likely the result of increased damage sustained during cycling. Both columns had identical geometries, axial load ratios, transverse reinforcement, and nearly identical material properties. Figures 1.6 and 1.7 show the load-displacement relationships for specimens 1 (cyclic loading) and 4 (monotonic loading) of Sezen, respectively.

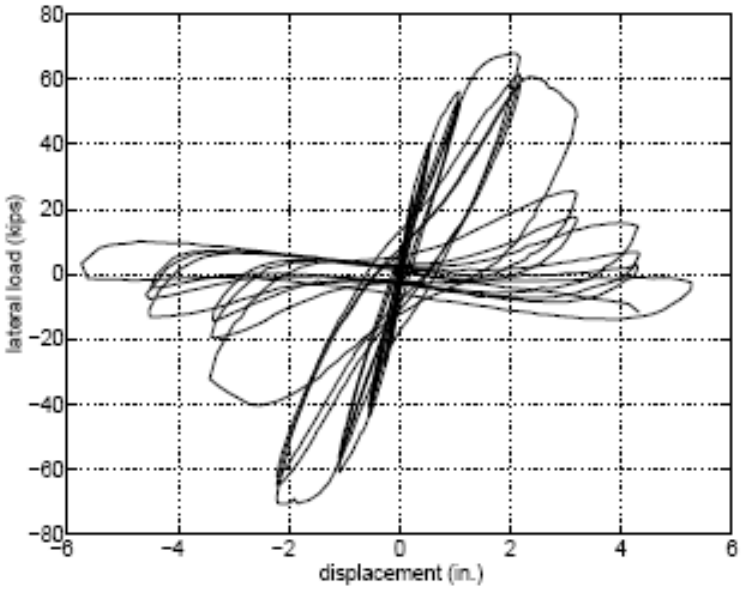

Figure 1.5: Load-displacement interactions for Sezen (2002) specimen 1

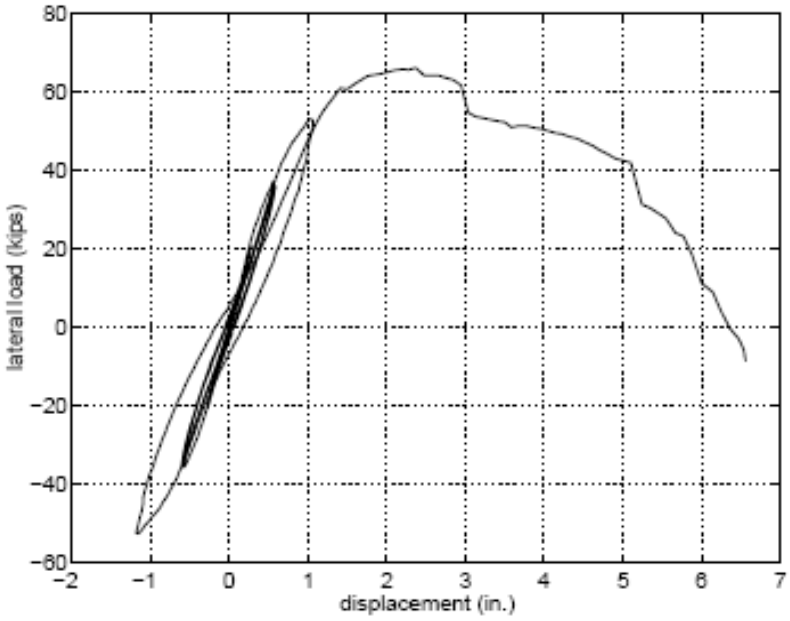

Figure 1.6: Load-displacment interaction for Sezen (2002) specimen 4

1.3 Effect of Displacement Protocol on Drift Ratio at Loss of Lateral Load Capacity.

1.3.1 Pujol, Sozen, and Ramirez (2006)

Research by Pujol et al. (2006) tested eight reinforced concrete column assemblies, each of which contained two specimens, for a total of 16 column specimens. They evaluated the effect of varying displacement histories on column drift capacity and stiffness. Variable testing parameters included axial load, amount of transverse reinforcement, and displacement history. All specimens reached yielding of the longitudinal reinforcement, which occurred at approximately 1% drift ratio (Pujol et. al., 2006).

Two series of tests were performed. The first series of test assemblies, designated 10-1-$2^{1/4}$, 10-2-$2^{1/4}$, and 10-3-$2^{1/4}$, were tested under the same axial load of 30 kips and contained No. 2 transverse reinforcement at a spacing of 2-1/4-in. Specimen 10-1-$2^{1/4}$ was tested with seven cycles with a maximum drift ratio of 1% and specimen 10-2-$2^{1/4}$ was tested with seven cycles with a maximum drift ratio of 2%. After the initial set of cycles, both specimens were subjected to cycles with a maximum drift ratio of 3%. Figure 1.7 taken from Pujol et al. (2006) shows that previous cycles with a maximum drift ratio of 2% resulted in a reduction in stiffness occurring at an earlier stage of the set of cycles with a maximum drift ratio of 3% than the specimens subjected to an initial set of cycles with a maximum drift ratio of 1% (Pujol et al., 2006).

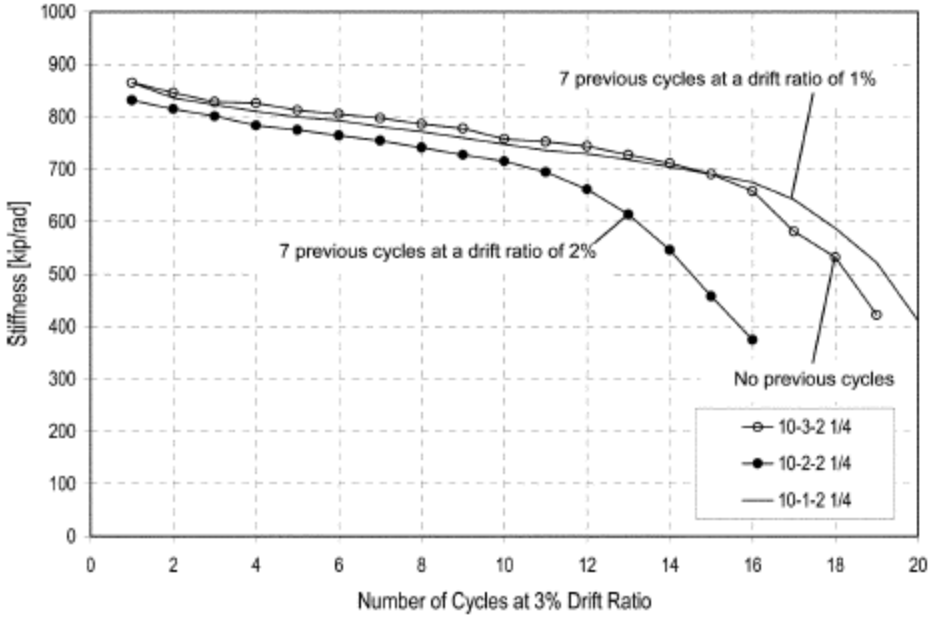

Figure 1.7: Average stiffness during cycles at 3% drift ratio. (Pujol et. al.)

The second series of tests was similar to the first in that both assemblies had the same axial load and transverse reinforcement ratios but displacement history between the two was changed. These assemblies were designated 10-2-3 and 10-3-3. Both had axial loads of 30 kips and transverse reinforcement consisting of No. 2 bars at a spacing of 3-inches. Assembly 10-2-3 was tested with seven cycles with a maximum drift ratio of 2% prior to being subjected to cycles with a maximum drift ratio of 3%. Assembly 10-3-3 was subjected only to cycles with a maximum drift ratio of 3%. The results were consistent with the first series of tests performed. Specimens subjected to a set of cycles with a maximum drift ratio of 2% prior to the set of cycles with a maximum drift ratio of 3% experienced greater loss of stiffness

during latter sets of cycles (Pujol et al., 2006). Both series of tests showed that displacement history affects the drift ratio at loss of lateral load capacity of columns. Pujol also observed that displacement cycles below the yield level did not result in a noticeable reduction in stiffness. Rather, it was the number of displacement cycles in the inelastic range that did affect the overall column drift capacity (Pujol et al., 2006).

Transverse deformations also were affected by the type of displacement history. Results indicated that cycles with a maximum drift ratio of 1% did not cause accumulation of transverse strains with increasing number of cycles. Cycles at larger drift levels did result in accumulation of transverse strains (Pujol et al., 2006). Furthermore, Pujol (2006) noted that large transverse strains may indicate loss of confinement in the concrete core and were associated with rapid stiffness decrease.

Pujol (2006) concluded that seven or less displacement cycles at drift ratios less than the drift ratio at yield would not have a noticeable effect on the drift capacity of the reinforced concrete column (Pujol et al., 2006). Column drift capacity was found to be affected by the displacement history only when subjected to drift cycles beyond yield and decreases in stiffness were observed to be a function of the amplitude and number of cycles performed (Pujol et al., 2006).

1.3.2 Laplace, Sanders, Saiidi, Douglas, and Azazy (2005)

One-third scale circular, reinforced concrete columns for bridge application were built with varying details and tested under different displacement demands to evaluate column ductility response. The first column was detailed to match columns

built prior to 1971 seismic codes. The second two columns were detailed to current seismic codes. The first column contained a relatively light amount of transverse reinforcement, with hoops providing a 0.15% transverse reinforcement ratio. Additionally, a splice joint was located just above the column-footing interface. The second column contained spiral wire which provided a ratio of 1% transverse reinforcement with no lap splices. All three columns contained a longitudinal reinforcement ratio of 2%.

Two columns, one with pre-1971 details and one detailed in compliance with current standards, were tested under incrementally increasing displacements. The third column, also detailed according to current standards, was subjected to one, large displacement demand followed by significant aftershocks (Laplace et al., 2005). The magnitude of the loading history was defined in terms of the percentage of the acceleration due to gravity.

Test results showed that the column detailed according to pre-1971 standards was less ductile than both columns built to current standards, which was expected. The first of the newer-detailed columns was able to sustain a demand level of 1.4g PGA (Laplace et al., 2005). The second column was able to withstand the first demand level of 1.23g PGA without significant damage to the core, and a second demand level of 0.88g PGA without further increase in damage (Laplace et al., 2005). The final demand level of 1.23g PGA did increase damage to the core but did not cause the column to fail (Laplace et al., 2005).

The results indicated that damage levels between the two columns with newer detailing standards were not equal (Laplace et al., 2005). The large amplitude motion applied initially to the second column produced significantly less damage than was sustained by the first column with the same details but with cyclic loading (Laplace et al., 2005). The final condition of the second column was improved over that of the first (Laplace et al., 2005). Figure 1.9 below shows that a higher peak capacity of approximately 8% was measured for the second column (Laplace et al., 2005). The researchers attributed this difference to the damage done by cycling.

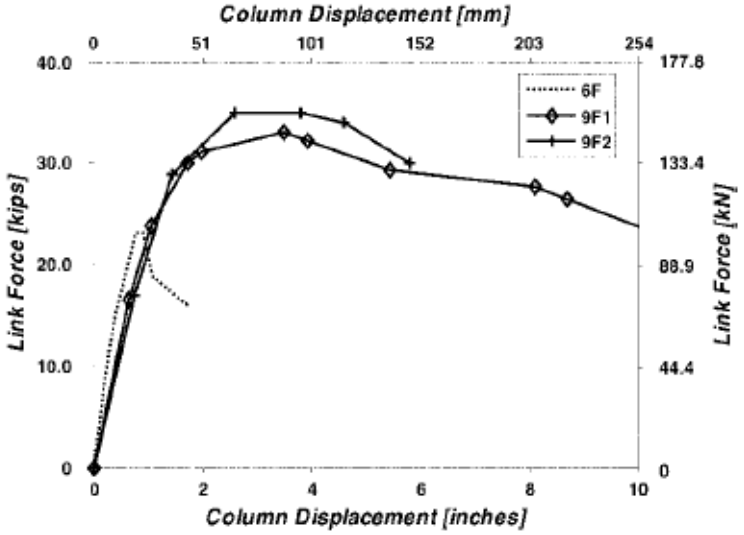

Figure 1.8: Column Response (Laplace et al., 2005)

1.3.3 Matchulat (2009), Lynn (2001), and Sezen (2000) Experimental Research

Few tests in North America have been conducted to study the drift at axial failure of reinforced concrete columns found in older buildings. A number of tests have been performed at the University of California at Berkeley. In addition to the existing data set developed at Berkeley, columns were recently constructed at the University of Kansas by Matchulat (2009) and Purdue University by Henkhaus to increase the breadth of the database established at Berkeley. The following table summarizes the properties of specimens previously tested and found in the literature.

Table 1.1: Column properties for tests by Matchulat (2009), Lynn (2001), and Sezen (2000).

Specimen	b (in.)	ρ_{long}	A_{st} (in^2)	s (in.)	f'_c (ksi)	f_{yl} (ksi)	f_{yt} (ksi)	P (kips)	V_{test} (kips)	$\Delta_{failure}$ (in.)
Matchulat (2009)										
1	18	0.025	0.22	18	4.80	64	54	500	93	1.0
2	18	0.025	0.22	18	4.88	64	54	340	82	1.5
Lynn (2001)										
3CLH18	18	0.030	0.22	18	3.71	48	58	113	61	2.4
2CLH18	18	0.020	0.22	18	4.80	48	58	113	54	3.6
3SLH18	18	0.030	0.22	18	3.71	48	58	113	60	3.6
2SLH18	18	0.020	0.22	18	4.80	48	58	113	52	4.2
2CMH18	18	0.020	0.22	18	3.73	48	58	340	71	1.2
3CMH18	18	0.030	0.22	18	4.01	48	58	340	76	2.4
3CMD12	18	0.030	0.38	12	4.01	48	58	340	80	2.4
3SMD12	18	0.030	0.38	12	3.73	48	58	340	85	2.4
Sezen (2000)										
2CLD12	18	0.025	0.38	12	3.06	64	68	150	73	5.8
2CHD12	18	0.025	0.38	12	3.06	64	68	600	78	2.2
2CVD12	18	0.025	0.38	12	3.03	64	68	Var.	70	3.4
2CLD12M	18	0.025	0.38	12	3.16	64	68	150	67	5.9

Notation: b = square column width; ρ_{long} = longitudinal reinforcement ratio; A_{st} = area of transverse reinforcement; s = hoop spacing; f'_c = concrete compressive strength; f_{yl} = longitudinal steel yield strength; f_{yt} = transverse steel yield strength; P = axial load; V_{test} = peak recorded shear; $\Delta_{failure}$ = displacement at axial failure

The specimens constructed as part of this study were proportioned to be similar to those previously tested, with the goal of exploring variations in loading protocol. For example, shear-critical versus flexure-shear failure, variations in longitudinal reinforcement ratio, and the displacement history could all be explored. In addition, this study is also intended to examine behavior past the point of axial failure, investigating the residual strength of columns.

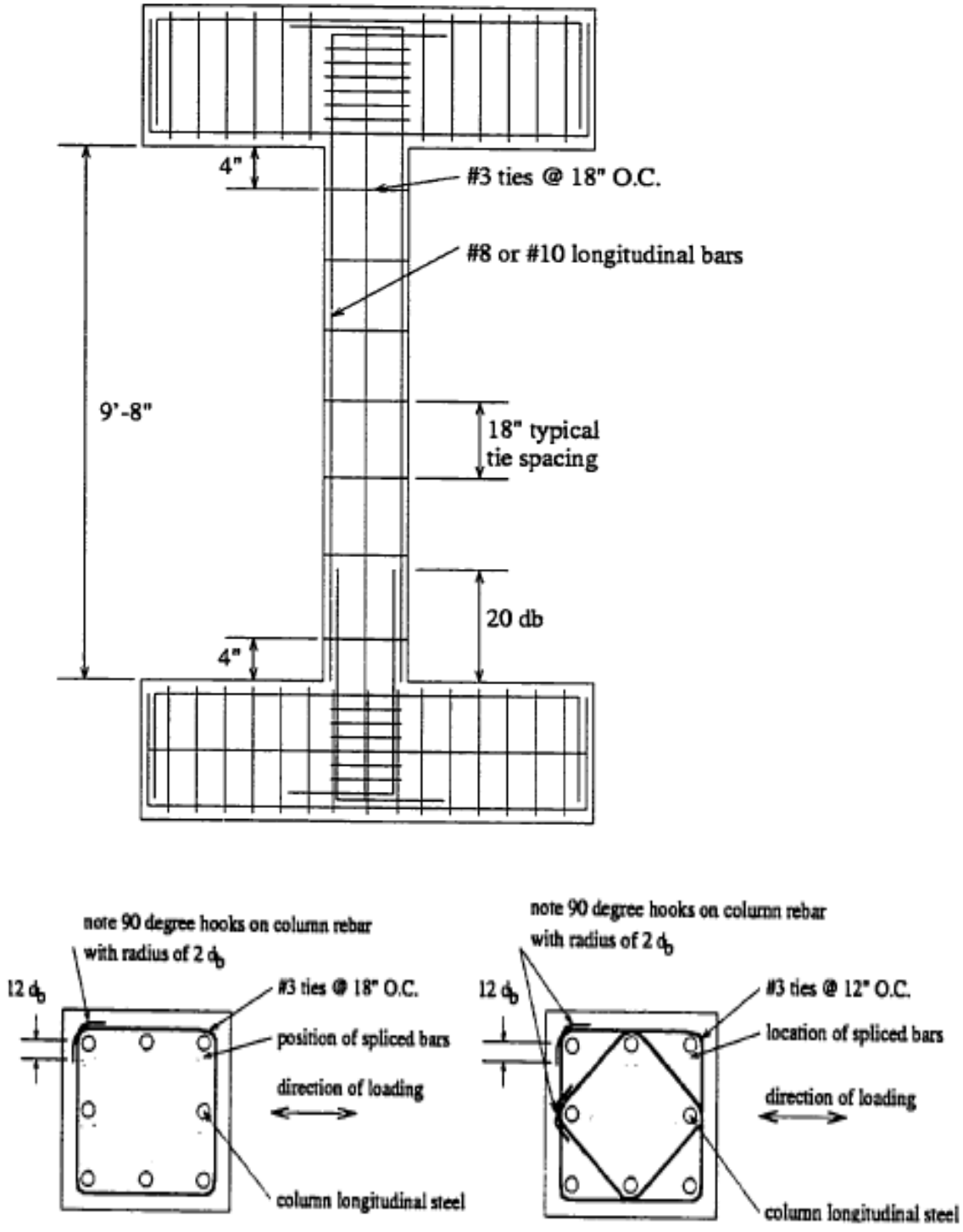

Figure 1.9: Typical column detailing for tests by Matchulat (2009), Lynn (2001), and Sezen (2000).

1.4 Objectives and Scope

This research program aims to expand upon existing data on drift at axial failure of columns found in older reinforced concrete buildings. Two column specimens were fabricated with detailing characteristics similar to those previously tested by Matchulat (2009) and Sezen (2000). The first specimen was intended to study the effect of longitudinal reinforcement ratio on the axial mode of failure of shear-critical columns. The second specimen, similar to previous specimens tested by Sezen (2000), was intended to study the effect of varying the number of cycles at each displacement level on drift ratio at axial failure of columns that experience shear failure after yielding of the longitudinal reinforcement. The two square columns had the same geometric cross sections and elevation dimensions, but varied reinforcing schedules and axial load levels. Data was obtained up to and after loss of axial load capacity, providing valuable insight into the behavior of the columns and their residual strength.

CHAPTER 2: EXPERIMENTAL PROGRAM

2.1 Introduction

The following chapter describes the methods used for construction and testing of the two full-scale column assemblies. Formwork, specimen casting, and strain gauge application were performed at the Structural Testing Laboratory at the University of Kansas. Further instrumentation and testing occurred at the MAST Laboratory at the University of Minnesota, which is part of the Network for Earthquake Engineering Simulation (NEES). Load and displacement protocol as well as specimen characteristics including reinforcing steel properties, steel placement and concrete strengths are presented in Section 2.3.

2.2 Specimen Description

Column geometry was chosen to simulate cross-sections typical to those found in existing reinforced concrete buildings constructed prior to 1971. Because the existing data set of columns tested to axial failure is very small, cross section dimensions and reinforcement details were similar to those of columns tested by Lynn (2001) and Sezen (2000). A square 18-inch column cross-section was selected and the column clear height was 9-feet, 8-inches. Top and bottom beams were constructed to simulate fully-fixed connections at floor locations. Top and bottom beam dimensions had a length of 7-feet, a width of 2-feet, 4-inches and a depth of 2-feet, 6-inches. The reinforcement in the beams was conservatively proportioned to force failure to occur in the column section of the assembly.

Specimen geometry was identical for columns 3 and 4. However, reinforcing steel in both the longitudinal and transverse directions varied between specimens. Column 3 had 8 No. 10 bars spaced evenly throughout the cross-section perimeter for a longitudinal reinforcing ratio of approximately 3%. Transverse reinforcement consisted of No. 3 hoops with 90-degree bends and 12db extensions, spaced at 18-in. on center throughout the column height as shown in Fig. 2.2.

Column 4 had 8 No. 9 bars for a longitudinal reinforcement ratio of approximately 2.5%. Transverse reinforcement consisted of No. 3, 90-deg. closed hoops spaced at 12-in. on center, and diamond-shaped hoops at the same spacing, following the pattern shown in Fig. 2.3. All hoops had 90-deg. bends with 12db extensions.

Reinforcement had a clear cover of 2.5 in. Neither column contained splices. The longitudinal reinforcement was anchored into the top and bottom beams using standard hooks.

The columns were fixed to a single reinforced concrete base block in order to adjust to the configuration of the crosshead. The dimensions of the concrete base block were 8-ft., 6-in. long by 3-ft. wide by 3-ft., 8-in. in height. The concrete base block was post-tensioned to the reaction floor with 12 2-1/2-in. diameter and 6 2-in. diameter steel threaded rods.

Specimen and cross-sections dimensions are shown in Figs. 2.1 to 2.3.

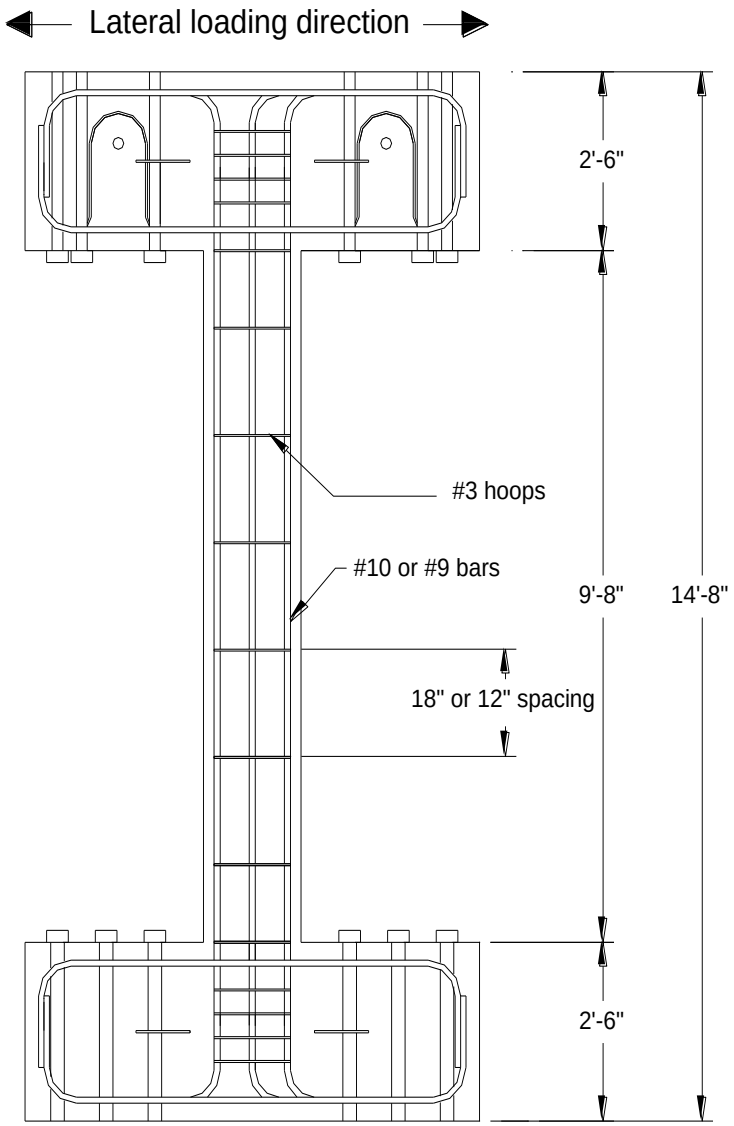

Figure 2.1: Column profile.

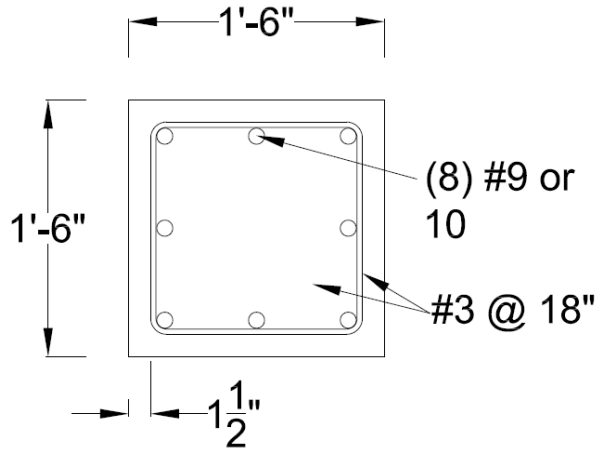

Figure 2.2: Specimen 3 cross-section.

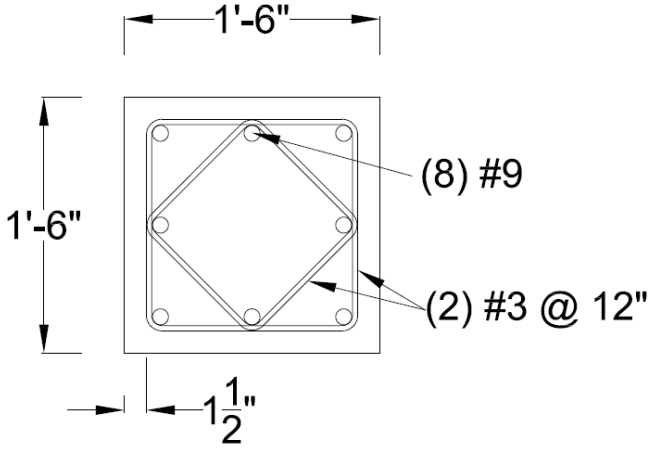

Figure 2.3: Specimen 4 cross-section.

2.3 **Material Properties**

2.3.1 **Concrete**

A target compressive strength of 3000 psi was selected in order to be consistent with previous research as well as represent properties found in typical construction at the study time period. The two specimens were cast separately, with twenty-four standard compressive cylinders cast for each of the columns in addition to two flexure beam specimens. Curing conditions for cylinder specimens and flexure beams were the same to those of the column to maintain continuity.

Lawrence Ready Mix Industries supplied the concrete for both of the columns and beams. Table 2.1 shows detailed constituent properties and quantities. A total amount of five cubic yards was required for each of the columns and corresponding material tests.

To track the curing behavior of the specimens, cylinders were tested in compression on days 7, 14, 21, and 28, as well as on the final day of testing. ASTM C 39 (2009) procedures were adhered to. Additionally, flexure beam tests and modulus tests were carried out on the final day of testing. Table 2.2 shows the various concrete characteristics for each of the columns.

Table 2.1: Concrete constituent quantities

Constituent	Quantity
Type I/II Cement	250 lb.
Class C Fly Ash	125 lb.
Water	190 lb.
Water/Cement Ratio	0.51
C-33 Coarse Aggregate	1673 lb.
C-33 Fine Aggregate	1660 lb.
Water Reducer	11.3 oz.

Table 2.2: Measured concrete properties for specimens 3 and 4

Measured Concrete Property	Column 3	Column 4
Slump	2.25 in.	2.75 in.
7-Day Compressive Strength	1590 psi	2000 psi
14-Day Compressive Strength	2350 psi	2750 psi
21-Day Compressive Strength	2320 psi	2800 psi
28-Day Compressive Strength	2570 psi	2870 psi
Test Day Compressive Strength	2510 psi	2700 psi
Flexural Beam Strength, f_r	690 psi	670 psi
Modulus of Elasticity, E_c	3270 ksi	3270 ksi

2.3.2 Reinforcing Steel

Figures 2.4 through 2.6 show the stress-strain relationships for the longitudinal and transverse reinforcing steels. The longitudinal reinforcing steel for

both specimens was ASTM A706 grade 60, while the transverse reinforcement was ASTM A615 grade 60. The longitudinal reinforcement of specimen 3 consisted of No. 10 bars, while specimen 4 had No. 9 bars. The transverse reinforcement for both specimens consisted of No. 3 hoops. The average yield stress, f_y, was observed to be 65 ksi, 64 ksi, and 54 ksi for Nos. 10, 9, and 3 bars, respectively.

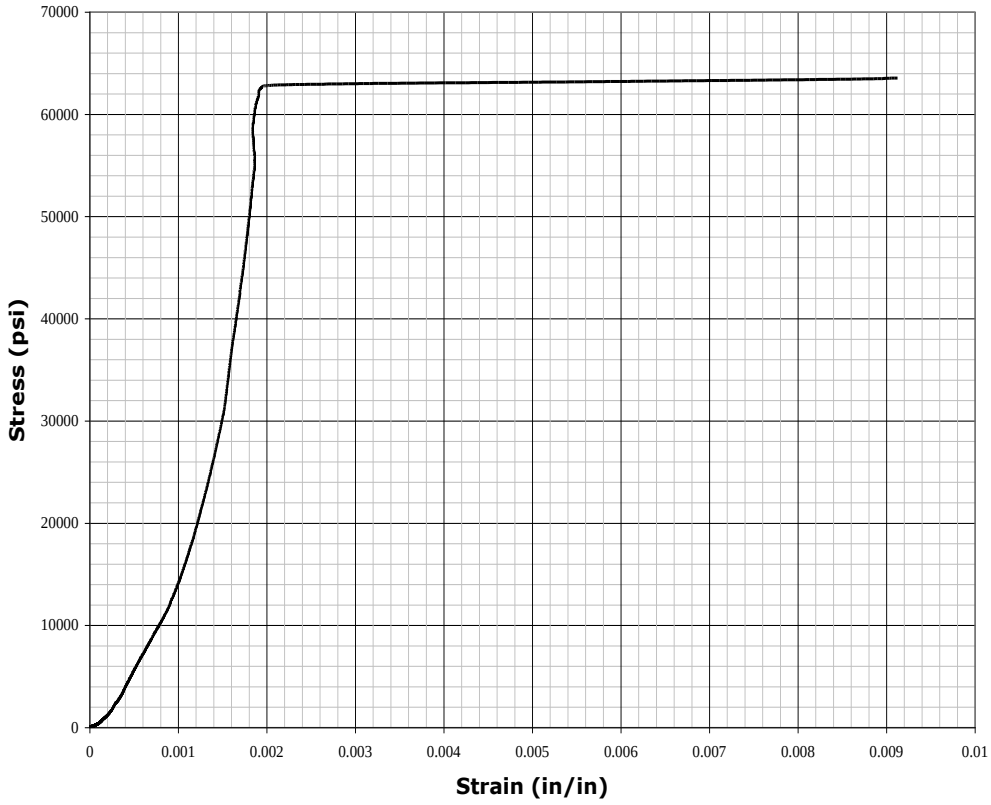

Figure 2.4: No. 10 ASTM A706 longitudinal reinforcing stress-strain relationship

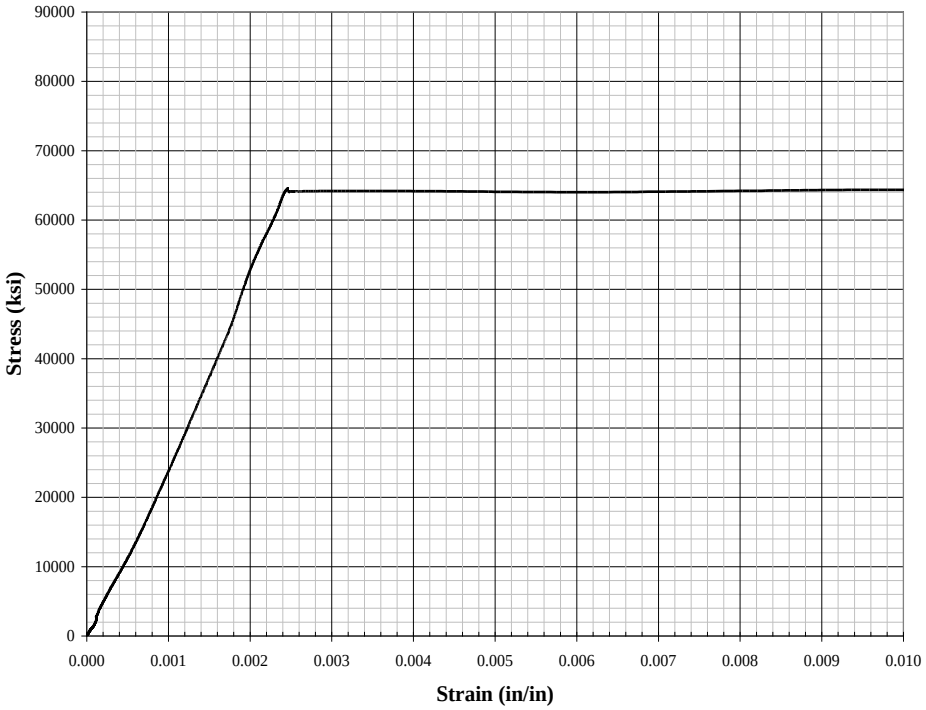

Figure 2.5: No. 9 ASTM A706 longitudinal reinforcing stress-strain relationship

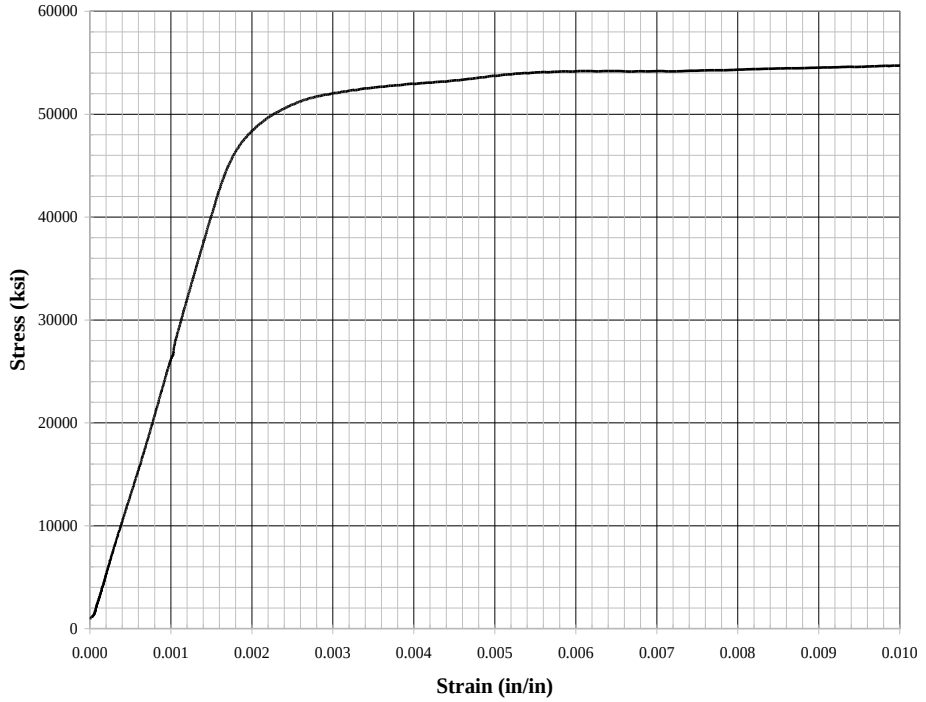

Figure 2.6: No. 3 ASTM A615 transverse reinforcing stress-strain relationship

2.4 Construction

Both columns were cast horizontally at the Structures Laboratory at the University of Kansas. Stick framing, consisting of 2x4 stud dimensioned lumber in addition to 3/4-in. plywood, was used to build the forms. Formwork built for columns 1 and 2 by Matchulat (2009) was used for columns 3 and 4.

Reinforcing steel cages were constructed and lowered into place in the formwork just prior to casting. Cages were put together using standard wire ties. Bar chairs were placed on the longitudinal and transverse reinforcement to provide a clear cover of 2-1/2 inches.

Reinforcing bars were sanded and smoothed at locations where strain gauges were attached. A total of 60 CEA-06, 1/4-in. long, 120-ohm gauges were attached to the longitudinal reinforcing bars. Additionally, 16 CEA-06, 1/8-in. long, 120-ohm gauges were attached to the transverse reinforcement. Specifications were followed for the application of the gauges. Figures 2.7 and 2.8 show the formwork and reinforcing cage prior to casting.

Columns were cured in the horizontal position. Formwork was removed four days after casting. After the curing period ended and prior to moving the columns for transportation to MAST, the columns were post-tensioned using two 1-1/2 in. diameter steel rods attached to anchors cast into the column. Each rod was tensioned to 30 kips using Torquenuts. The post-tensioning force was intended to prevent cracking of the specimens during transportation and tilting.

Figure 2.7: Specimen reinforcing cage

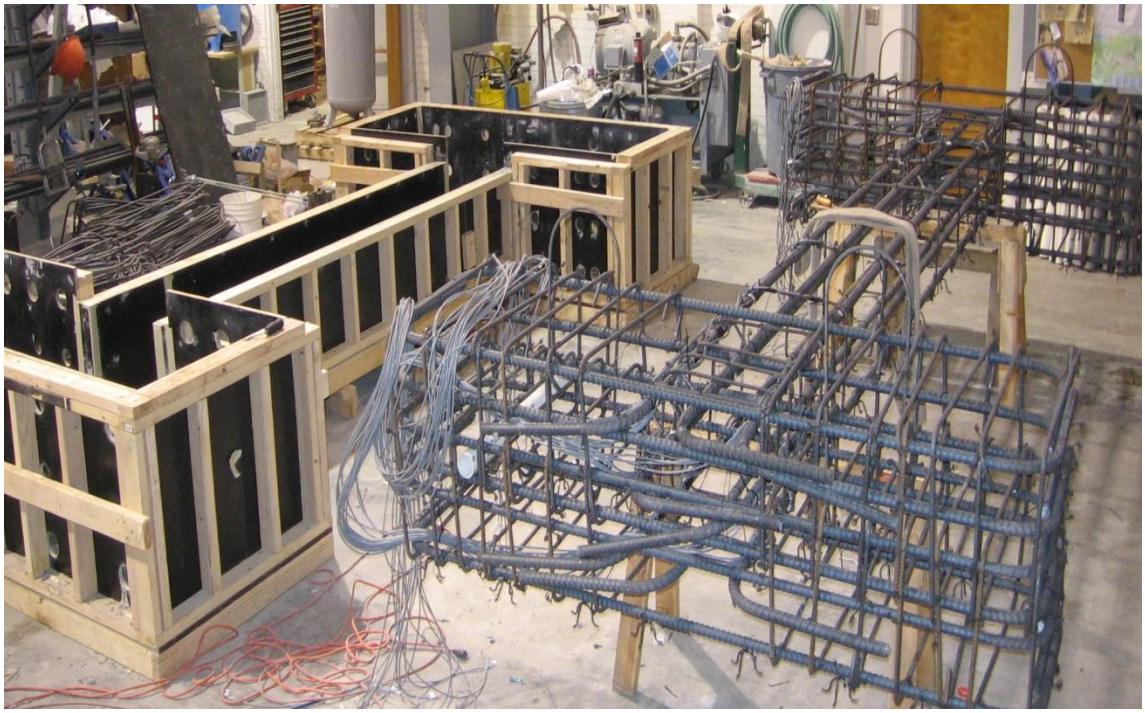

Figure 2.8: Specimen reinforcing cage and formwork

2.5 Test Setup

The columns arrived at the MAST laboratory at the University of Minnesota in their horizontal casting position. The columns were tilted into the vertical testing position by using a support steel frame and the overhead crane. The columns were moved into place underneath the cross-head by systematically "walking" them through various steps by lifting and shifting the specimens until they reached their testing location.

The base block was fixed to the strong floor by six 1-1/2 in.-diameter A193 B7 steel rods, which were post-tensioned using torquenuts. Prior to post-tensioning, UltraCal 30 grout was placed between the bottom plane of the base block and the strong floor to ensure uniform distribution of stresses.

The bottom beam was fixed to the strong floor using 12-2 in.-diameter A193 B7 steel rods. UltraCal 30 grout was applied between the base block and the bottom beam to provide a uniform contact surface between the two.

The interface between the cap beam and the cross head was assembled similar to the interface between the bottom beam and base block, however it was done so upon the completion of the instrumentation. Just prior to beginning to test, the top beam was tensioned to the cross head through the use of 18 1-1/2 in.-diameter A193 B7 steel rods post-tensioned using torquenuts and 1-1/2 in.-thick plate washers. UltraCal 30 grout was applied between the two surfaces to maintain uniform distribution of stresses.

Figures 2.9 through 2.12 show the final testing configuration. A total of six hydraulic actuators, four vertically and two horizontally were attached to the cross head. The capacities of the actuators were 330 kips and 440 kips, for the vertical and horizontal directions, respectively.

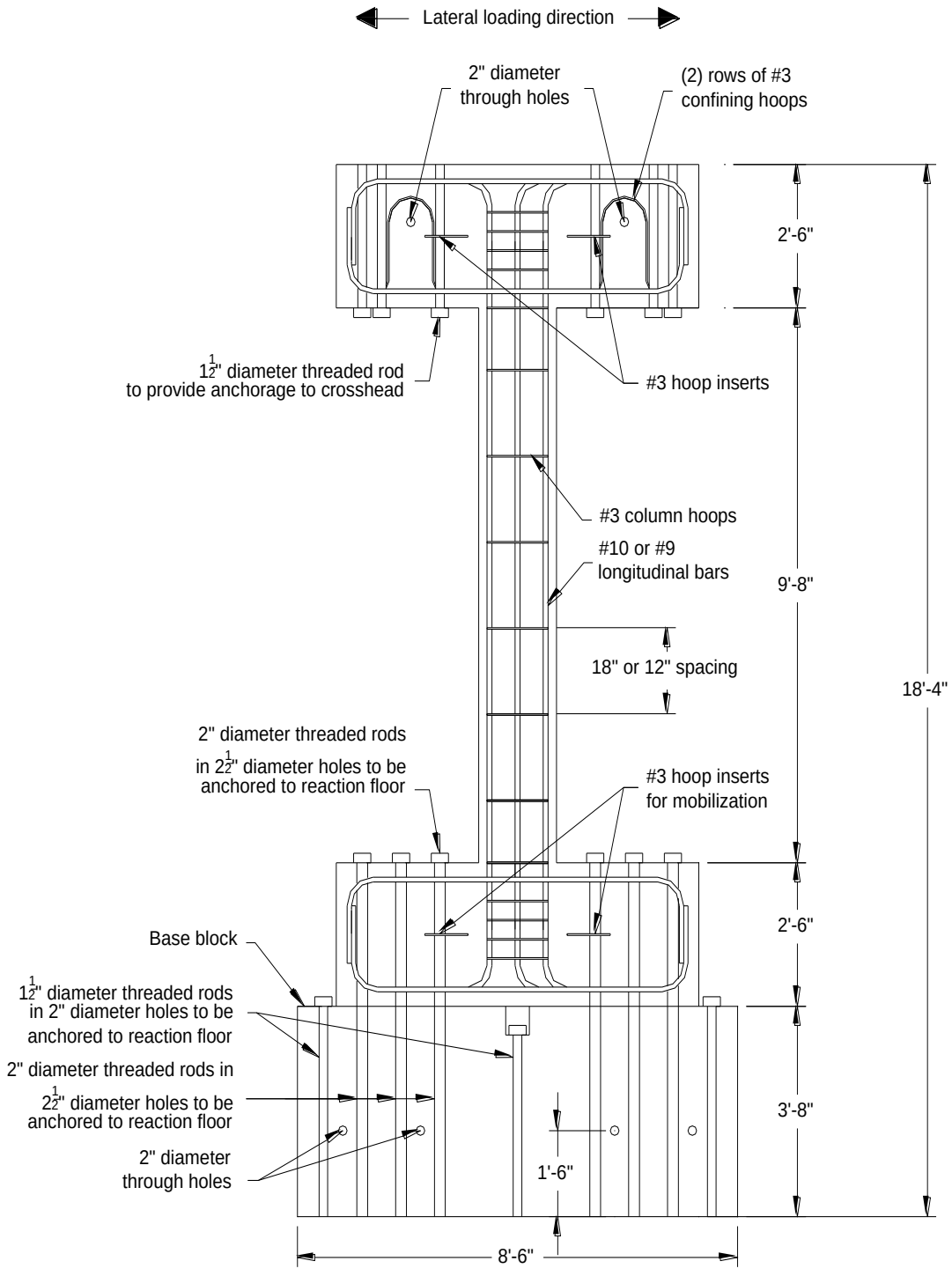

Figure 2.9: Assembly profile

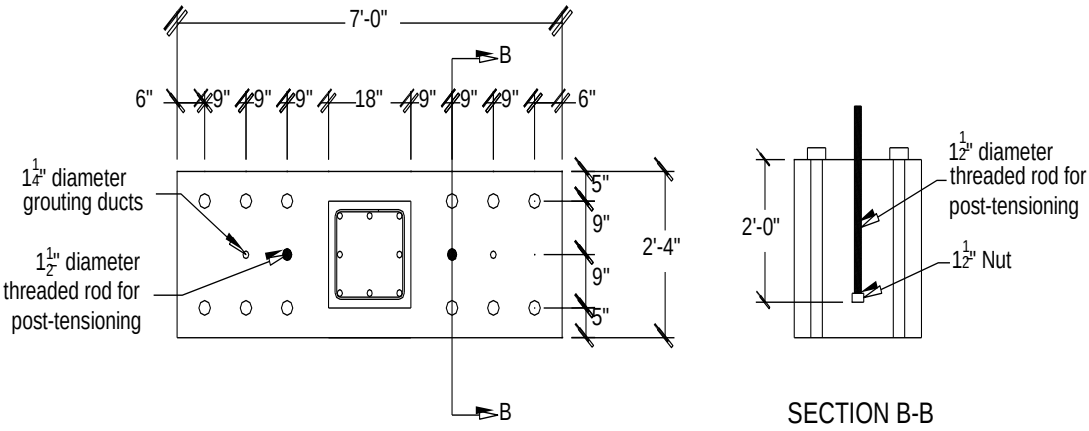

Figure 2.10: Bottom beam hole layout

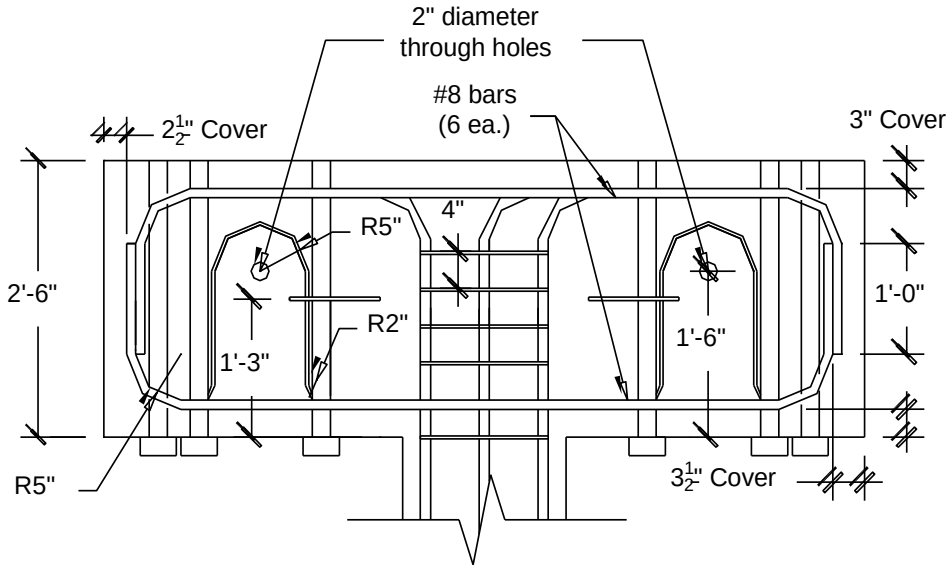

Figure 2.11: Top beam-column connection

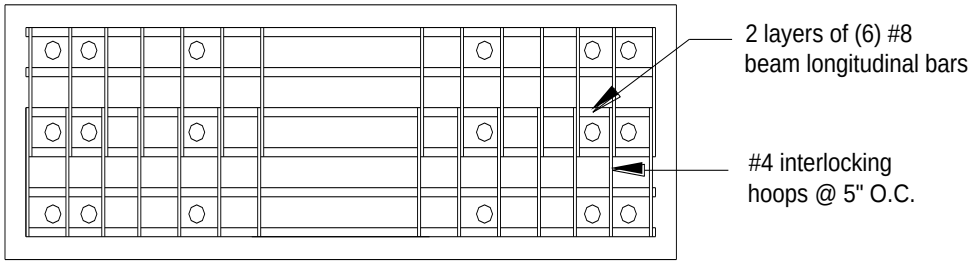

Figure 2.12: Top beam reinforcing layout

2.6 Loading and Displacement Protocol

The testing protocol for specimens 3 and 4 was similar, with the only two differences being the axial load and the number of cycles per drift level. Specifically, column 3 was subjected to sets of three consecutive cycles with the same displacement amplitude. After each set of three cycles was completed, the process was repeated with an increase in displacement amplitude for the next set. In the case of column 4, each set consisted of six displacement cycles with the same amplitude. Other than the number of cycles per drift level, the displacement protocol for both specimens was similar, with the same increments in drift ratio between sets of cycles. Figure 2.13 shows the lateral displacement protocol for column 3.

Axial load was kept constant throughout the test, until axial load failure of the column was detected. The axial loads applied to column 3 and column 4 were 500 kips and 340 kips, respectively. Sets of lateral displacements with increasing amplitude were applied to the columns until axial failure was reached.

Prior to axial failure, defined as a ten percent reduction in the axial load the column could carry, the axial compression force was maintained by the vertical actuators operating in force control. Horizontal actuators were programmed to operate in displacement control as necessary to reach the desired drift ratio. At the point of axial failure, the vertical actuators were programmed to switch to displacement control and maintain the vertical displacement constant and equal to the value measured when the triggering event was recorded, in order to avoid crushing the columns. This was done because part of the investigation into the behavior of these columns included the analysis of post-failure behavior. Post-failure behavior was tracked until damage to the column was extremely severe, with the concrete in the core being completely destroyed and the residual force being carried almost entirely by the buckled longitudinal reinforcement.

After each axial failure event, when the columns returned to a stable condition, an attempt was made to return to the initial axial compressive force. If the prior axial load could not be achieved, then a reduced axial force was applied and cycling continued following the lateral displacement protocol.

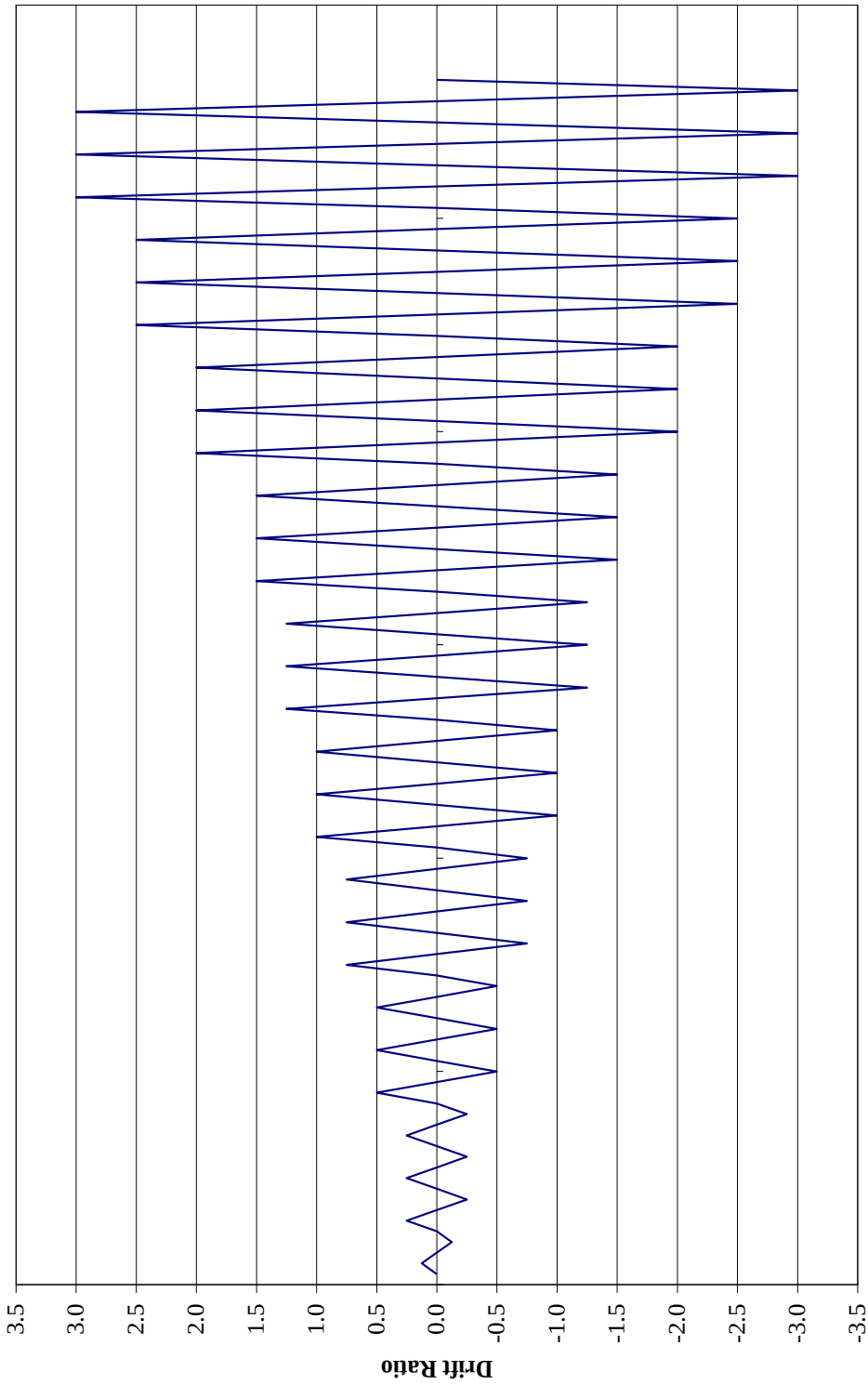

Figure 2.13: Displacement protocol for Specimen 3

2.7 Instrumentation

A total of 76 Strain gages, 23 linear variable differential transducers (LVDTs), and 11 string potentiometers were attached to each of the columns. Additional sensors tracked the motion of the cross head. During testing, data was recorded with a sampling frequency of 1 Hz. Because each test took several days to complete, data was recorded at a reduced sampling rate of 0.1 Hz overnight. Offset voltage readings were recorded before all other test data was acquired.

Of the total 76 strain gages, 60 were attached to the longitudinal reinforcing bars at locations of largest moment demand (the top and bottom of the columns). The remaining 16 gages were attached to the transverse reinforcement at these same relative locations. As shown in Fig. 2.14, the longitudinal gages were numbered in groups starting at the top of the column and increasing down the column height. For example, "LM5" indicates a longitudinal strain gage located on the left side of the front face, middle bar, and five spots from the first gage. Longitudinal strain gages were spaced 8-in. apart within the top and bottom beams and 6-in. apart within the column cross-section. A total of five longitudinal gages were attached to each of the three longitudinal bars experiencing the largest strain demand on each of the faces of the column. Longitudinal gages were extended not only in the column but also into the top and bottom beams to capture the effects of bar slip.

Eight transverse reinforcement strain gages were applied at the top and bottom of the column. Four gages were applied to the hoops nearest the beam-column

interface, at the top and bottom of the column. The remaining four gages were attached to the second nearest hoop to the beam-column interface.

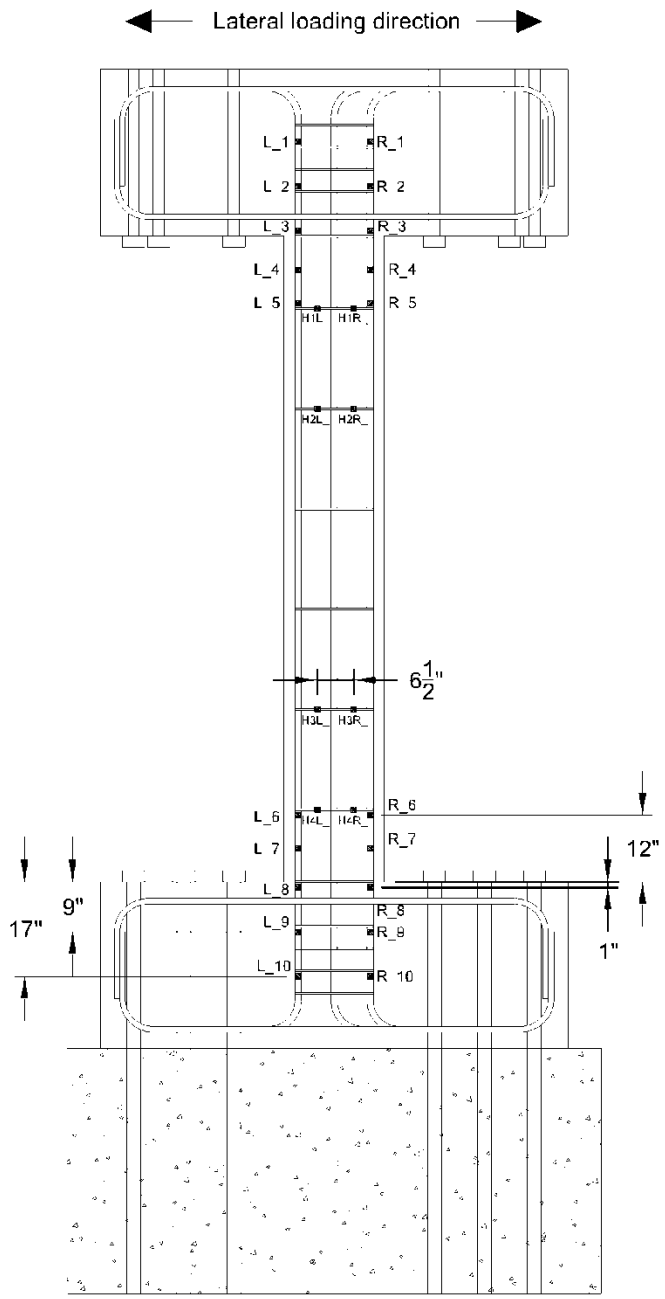

Figure 2.14: Strain gage layout and designation

A total of 23 LVDTs were fixed to the column to track the deformation along the height. The LVDTs were mounted on the column using post-installed anchor rods epoxied at 19-in. intervals throughout the height of the column (Fig. 2.15). Two LVDTs were positioned horizontally to measure the lateral expansion of the column core. Another LVDT was positioned horizontally at the bottom beam to record rigid body translation. Six LVDTs were attached diagonally within the column to capture shear displacements. The remaining 14 LVDTs were aligned vertically along the height of the column to measure rotations, slip, and flexural deformations. Figure 2.15 shows the location of the LVDTs. Similar to the strain gages, LVDTs were designated according to their orientation (V meaning vertical, D meaning diagonal, etc.) and their location relative on the column height, with "1" corresponding to the top of the column.

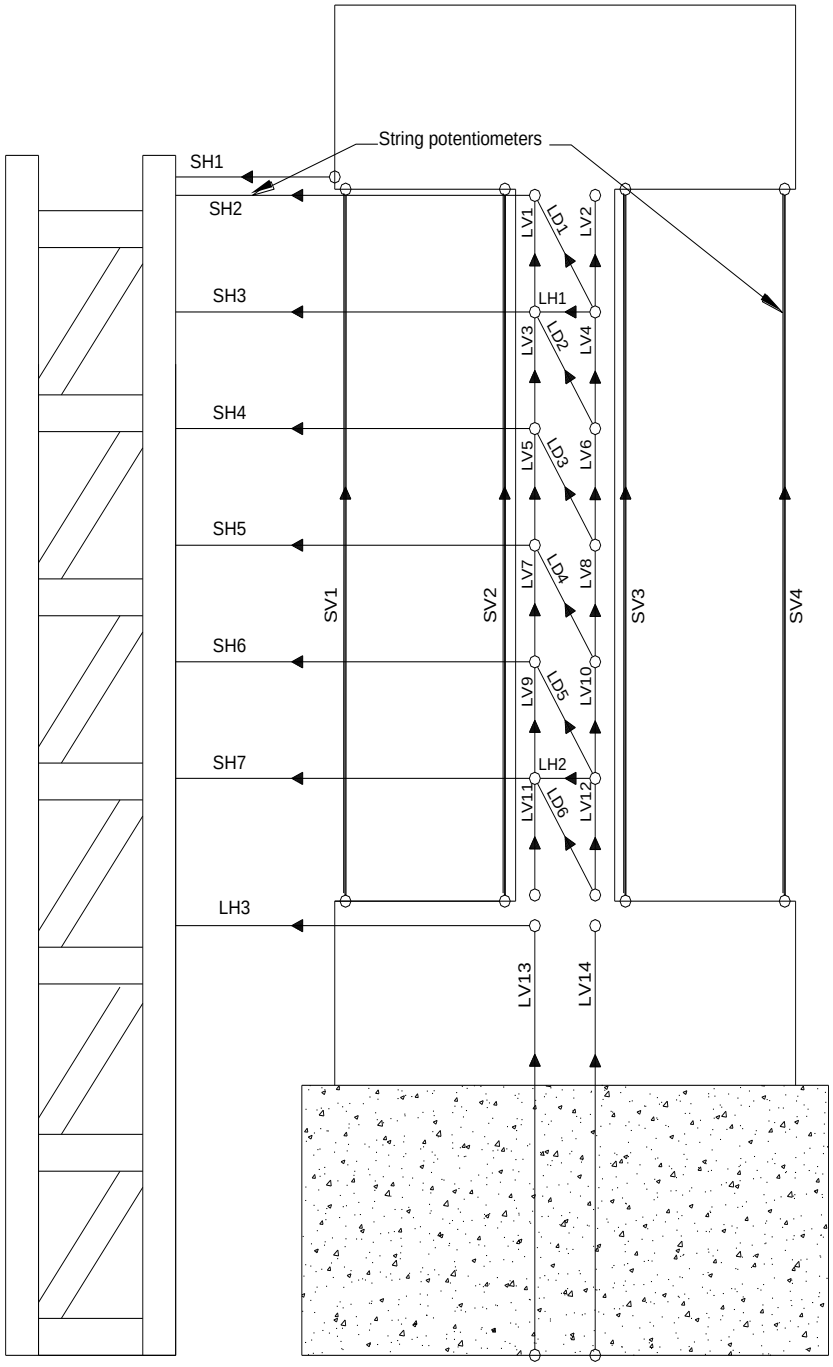

Figure 2.15: Linear Variable Differential Transducers (LVDT) layout

String potentiometers were attached to a reference frame built adjacent the column and fixed to the reaction floor. Seven string pots were used to track lateral displacement at 19 in. intervals throughout the column height. These string potentiometers were designated SH followed by a number. Designations started with SH1 at the top of the beam, with numbers increasing towards the base of the column. A total of four string pots were oriented in the vertical direction, tracking the displacement and rotation between the top and bottom beams. The vertical string pots were designated, SV1, SV2, etc. The number in the designation increased with increasing distance from the instrumentation column, with SV1 being closest to the instrumentation column and SV2 and SV3 being closest to the test column. String pot locations are shown in Fig. 2.16.

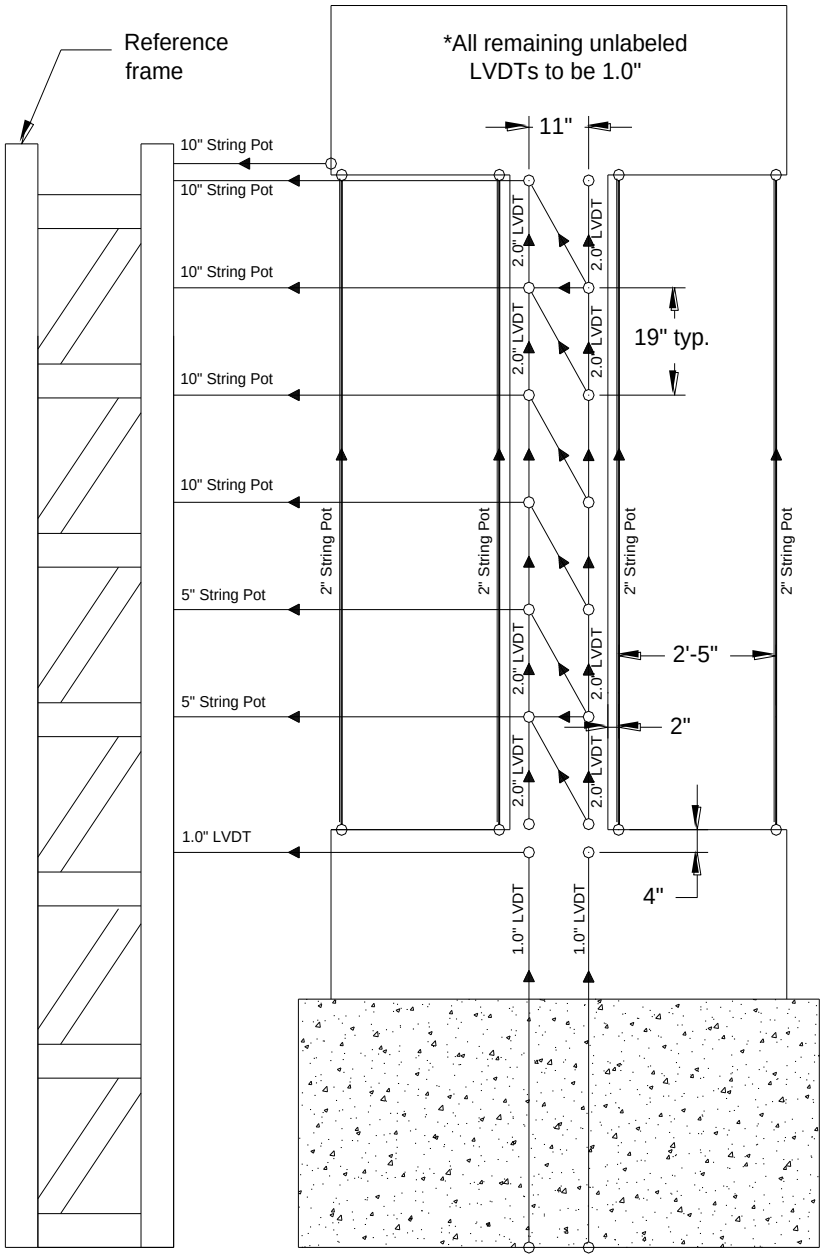

Figure 2.16: Strain Potentiometer layout

2.8 Telepresence

The use of four multi-media towers provided still image and streaming video of both tests. Pictures were taken at each displacement level in order to be used in the analysis of the photogrammetric grid placed on the top, backside of the column, as well as to capture the progression of damage during testing.

Figure 2.17: Telepresence towers. Imagine provided by MAST laboratory.

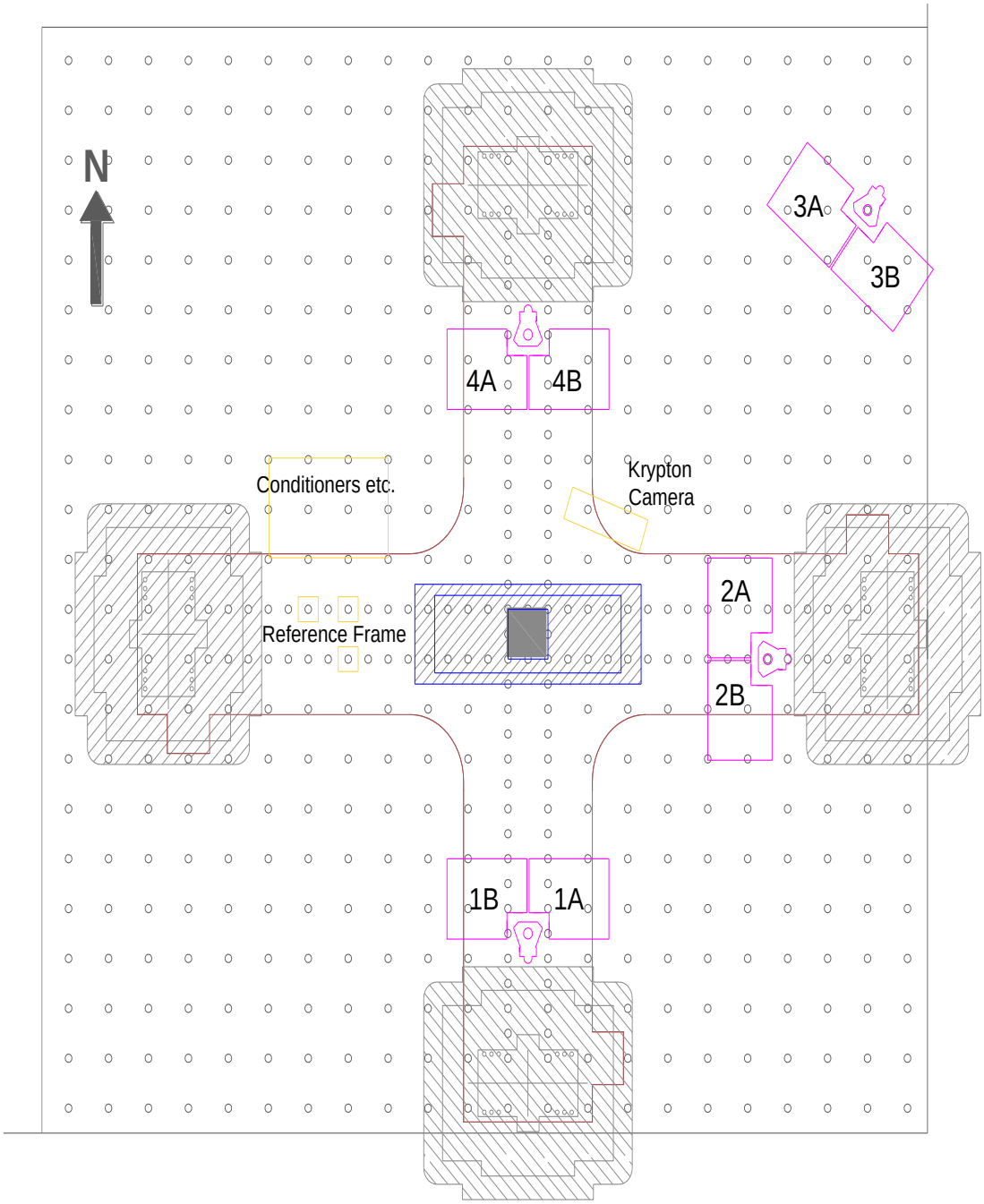

Figure 2.18: Telepresence tower layout

2.8.1 Photogrammetric Measurements

Digital cameras were used to trace the movements of individual photo taggers placed at the top of the column, near the column beam interface, at the location of largest moment. A grid of 5x5 taggers was used to map the deformation at this region of the column. Taggers consisted of gray 11/16-in.-diameter circles with a 1/8-in.-diameter black circle at the center of the tagger.

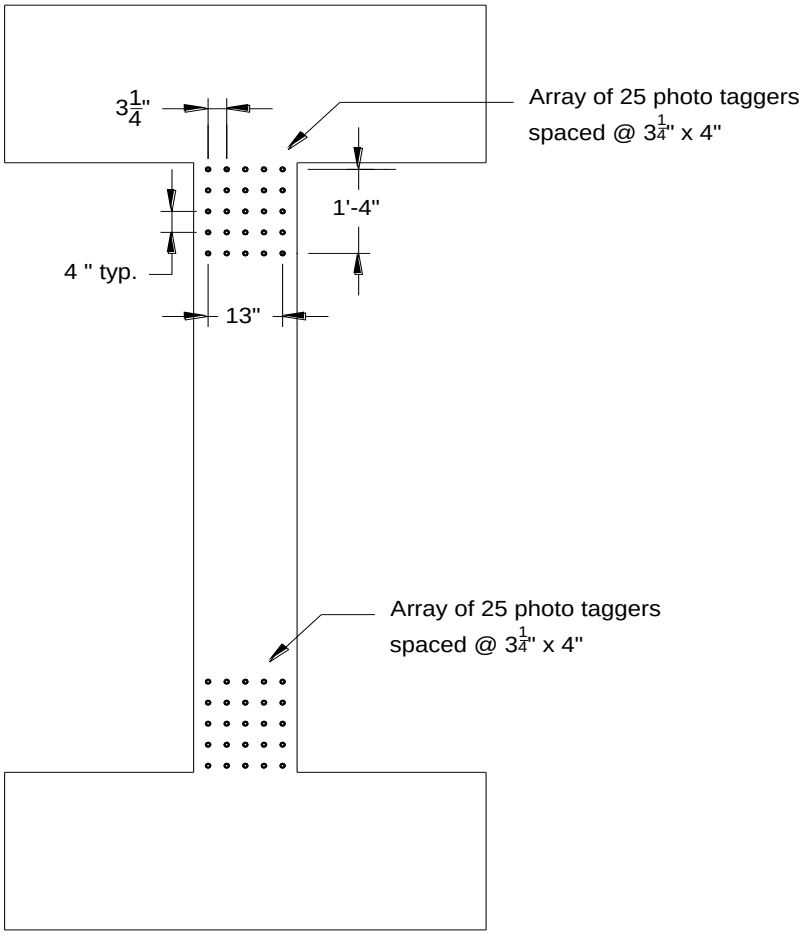

Figure 2.19: Tagger layout

2.8.2 Krypton Camera

In addition to the photo taggers at the top of the column, a 5x5 LED tagger grid was placed on the bottom of the column, also nearest the beam column interface, at the location of maximum moment. A proprietary system called Krypton was used to track the motion of the taggers and convert them to coordinates in three dimensional space. The Krypton system camera was mounted on a support frame located to the side of the column. A reference frame was built to establish a coordinate system by which the grid could be referenced. The Krypton system recorded in three dimensions the location coordinates of each LED tagger during the column displacement cycles. Measurements from the LEDs provided data to calculate deformation components of the column due to shear, flexure, and slip. Figure 2.20 shows the placement and numbering for the LED grid.

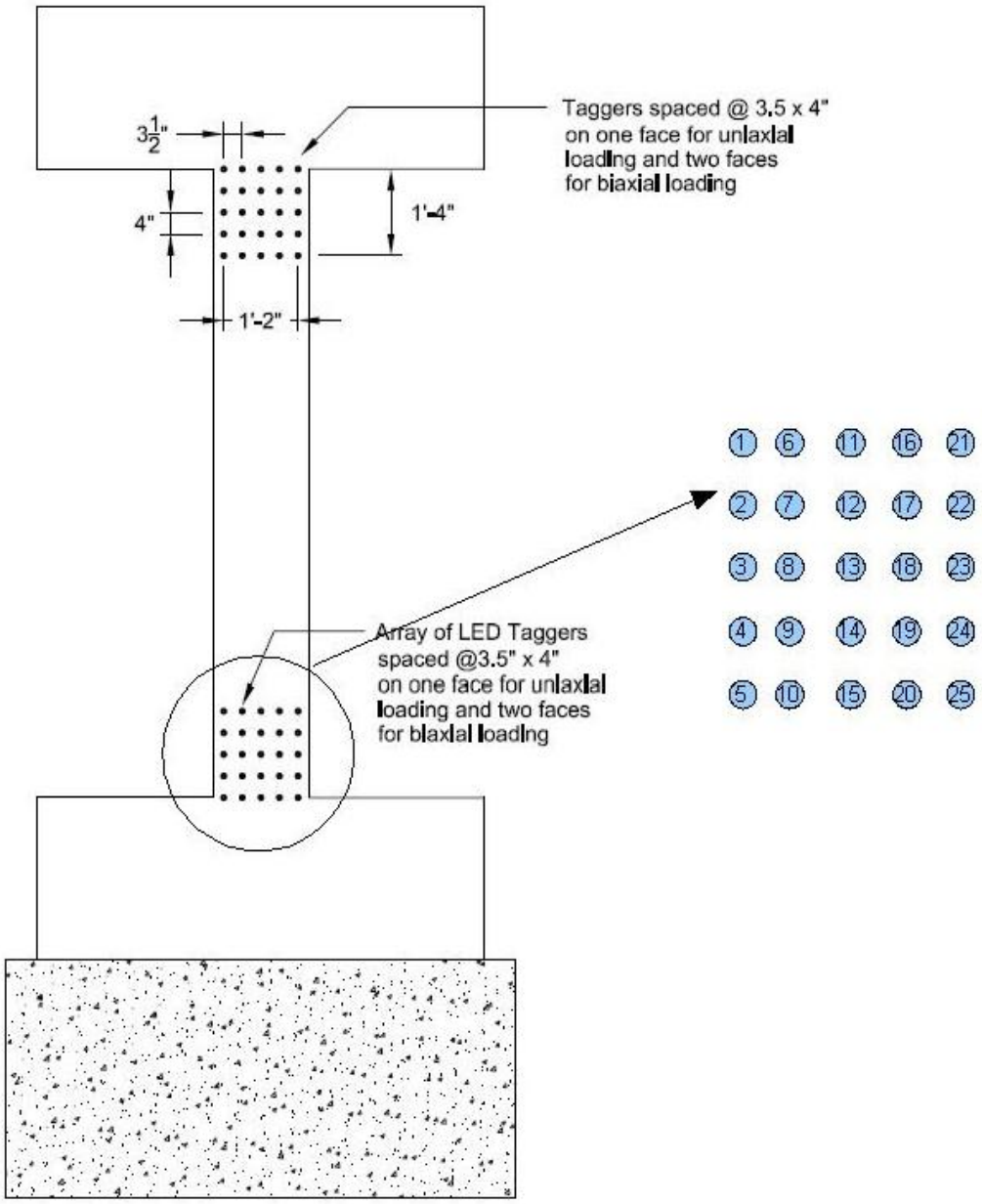

Figure 2.20: Krypton system LED tagger grid layout

CHAPTER 3: TEST RESULTS

3.1 Introduction

Two full-scale reinforced concrete columns, with details similar to those found in buildings constructed prior to 1971, were tested under constant axial compression and increasing lateral load reversals until failure. Test results and the corresponding theoretical estimates are presented within this Chapter. Drift ratios presented in this Chapter were calculated by dividing the lateral displacement by the nominal column height of 116 inches. Theoretical calculations presented in this Chapter include the moment-curvature response and deflection components. Experimental measurements discussed include column strains and axial and shear failure events. The following observed results include lateral load deflection, deflection components, crack propagation, and shear capacity.

3.2 Damage Progression—Specimen 3

A constant, compressive axial load of 500 kips, corresponding to $0.50f'_cA_g$ was applied during the first stage of the test. The lateral displacement protocol was the same as that used for two specimens previously tested by Matchulat (2009). The displacement protocol used with this specimen consisted of three load cycles per drift ratio.

The first displacement cycle, with a maximum drift ratio of 0.125%, was used to verify concrete properties within the linear range as well as proper functioning of the instrumentation. Cracks were marked immediately following the positive and

negative peak displacements of the first cycle corresponding to each level of drift demand.

Hairline, flexural cracks were noticed at the top of the column following the first positive peak displacement of the 0.25% drift ratio, as shown in Fig. 3.1. The maximum measured shear force was approximately 43 kips. At the first negative and positive peaks of the set of displacement cycles with a maximum drift ratio of 0.5%, the maximum measured shear force was approximately 60 kips. Flexural cracks on the tension face of column continued to spread into the tension zone at the top and base of the column, as can be seen in Figs. 3.2 and 3.3.

Flexural cracks continued to propagate during the set of displacement cycles with a maximum drift ratio of 0.75%, growing in both length and width. A change in orientation from horizontal, flexural cracks to inclined shear cracks was noticed at this drift level. Cracks began to spread into both the tension and compression zones. The cracks developed at locations of transverse reinforcement, indicating that they originated at the steel-concrete interface. Figures 3.4 and 3.5 show crack mapping corresponding to the set of displacement cycles with a maximum drift ratio of 0.75%.

Shear cracks continued to propagate during the set of cycles with a maximum drift ratio of 1%. At the first negative peak, a large shear crack approximately one-eighth inch wide formed through the center of the column. The angle of inclination of the crack with respect to the horizontal axis was observed to be approximately 77 degrees. Local displacement readings near the top of the column during the third set of displacement cycles indicated significant lateral expansion. The lateral expansion

was observed in measurements from the diagonal LVDT, (LD2, Fig. 3.10b) as well as larger readings in the top horizontal LVDT (LH1, Fig. 3.10a). Readings from the aforementioned instruments indicate yielding and/or loss of anchorage of the transverse reinforcement and a relative lack of confinement of the column core. Horizontal LVDT readings from the top of the column indicated a lateral expansion of the column of approximately four-tenths of an inch. The large shear crack can be seen in Fig. 3.6, propagating up from the bottom west end of the column to the upper east end of the column. Although the width of the shear crack and the significant loss of stiffness observed in the shear-deflection curve (Fig. 3.21) suggest that shear failure occurred at this point, the column was able to continue to sustain the 500 kip axial load applied.

Cracking widths continued to increase during the set of displacement cycles with a maximum drift ratio of 1%. Damage continued to increase at the points of maximum moment at top and bottom of the column, with some crack widths reaching nearly one-tenth an inch during this set of cycles. The maximum shear force recorded during the first positive peak of the cycle was approximately 69 kips.

Significant loss in stiffness occurred during the set of cycles with a maximum drift ratio of 1.25%.

Axial load failure occurred at the positive peak of the first cycle with a maximum drift ratio of 1.5%, at a displacement of 1.82 in. At this point, the control system shifted from load control in the vertical direction to displacement control, maintaining the vertical displacement that was measured when the triggering criterion

was observed. After switching to displacement control, the column stabilized under a reduced axial load of 447 kips (A reduction in axial load capacity of 53 kips). The system was transitioned to load control under the reduced axial load and maintaining the lateral displacement, an attempt was made to return to the original axial load of 500 kips. The column was not able to withstand the increase in axial load, triggering the vertical actuators into displacement control again when the axial load reached 477 kips. Following this second failure event, load was reduced to 400 kips and the lateral displacement protocol resumed.

Subsequent failure events took place during the same displacement cycle. The third failure event took place while unloading, at a displacement of 0.46 in. After this third failure event, the axial load was further reduced to 300 kips and the vertical actuators again transitioned to load control. Lateral displacement resumed and another axial failure event was recorded when loading in the negative direction of the same cycle at a displacement of 0.78 in. After this axial failure event the column was stabilized at an axial load of 250 kips. Axial load was reduced to 200 kips, and the lateral displacement resumed.

The column was able to maintain a 200 kip axial load throughout the second displacement cycle with a maximum drift ratio of 1.5%. Half way during the third cycle, at approximately zero lateral displacement, another axial failure event occurred. The column was stabilized at an axial load of 180 kips. The axial load was again reduced to 150 kips and lateral displacement resumed. The axial load of 150 kips was maintained on the column through the first positive peak of the cycle with a

maximum drift ratio of 2%. The lateral displacement protocol was interrupted at the end of the first quarter of the displacement cycle with a maximum drift ratio of 2%. At this point the lateral displacement was kept constant and the vertical displacement increased at constant rate to obtain a measure of the residual axial capacity in the column.

Figures 3.7 and 3.8 show the final column state. The most severe damage was observed at the top of the column, in the maximum moment region. Opening of the second hoop from the top allowed unrestrained buckling of the longitudinal bars to occur. Figure 3.8 shows the second hoop from the top just prior to opening, and Fig 3.9 shows the hoop failing at the right-side corner, which removed the lateral restraint of the longitudinal bars. As seen in the figures, a mushroom shaped deformation pattern took place in the longitudinal reinforcement, consistent with previous tests (Matchulat, 2009). This deformation pattern indicates that once the transverse steel experienced anchorage failure and was consequently unrestrained from opening, the axial load acted to "squash" the reinforcing steel.

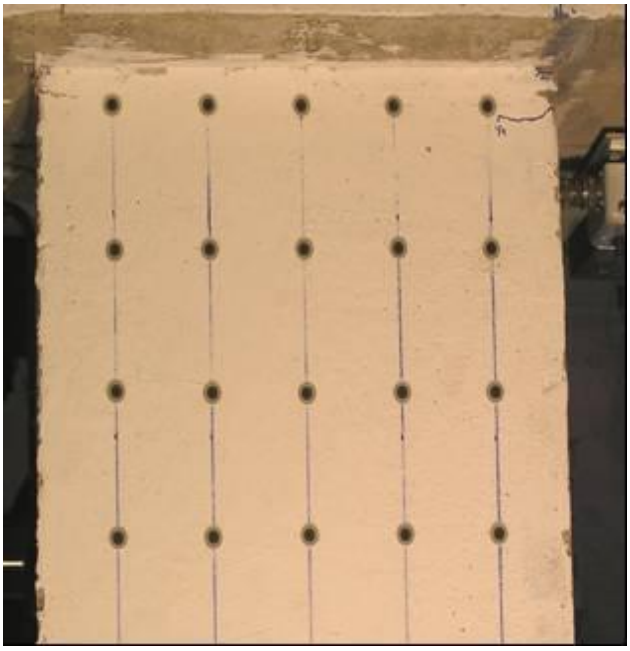

Figure 3.1: Crack pattern at top of Specimen 3 for a maximum drift ratio of 0.25%.

Figure 3.2: Crack pattern at top of Specimen 3 for maximum drift ratio of 0.50%.

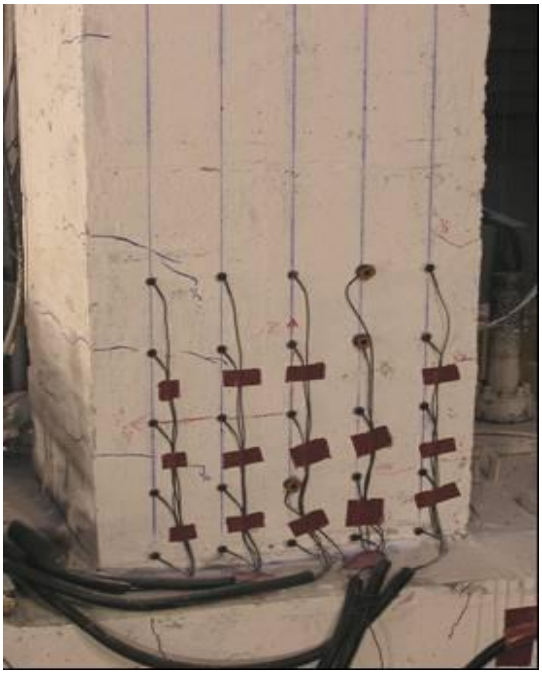

Figure 3.3: Crack pattern at bottom of Specimen 3 for a maximum drift ratio of 0.50%.

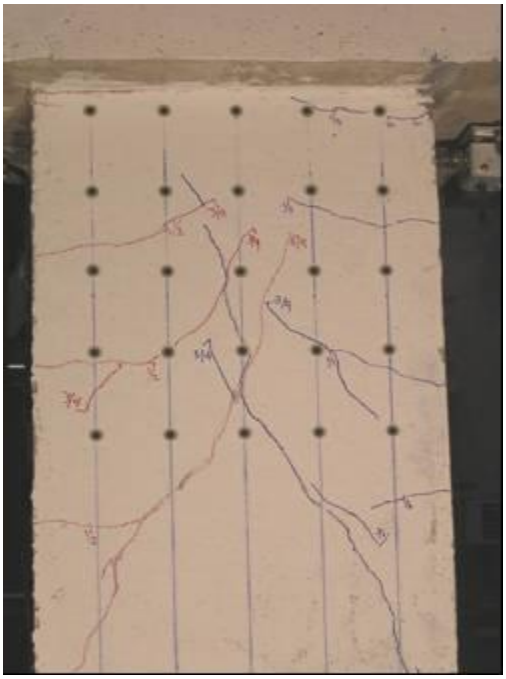

Figure 3.4: Crack pattern at top of Specimen 3 for a maximum drift ratio of 0.75%.

Figure 3.5: Crack pattern at bottom of Specimen 3 for a maximum drift ratio of 0.75%.

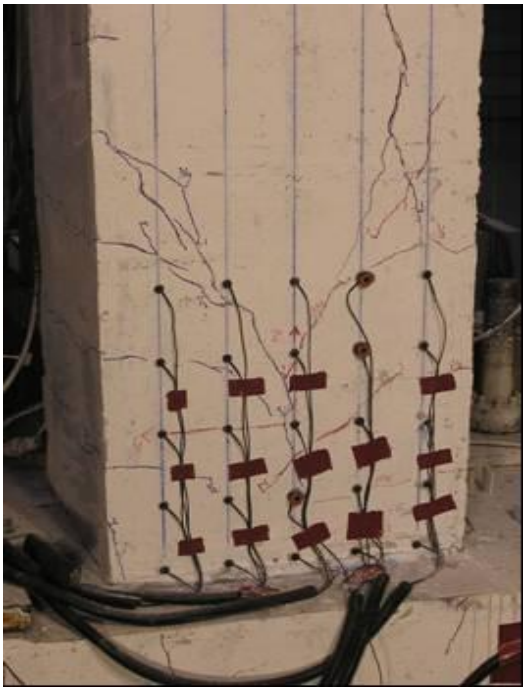

Figure 3.6: Crack pattern at bottom of Specimen 3 for a maximum drift ratio of 1%. The inclined crack shown developed at this stage of loading.

Figure 3.7: Condition of Specimen 3 after a maximum drift ratio of 2%.

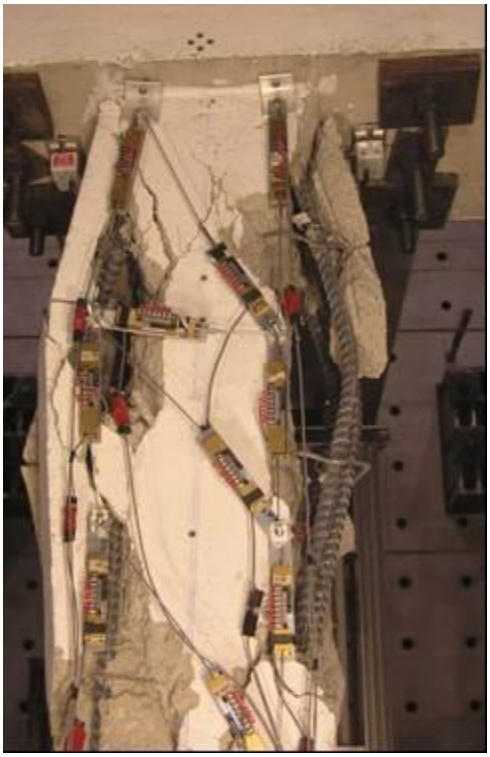

Figure 3.8: View of the top of Specimen 3 just prior to noticing the opening of the hoop.

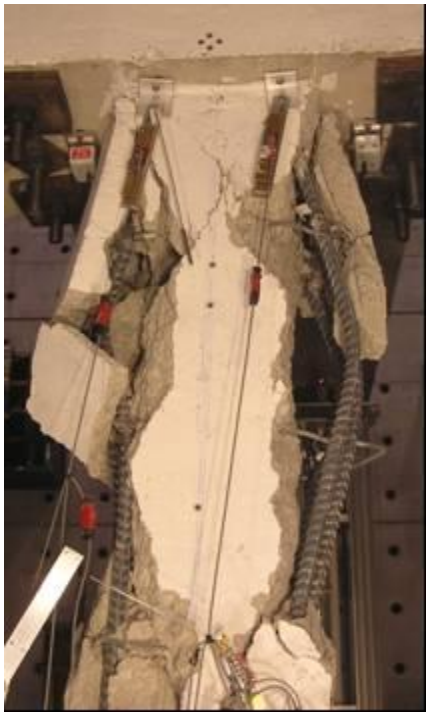

Figure 3.9: View of the top part of Specimen 3 just after opening of hoop was noticed.

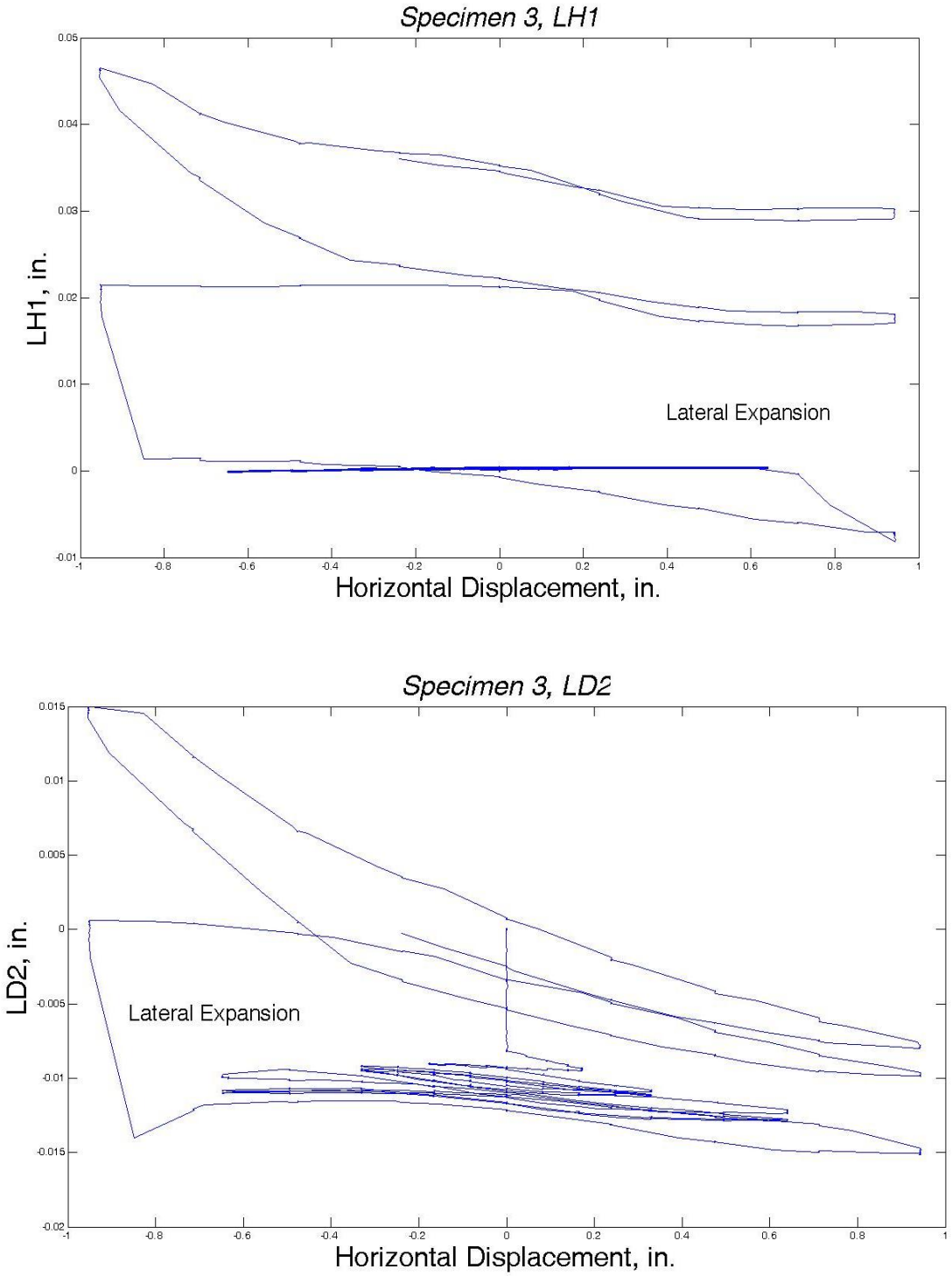

Figure 3.10: (a) Horizontal expansion measured with LVDT LH1 (b) and Diagonal expansion measured with LVDT LD2.

3.3 Damage Progression—Specimen 4

Specimen 4 was subjected to a constant, compressive axial force of 150 kips, which corresponded to approximately to $0.15f'_cA_g$. The displacement protocol changed from Specimen 3 in that 6 cycles at each drift level were imposed on the column. See Section 2.6 for details.

A "test" cycle with a maximum drift ratio of 0.125% was performed to verify that the instrumentation and loading equipment were functioning properly. No cracks were noticed in the column prior to or within this range of testing.

The first cycle with a maximum drift ratio of 0.25% produced a measured maximum shear force at the positive displacement peak of 31 kips. A slightly lower magnitude of 26 kips was recorded at the first negative peak of displacement of this set of cycles. Small flexural cracks were observed at the top and bottom tension regions of the column during peak displacements. Cracks for this cycle are shown in Fig. 3.11.

The first cycle with a maximum drift ratio of 0.5% had a maximum shear force of 44 kips at the first positive peak and 40 kips on the first negative peak. Flexural cracks continued to grow and shear cracks began to form.

A shear force of 54 kips was recorded at the positive peak of the first displacement cycle with a maximum drift ratio of 0.75%. During this set of cycles shear cracks were noticeable, observed in Fig. 3.12, and began to extend into the compression zone of the column. The cracks formed at an angle with respect to the horizontal of approximately 70 degrees.

A shear force of 60 kips was recorded at the positive peak of the first cycle with a maximum drift ratio of 1%. The measured shear force was approximately the same for the negative peak of this displacement cycle (59 kips). Cracks extended far into the compression zone of the column as well as further down the column height. As shown in Fig. 3.13, cracks tended to initiate at hoop locations.

Behavior was similar for the set of displacement cycles with a maximum drift ratio of 1.25%. It was noticed that shortening of the column for this set of cycles increased at a higher rate than previous displacement sets.

The shear force recorded at the peak of the first cycle with a maximum displacement of 1.5% was 70 kips. Horizontal LVDT readings at the top of the column indicated significant growth in lateral expansion of the column. During the first cycle, LVDT LH1 (Fig. 3.20) recorded a lateral expansion greater than 0.25 in., which continued to increase throughout the set of displacement cycles with a maximum drift ratio of 1.5%. As shown in Fig. 3.14, the presence of shear cracks at the top of the column was associated with significant lateral expansion of the column core.

Table 3.1: Axial Failure Events for Specimens 3 and 4.

Column	Event	Max. D.R. Sustained Prior to Failure Event (%)	D.R. at Failure Event (%)	Axial Load Prior to Failure Event (kips)
3	1	1.50	+1.12	500
	2	1.50	+1.01	400
	3	1.50	+0.39	300
	4	1.50	-0.78	250
	5	1.50	-0.78	200
4	1	2.50	-2.84	150
	2	3.00	+2.20	150
	3	3.00	+2.88	114
	4	3.00	+2.88	114
	5	3.00	+1.11	75

The first cycle with a maximum drift ratio of 2% caused a large lateral expansion of the core. Horizontal LVDT LH1 (Fig. 3.20) at the top of the column recorded an expansion greater than 0.5 in. The expansion of the core at this stage of loading is noticeable in Fig. 3.15. The loss of shell concrete at the top, backside of the column can be observed in Fig. 3.16. The shear force at the peak displacement dropped to approximately 14 kips at the end of this set of cycles (maximum drift ratio of 2%) indicating that shear failure took place and the subsequent damage caused a significant reduction in lateral stiffness. The relationship between vertical displacement and lateral force changed from a parabolic shape with positive slope during the previous cycles to a parabolic shape with negative slope (Fig. 3.20b),

indicating that the damage to the concrete core was severe enough to start inducing buckling of the longitudinal reinforcement at large lateral displacements.

During the set of cycles with a maximum drift ratio of 2.5%, lateral stiffness was almost negligible (Fig. 3.22b). Spalling of the concrete shell increased as well as material loss at crack locations. This set of cycles was characterized by having negligible shear force caused by lateral displacement. As shown in Fig. 3.17, although there were cracks extending through the core of the column, the confinement provided by the transverse steel was sufficient to maintain the integrity of the core. However, the outer shell of the column had spalled off exposing the reinforcing steel and the concrete in the core. Figure 3.17 shows that the longitudinal reinforcing steel had not buckled significantly and that anchorage failure of the hoops had not taken place, preserving the ability of the transverse reinforcement to confine the concrete core.

During the first cycle with a maximum drift ratio of 3%, axial failure occurred while loading in the negative direction at a lateral displacement of 3.35 in. Severe damage to the concrete in the core led to anchorage failure of the hoops, which opened at the top of the column resulting in sudden buckling of the longitudinal reinforcement. Figure 3.18 shows the opening of the hoops at the top corner of the column. After the trigger set for the vertical actuators caused them to transition from load to displacement control, the column stabilized at an axial load of 136 kips. The vertical actuators were transitioned to load control and the axial load increased to 150 kips. In this case, the column was able to withstand the original axial load and the

lateral displacement protocol was resumed. While sustaining an axial load of 150 kips the lateral displacement was increased to the peak of the negative cycle (3.6 in.) and brought back to zero to finalize the first cycle. The second cycle was started and axial failure took place while loading in the positive direction at a displacement of 2.6 in. (2.25% drift ratio). After transitioning to displacement control, the vertical actuators stabilized at an axial load of approximately 100 kips. An attempt was made to re-load the column but axial failure occurred at a load of 114 kips. The lateral displacement protocol resumed under a reduced axial load of 90 kips, and a second attempt was made to reach the maximum displacement of 3.6 inches. Axial failure occurred again at a displacement of 3.4 inches. Lateral displacement resumed under a reduced axial load of 87 kips. Another failure event took place at the peak displacement of 3.6 inches, and the axial load was reduced to 75 kips. The lateral displacement protocol resumed under the load of 75 kips and another axial failure event took place while unloading at a displacement of 1.31 in. Axial load was reduced to 50 kips and the displacement protocol resumed. The column brought back to a zero displacement configuration and subsequently tested under increasing vertical displacement to measure the residual axial capacity, which remained nearly constant at approximately 50 kips. Figure 3.19 shows the final condition of the column. Nearly the entire core had deteriorated.

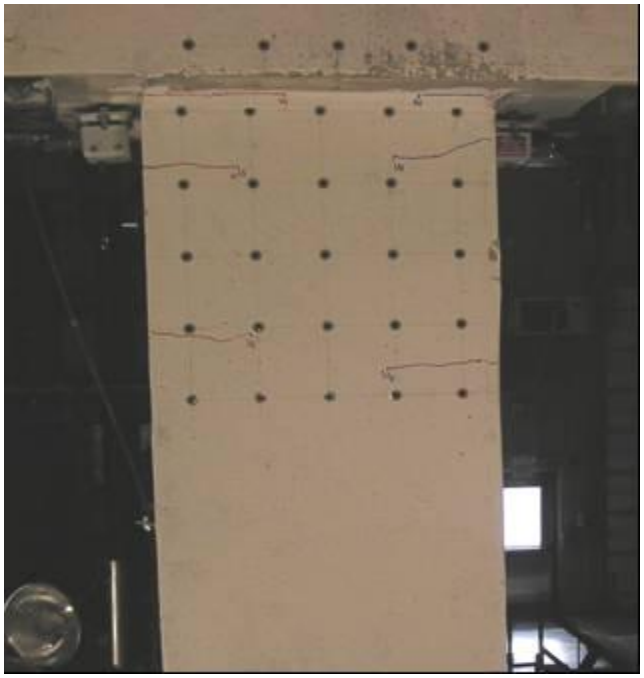

Figure 3.11: Crack pattern at the top of Specimen 4 for a maximum drift ratio of 0.25%.

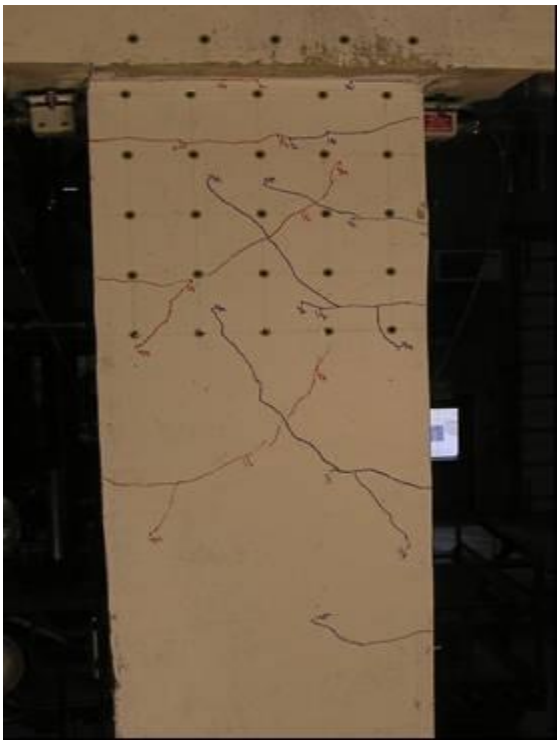

Figure 3.12: Crack pattern at the top of Specimen 4 for a maximum drift ratio of 0.75%.

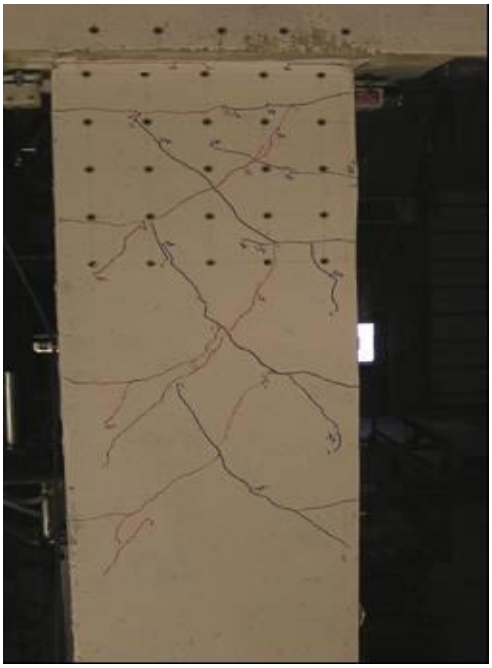

Figure 3.13: Crack pattern at the top of Specimen 4 for a maximum drift ratio of 1%.

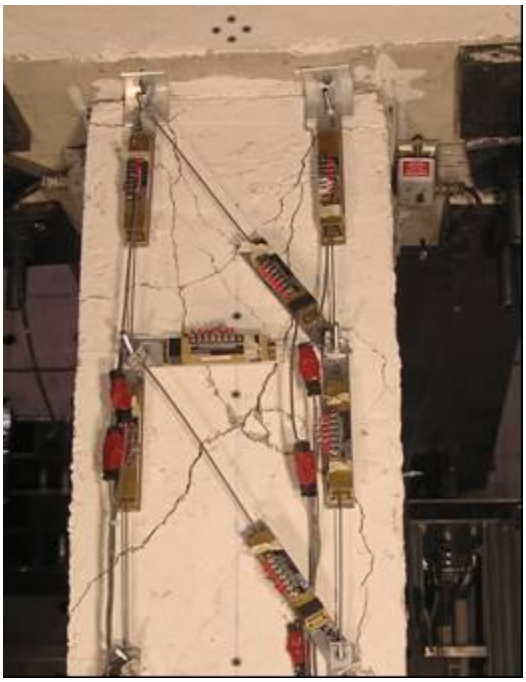

Figure 3.14: Crack pattern at the top of Specimen 4 for a maximum drift ratio of 1.5%. Significant widening of inclined cracks was noticeable at this stage of loading.

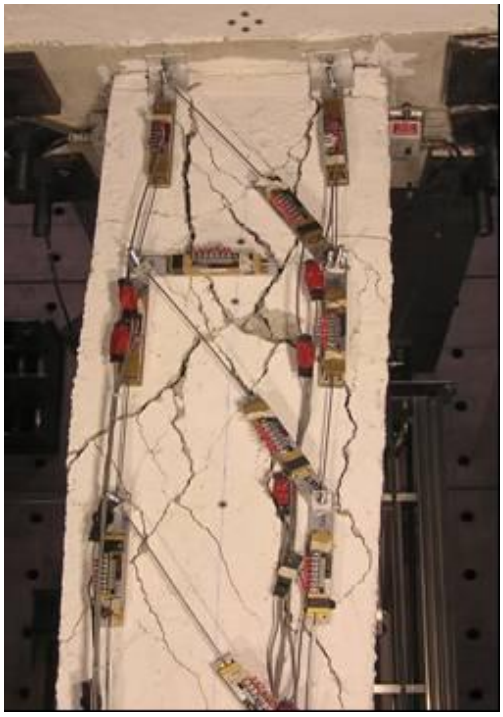

Figure 3.15: Crack pattern at the top of Specimen 4 for a maximum drift ratio of 2%.

Figure 3.16: Crack pattern at the top of Specimen 4 for a maximum drift ratio of 2%.

Figure 3.17: Crack pattern at the top of Specimen 4 for a maximum drift ratio of 2.5%.

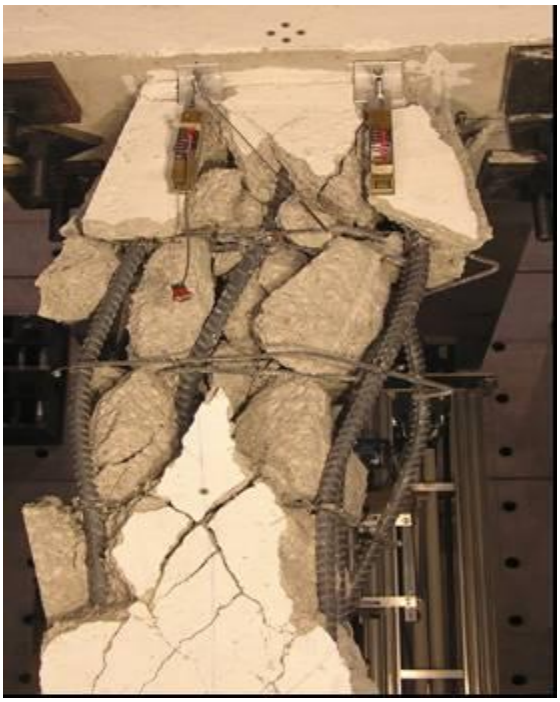

Figure 3.18: Condition of Specimen 4 for a maximum drift ratio of 3%. Damage to the concrete of the core and anchorage failure of the hoop caused buckling of the longitudinal reinforcement.

Figure 3.19: Final condition of Specimen 4.

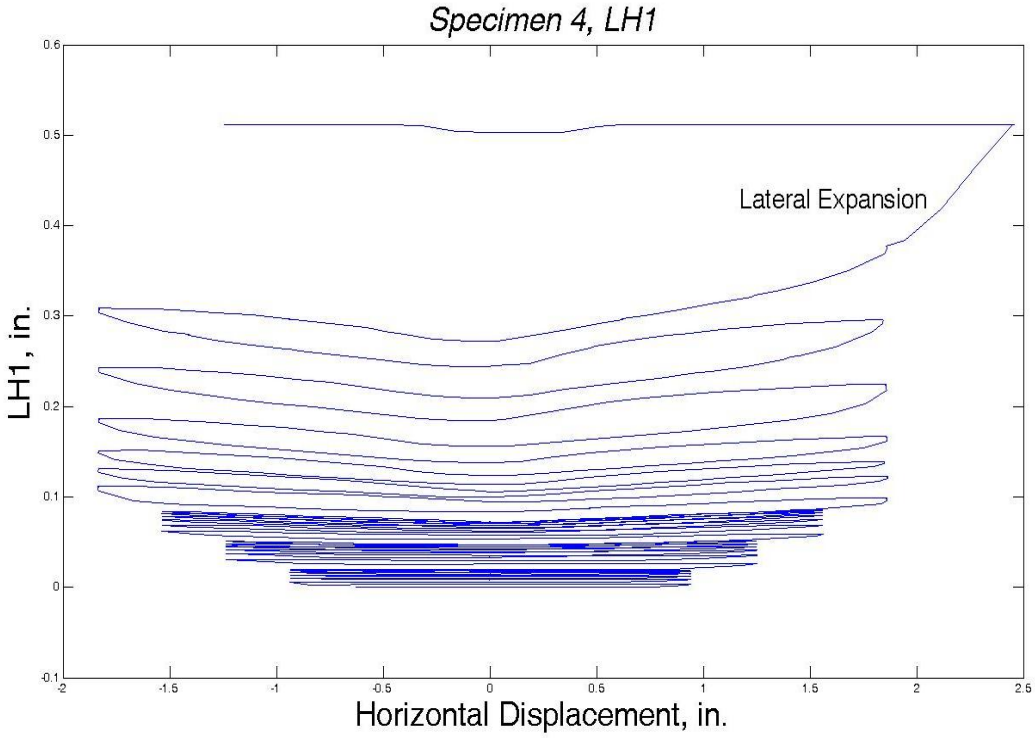

Figure 3.20: Horizontal expansion measured with LVDT LH1.

3.4 Load-Deflection Response

Both columns 3 and 4 experienced shear failure prior to axial failure. In the context of these tests, shear failure is defined by a significant loss of lateral stiffness associated with the appearance or sudden widening of an inclined crack. The drift ratio at shear failure is defined by a change in slope of the load-deflection curve under increasing displacement. The behavior of both columns up to the point of shear failure was relatively linear, with some softening of the response occurring prior to shear failure. Column 3 exhibited brittle behavior which was to be expected based on theoretical strength calculations and observations from previous tests with similar

loading protocols and column detailing Matchulat (2009). Column 4 behaved in a ductile manner, also consistent with a significantly lower axial load ($0.15f'cA_g$) and closer spacing of the transverse reinforcement.

Column 3 reached a maximum lateral load of 70 kips at a corresponding drift ratio of 1%. In the set of cycles following shear failure, the maximum lateral force was reduced by over 70%. Column 4 reached a maximum lateral load of 70 kips at a corresponding drift ratio of 2%. The reduction in lateral stiffness was not as sudden as it was in column 3 despite the increased number of cycles per drift level. A significant reduction in peak lateral load (from 70 to approximately 45 kips) was observed between sets of cycles with maximum drift ratios of 1.5% and 2% (Fig. 3.21). The reduction in lateral stiffness between subsequent cycles was much higher for the set with a maximum drift ratio of 2%. By the end of the set of cycles with a maximum drift ratio of 2% the lateral stiffness was nearly negligible.

There are many similarities between column 3 and columns 1 and 2 tested by Matchulat (2009). All three columns had similar cross-section dimensions and transverse reinforcement spacing, and according to theoretical computations, all three columns were expected to fail in shear prior to yielding of the longitudinal reinforcement. Of the two columns tested by Matchulat (2009), the most similar to column 3 was column 1, which had the same dimensions and axial load, with the only difference being the longitudinal reinforcement ratio.

In terms of behavior, the response of column 3 was similar with that of columns 1 and 2. Given the low amount of transverse reinforcement, there was a

significant reduction in stiffness after shear failure, which occurred at a drift ratio of approximately 1%. While in columns 1 and 2 shear and axial failure were simultaneous, in column 3 axial failure was not immediately triggered by shear failure. Also, in column 1 the combined shear and axial failure led to a total, sudden loss in lateral stiffness. In that respect, the behavior of column 3 was less brittle because axial failure did not lead to an immediate loss in lateral stiffness, although the rate at which the lateral stiffness decreased was very significant. In column 3 a shear crack was first observed at a drift ratio of 0.75% (during the negative peak of the first loading cycle). However, a sudden widening of this crack leading to axial failure occurred during the loading cycles with a maximum drift ratio of 1%.

Table 3.2: Shear Failure Events for Specimens 1 through 4.

Column	Max. Lateral Force (kips)	Drift Ratio at Shear Failure (%)	Drift Ratio at First Axial Failure (%)
1	92.7	0.90	0.90
2	81.5	1.27	1.27
3	70.3	1.03	1.12
4	70.3	2.00	2.89

As previously mentioned, column 3 first suffered axial failure after it reached the peak of the first displacement cycle with a maximum drift ratio of 1.5%. Axial failure occurred while unloading at 1.3 in. of lateral displacement, which corresponds to a drift ratio of 1%. Following this initial failure event, loading resumed under a lower axial load and the column was able to sustain 400 kips (80% of the initial

capacity). The second failure event also occurred while unloading during the same displacement cycle, at a drift ratio of 0.34%. After the second failure event the axial load was reduced to 300 kips. Two more failure events took place while cycling with the same maximum lateral displacement (1.5% drift ratio), one at 250 kips and again at 200 kips. At the end of the set of displacement cycles with a maximum drift ratio of 1.5% the column was able to maintain an axial load of 150 kips with a corresponding axial strain of 0.011.

The trigger criteria for detecting axial failure events in columns 2 through 4 were set to have a shorter response time than column 1. The reason was to prevent excessive damage to the column due to unstable behavior. In column 1 the load dropped from 500 to 100 kips during the first failure event, during the set of displacement cycles with a maximum drift ratio of 1% Matchulat (2009). In column 3 the loss of axial capacity was more progressive nature in that it occurred through several failure events. However, these failure events which caused the axial capacity to drop from 500 kips to 150 kips all occurred during the set of cycles with a maximum drift ratio of 1.5%.

While column 1 experienced simultaneous shear and axial failures after a maximum drift ratio of 1%, column 3 suffered shear failure after a maximum drift ratio of 1% and axial failure after a maximum drift ratio of 1.5%. In column 1 the sudden and brittle nature of the axial failure caused the column to lose its lateral stiffness immediately.

Column 4 behaved unlike any of the columns tested previously at the MAST facility (columns 1 and 2 tested by Matchulat (2009) and column 3 discussed in this report), which was to be expected given the difference in the detailing of the transverse reinforcement. The detailing of this column was similar to that of four columns tested by Sezen (2000) and the axial load was the same as specimens 2CLD12 and 2CLD12M. The main difference between column 4 and columns 2CLD12 and 2CLD12M tested by Sezen (2000) was the loading protocol. Column 4 had six cycles at each displacement level instead of 3 (Specimen 2CLD12) or monotonic loading (Specimen 2CLD12M) used in the specimens tested by Sezen (2000). The lateral load-displacement relationship for column 4 is shown in Fig. 3.21b. Theoretical estimates indicated that the higher amount of transverse reinforcement in this column would cause yielding of the longitudinal reinforcement occurring prior to shear failure, resulting in a more ductile response.

Table 3.3: Test Parameters for specimens tested by Sezen (2000).

Specimen	Axial Load (kips)	Gross Axial Capacity (kips)	Axial Load Ratio	Number of Cycles per Drift Ratio	Drift Ratio at Shear Failure (%)	Drift Ratio at Axial Failure (%)
2CLD12	150	512	0.15	3	2.6	5.0
2CHD12	600	512	0.60	3	0.88	1.9
2CVD12	Variable	512	0.25-0.60	3	1.9	2.9
					2.9	2.9
2CLD12M	150	512	0.15	3-1	2.9	5.5

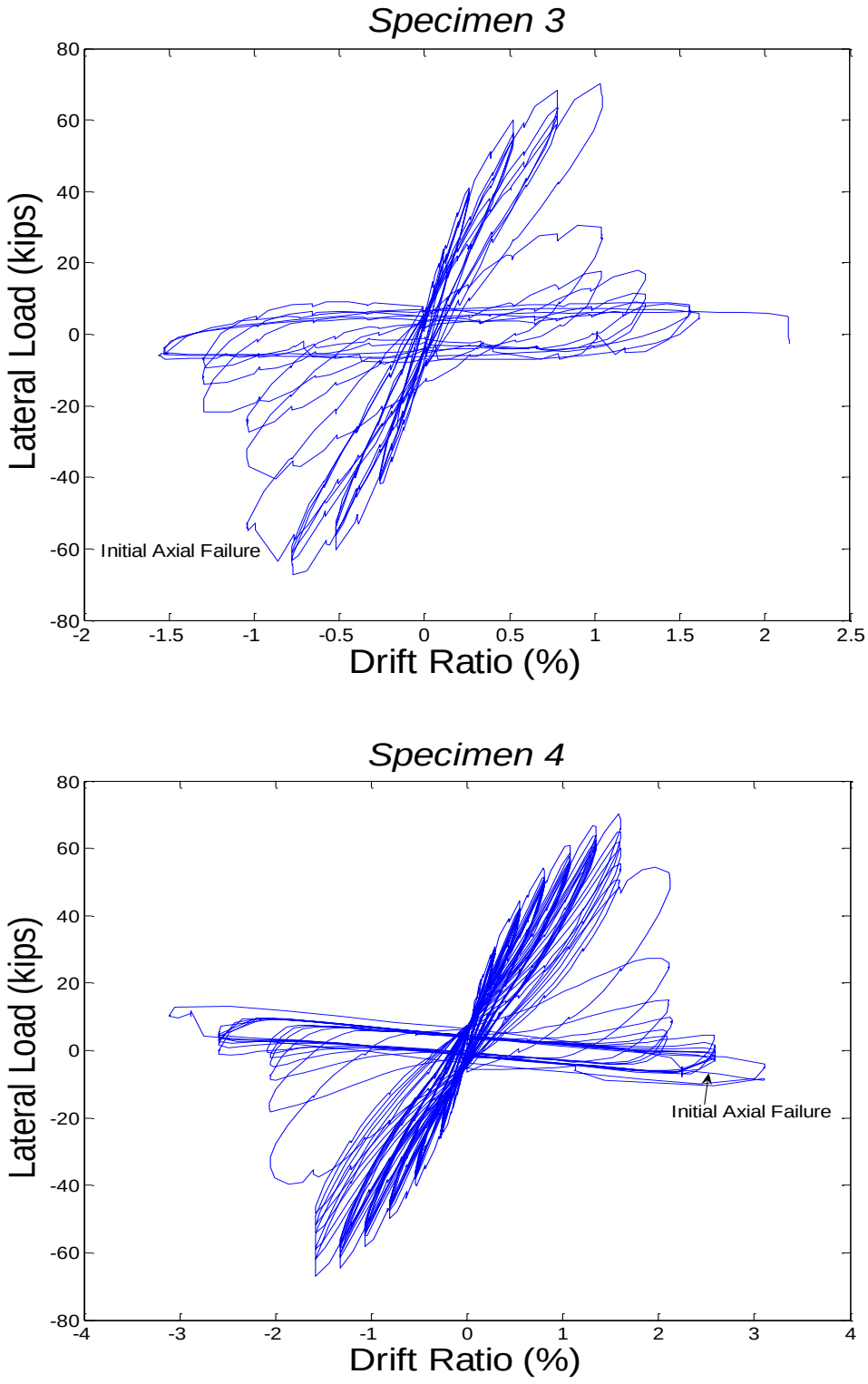

Figure 3.21: Measured lateral-load vs drift ratio. (a) Column 3, (b) Column 4

Unlike the first three columns tested, the first axial failure event for column 4 occurred at a significantly higher drift ratio, after yielding of the flexural reinforcement and after shear failure had occurred. The first axial failure event occurred as the column was being cycled to the negative peak of the first cycle with a maximum drift ratio of 3%, at approximately 3.3 in. of lateral displacement. After the loss of axial capacity, axial load was increased back to 150 kips and displacement resumed. Soon after a second failure event ensued and axial load was reduced to 90 kips. From this point the column was never able to sustain more than 90 kips, with the load being reduced to 50 kips by the end of the test. Between the first axial failure event and the end of the test, column displacement in the vertical direction increased from three-tenths of an inch to nearly one inch, which corresponds to axial strains of 0.0026 and 0.0081, respectively.

Figure 3.22 shows the relationship between axial strain and drift ratio for columns 3 and 4. Column 4 clearly exhibits a change in behavior prior to axial failure as can be noticed by the change in shape of the curve in Fig. 3.22b. The change in shape from convex upward to convex downward is indicative of damage to the concrete core and redistribution of internal compression forces from the concrete to the steel.

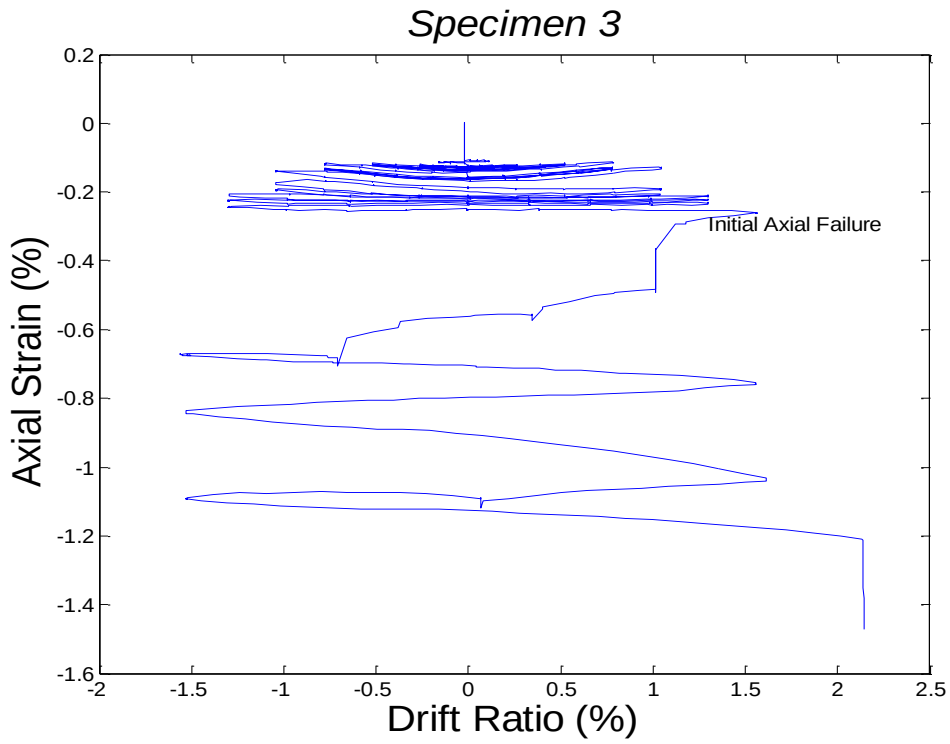

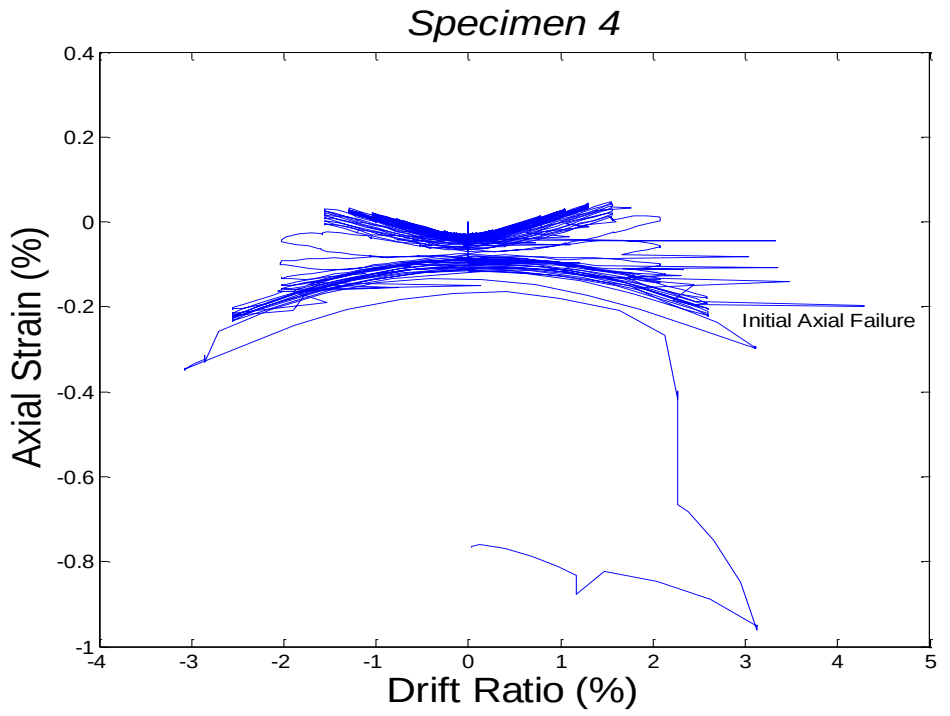

Figure 3.22: Measured axial strain vs. drift ratio for: (a) Column 3, (b) Column 4

3.5 Moment-Curvature

Moment curvature relationships were developed for each of the columns tested. Because the amount of confinement was relatively low, the stress-strain model proposed by Hognestad (1952) was utilized in order to develop the theoretical moment-curvature response. The following procedure was used to develop the moment-curvature relationships:

- It was assumed that plane sections remained plane after bending. A linear strain distribution was assumed as a result.
- The column cross section was divided into layers. The strain calculated at the centroid of each layer was assumed to be equal to the strain across the entire layer.
- The stress-strain relationship for the reinforcing steel was assumed to be elastic-perfectly plastic.
- Tensile stresses in the concrete were ignored.

The following set of equations (3.1), (3.2), and (3.3) proposed by Hognestad (1952) was used to determine the concrete stress at any given layer.

$$f_c = \begin{cases} f''_c \cdot \left[\dfrac{2\varepsilon_c}{\varepsilon_o} - \left(\dfrac{\varepsilon_c}{\varepsilon_o} \right)^2 \right] & \text{for} \quad \varepsilon_c \le \varepsilon_o \\ f''_c \cdot \left[1 - 0.15 \left(\dfrac{\varepsilon_c - \varepsilon_o}{\varepsilon_u - \varepsilon_o} \right) \right] & \text{for} \quad \varepsilon_c > \varepsilon_o \end{cases} \tag{3.1}$$

$$f''_c = 0.85 f'_c \tag{3.2}$$

$$\varepsilon_o = \frac{1.7 f'_c}{E_c} \tag{3.3}$$

where:

f_c = concrete stress (ksi)

f''_c = peak concrete stress (ksi)

f'_c = concrete compressive strength (ksi)

ε_c = concrete strain

ε_o = concrete strain at peak stress

ε_u = ultimate concrete strain = 0.0038

E_c = concrete modulus of elasticity (ksi)

Stress in the reinforcing steel was determined using the following two expressions (3.4).

$$f_s = \begin{cases} 29000\varepsilon_s & \text{for } \varepsilon_s \le 0.0022 \\ f_y & \text{for } \varepsilon_s > 0.0022 \end{cases} \tag{3.4}$$

where:

f_s = reinforcing steel stress (ksi)

ε_s = reinforcing steel strain

f_y = longitudinal reinforcing steel yield strength, measured to be 65 ksi for #10 bars, 64 ksi for #9 bars

An iterative approach was used to calculate moment and curvature pairs by choosing the neutral axis depth and peak concrete compressive strain and then adjusting the position of the neutral axis to balance the resulting forces. Figure 3.23 shows theoretical moment-curvature results compared with measured moment-curvature response in the maximum moment regions of the columns inferred from LVDT measurements. The vertical lines indicate the calculated curvature at yielding of the longitudinal reinforcement. Figure 3.23 shows that both columns exceeded the calculated curvature at yield prior to axial load collapse. The disparity between the theoretical and measured responses can be attributed to the progressive damage that occurred during cycling.

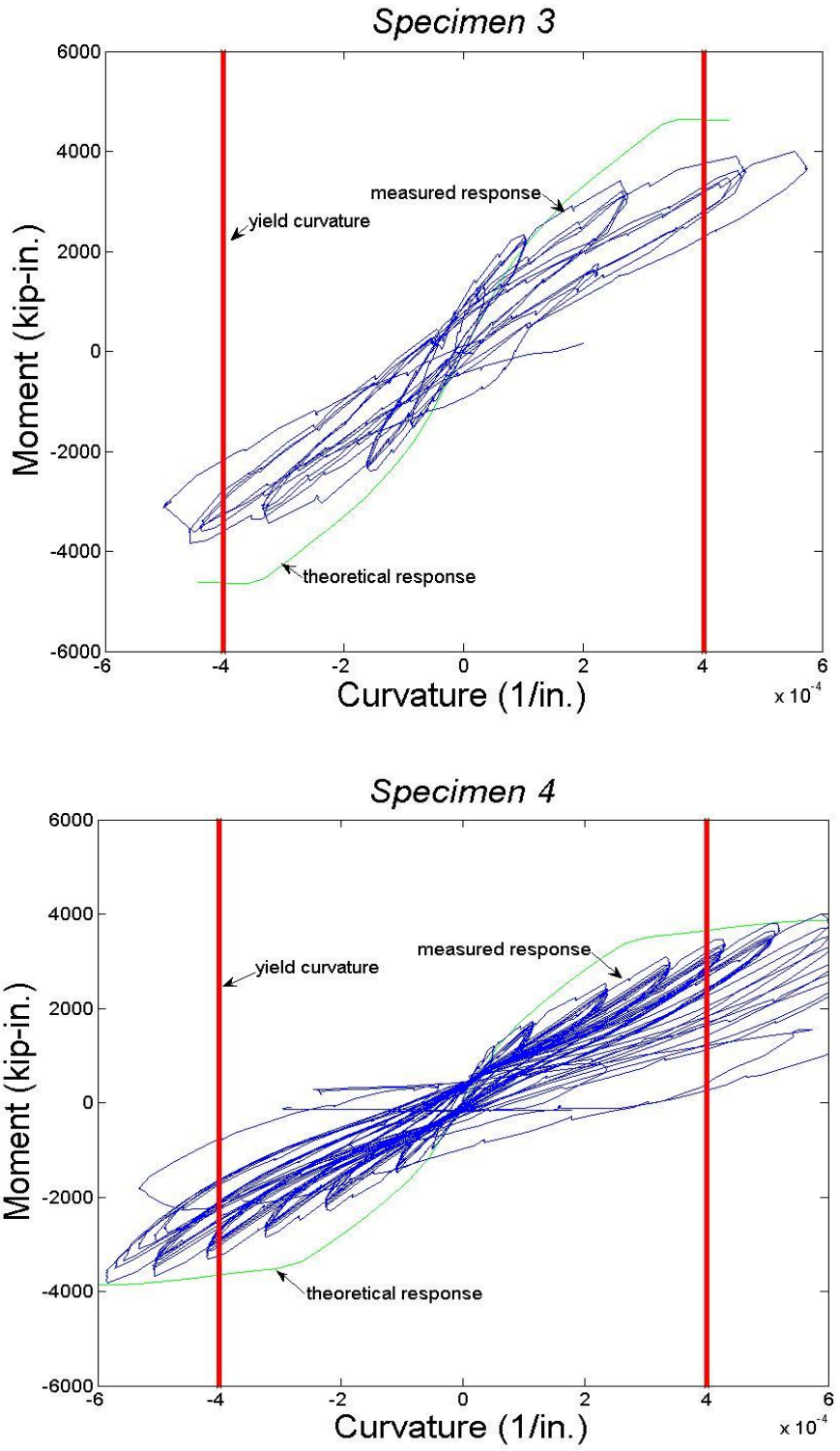

Figure 3.23: Moment-curvature relationship. (a) Specimen 3, (b) Specimen 4

3.6 Deflection Components

Theoretical deflection components due to flexure, shear, and slip are presented below. The total deflection at cracking and yield for each column was calculated as the summation of the three components. Deflection profiles are presented in Fig. 3.24, with references made to the calculated deflections at cracking and yield. The calculated values correspond to the top of the column.

The deflection due to flexure was calculated using the moment-area method. Equation (3-5) assumes a linear curvature distribution.

$$\delta_{flexure} = \frac{\varphi \cdot L^2}{6} \tag{3.5}$$

Where:

φ = curvature in column (1/in.)

L = height of column (in.)

The deflection caused by shear was calculated using Eq. (3.6) and relies on the assumption of uniformly distributed shear strain as well as linear material response.

$$\delta_{shear} = \frac{6 \cdot V \cdot L}{5 \cdot G \cdot A_g} \tag{3.6}$$

$$V = \frac{2 \cdot M}{L} \tag{3.7}$$

$$G = \frac{E_c}{2 \cdot (1 + \upsilon)} \tag{3.8}$$

where:

V = shear force (kips)

G = concrete shear modulus (ksi)

A_g = gross cross-sectional area of column (in^2)

M = moment at column end (in-kip)

E_c = concrete modulus of elasticity (ksi)

υ = Poisson's ratio = 0.20

Slip was calculated based on Eq. (3.9) which assumes that a uniform bond stress along the development length of the bar (Matamoros, 1999).

$$\delta_{slip} = \frac{L \cdot d_b \cdot f_s^{\,2}}{48 \cdot (d - d') \cdot E_s \cdot \sqrt{f'_c}} \tag{3.9}$$

where:

d_b = diameter of longitudinal bars (in.)

f_s = reinforcing steel stress (ksi)

d' = depth to first layer of reinforcement (in.)

d = depth to third layer of reinforcement (in.)

E_s = reinforcing steel modulus of elasticity (ksi)

f'_c = concrete compressive strength (ksi)

Additional deflections caused by rigid body rotation and horizontal slip were neglected, although measured values are included for reference in the following tables. The effects of these components were insignificant at the top of the column. Table 3.4 provides a summary of the calculated deflections at both cracking and yielding for both columns. Figure 3.24 indicates that the deflection of column 3 at axial failure was approximately equal to the calculated deflection at yield, and that column 4 significantly exceeded calculated deflection at yield prior to axial failure.

Table 3.4: Theoretical deflection components

	Cracking		**Yield**	
Components	**Specimen 3**	**Specimen 4**	**Specimen 3**	**Specimen 4**
Flexure	0.03 in.	0.03 in.	0.90 in.	0.89 in.
Shear	0.002 in.	0.002 in.	0.03 in.	0.02 in.
Slip	0.008 in.	0.01 in.	0.69 in.	0.51 in.
Total	0.04 in.	0.04 in.	1.62 in.	1.42 in.

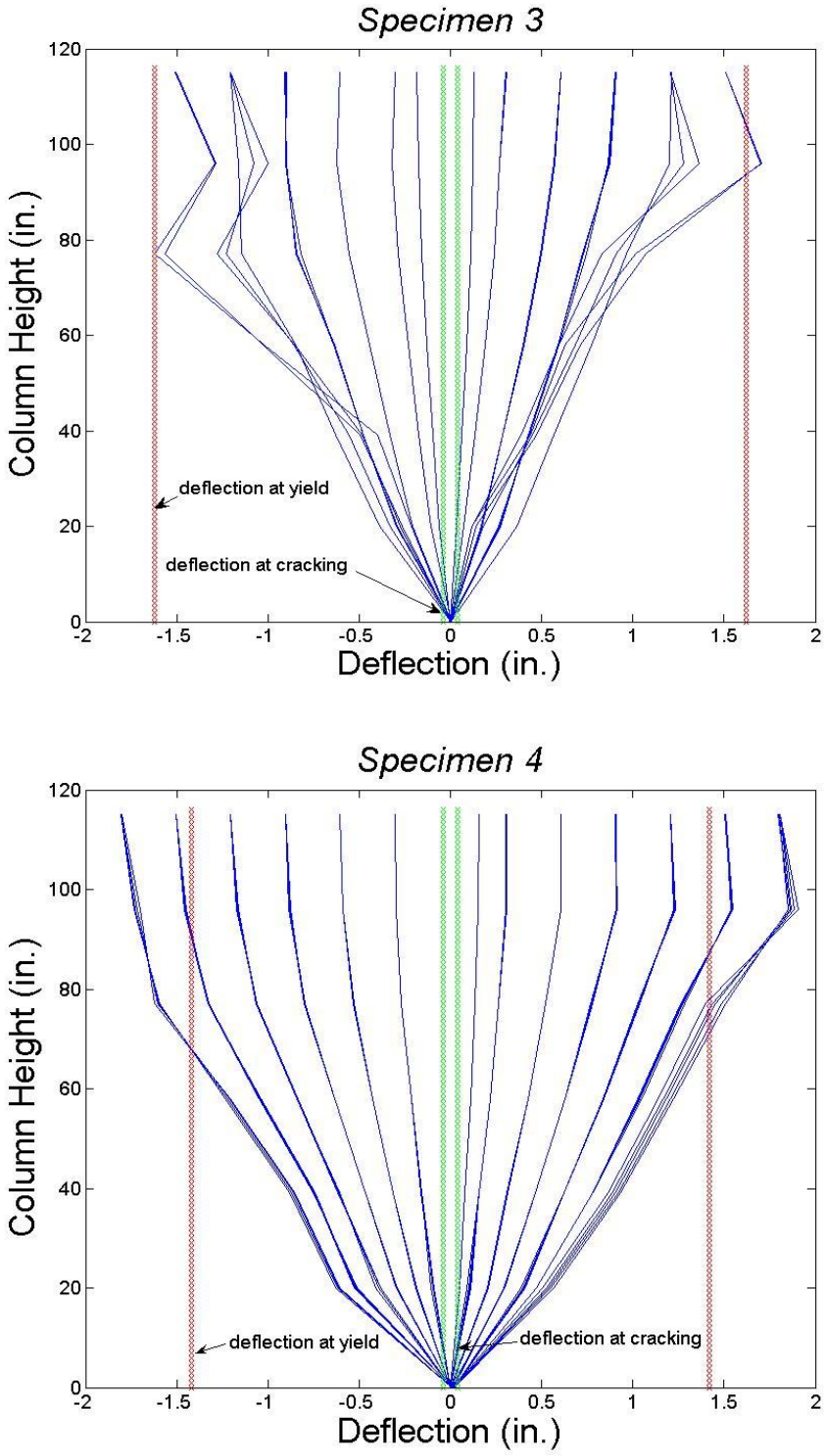

Figure 3.24: Deflection profiles (a) specimen 3 (b) specimen 4

3.6.1 Deflection Components by Krypton System

The following describes the analysis of distributed deformation measurements made using the Krypton System at the bottom of the column, in the maximum moment region. Results are for a discrete grid of points separated by 3.5-in. in the horizontal direction and by 4-in. in the vertical direction, as shown in Fig. 2.20. The grid was placed at this location with the intent of capturing the effect of damage on the deformation components. All analyses described below refer to the displacement at the top of the grid, which was located 17 in. from the base of the column. Deflection components for each set of readings were calculated using the method presented by Matamoros (1999).

Tables 3.5, 3.6(a) and (b) show the calculated components of the displacement measured with the Krypton system. The displacements recorded during the first two cycles were negligible for both specimens 3 and 4. While the drift ratio of specimen 3 ranged between 0 and 1% the largest deflection component inferred from the Krypton system readings was the deformation related to flexure. As cycling continued at drift ratios exceeding 1%, inferred shear and slip deformations became a larger percentage of the total deflection. At a drift ratio of 1%, the inferred shear deformation doubled, likely as a result of the formation of a dominant shear crack across the specimen's cross-section. At the point of axial failure, the deformation components related to shear and flexure were nearly equal, as can be observed in Table 3.5. The Krypton measurements support visual observations that the deformation component due to shear increased with the width of the shear cracks

during the larger displacement ramps. Figure 3.25 graphically shows the relative contribution of the components related to shear and flexure to the total deformation of the specimen.

In the case of specimen 4, the inferred deformation components related to shear and flexure were approximately equal in magnitude until the set of cycles with a maximum drift ratio of 1.25%. After this level of deformation was exceeded, measured deformations related to shear became an increasingly larger percentage of the total deformations. During the set of cycles with a peak drift ratio of 1.25% to 1.50%, deformations related to shear became almost 1.75 times the deformations related to flexure. During the latter displacement ramps, deformations related to shear were significantly larger during positive displacement cycles, indicating that greater shear damage was incurred while loading in that direction. Consistent with expectations, the relatively equal magnitude of the deformation components while cycling under 1.25% drift ratio is consistent with the larger amount of transverse reinforcement, and the greater shear strength of specimen 4 compared with specimens 1, 2, and 3.

Specimen 4 had a larger amount of transverse reinforcement and lower axial load demand than specimens 1, 2, and 3. It was also subjected to a larger number of cycles at each displacement level, six rather than three, which caused greater damage to the concrete. For both of these reasons, the total lateral deformation in the maximum moment region recorded with the Krypton system prior to axial failure (0.2 in.) was nearly twice of that measured in specimen 3. Although the core of the

column remained largely intact throughout the test, the effect of shear cracks on the lateral deformation became increasingly dominant in later cycles.

Table 3.5: Inferred deflection components for Specimen 3.

		Deflection Component				
Ramp	**Drift Ratio**	**Slip**	**Shear**	**Flexure**	**Rigid Body**	**Total**
	(%)	**(in.)**	**(in.)**	**(in.)**	**(in.)**	**(in.)**
1	0.50	0.015	0.004	0.006	0.006	0.03
2	-0.50	-0.018	-0.001	-0.008	-0.008	-0.04
3	0.50	0.019	0.003	0.008	0.007	0.04
4	-0.50	-0.018	-0.001	-0.008	-0.008	-0.04
5	0.50	0.018	0.003	0.008	0.007	0.04
6	-0.50	-0.018	-0.001	-0.009	-0.007	-0.04
7	0.75	0.034	0.006	0.017	0.014	0.07
8	-0.75	-0.034	-0.007	-0.018	-0.013	-0.07
9	0.75	0.034	0.007	0.017	0.013	0.07
10	-0.75	-0.034	-0.007	-0.017	-0.013	-0.07
11	0.75	0.033	0.008	0.017	0.013	0.07
12	-0.75	-0.034	-0.008	-0.017	-0.014	-0.07
13	1.00	0.045	0.015	0.024	0.016	0.10
14	-1.00	-0.046	-0.015	-0.024	-0.016	-0.10
15	1.00	0.041	0.018	0.025	0.016	0.10
16	-1.00	-0.045	-0.017	-0.024	-0.014	-0.10
17	1.00	0.041	0.018	0.025	0.017	0.10
18	-1.00	-0.045	-0.018	-0.024	-0.014	-0.10
19	1.25	0.052	0.027	0.032	0.018	0.13
20	-1.25	-0.046	-0.027	-0.024	-0.018	-0.12

Table 3.6(a): Inferred deflection components for Specimen 4

Ramp	Drift Ratio	Deflection Component						Ramp	Drift Ratio	Deflection Component					
		Slip	Shear	Flexure	Rigid Body	Total				Slip	Shear	Flexure	Rigid Body	Total	
	(%)	(in.)	(in.)	(in.)	(in.)	(in.)			(%)	(in.)	(in.)	(in.)	(in.)	(in.)	
1	0.13	0.000	0.000	0.000	0.000	0.00		19	0.50	0.035	0.009	0.011	0.017	0.07	
2	-0.13	0.000	0.000	0.000	0.000	0.00		20	-0.50	-0.035	-0.008	-0.006	-0.018	-0.07	
3	0.25	0.020	0.004	0.005	0.012	0.04		21	0.50	0.035	0.009	0.011	0.017	0.07	
4	-0.25	-0.020	-0.003	-0.004	-0.008	-0.04		22	-0.50	-0.036	-0.008	-0.006	-0.018	-0.07	
5	0.25	0.020	0.004	0.006	0.012	0.04		23	0.50	0.035	0.009	0.011	0.018	0.07	
6	-0.25	-0.020	-0.003	-0.004	-0.008	-0.04		24	-0.50	-0.036	-0.008	-0.006	-0.018	-0.07	
7	0.25	0.020	0.004	0.005	0.012	0.04		25	0.50	0.035	0.009	0.011	0.018	0.07	
8	-0.25	-0.020	-0.003	-0.004	-0.008	-0.04		26	-0.50	-0.035	-0.008	-0.006	-0.018	-0.07	
9	0.25	0.020	0.004	0.005	0.012	0.04		27	0.75	0.049	0.015	0.014	0.023	0.10	
10	-0.25	-0.021	-0.003	-0.004	-0.008	-0.04		28	-0.75	-0.049	-0.014	-0.014	-0.023	-0.10	
11	0.25	0.020	0.004	0.005	0.012	0.04		29	0.75	0.049	0.015	0.014	0.023	0.10	
12	-0.25	-0.021	-0.003	-0.004	-0.008	-0.04		30	-0.75	-0.049	-0.014	-0.015	-0.023	-0.10	
13	0.25	0.020	0.004	0.005	0.012	0.04		31	0.75	0.049	0.015	0.014	0.023	0.10	
14	-0.25	-0.021	-0.003	-0.004	-0.008	-0.04		32	-0.75	-0.049	-0.014	-0.015	-0.023	-0.10	
15	0.50	0.034	0.009	0.011	0.017	0.07		33	0.75	0.049	0.015	0.014	0.023	0.10	
16	-0.50	-0.035	-0.008	-0.006	-0.017	-0.07		34	-0.75	-0.049	-0.014	-0.015	-0.023	-0.10	
17	0.50	0.034	0.009	0.011	0.017	0.07		35	0.75	0.049	0.015	0.014	0.023	0.10	
18	-0.50	-0.035	-0.008	-0.006	-0.018	-0.07		36	-0.75	-0.047	-0.014	-0.015	-0.023	-0.10	

Table 3.6(b): Inferred deflection components for specimen 4

		Deflection Component							Deflection Component				
Ramp	Drift Ratio	Slip	Shear	Flexure	Rigid Body	Total	Ramp	Drift Ratio	Slip	Shear	Flexure	Rigid Body	Total
	(%)	(in.)	(in.)	(in.)	(in.)	(in.)		(%)	(in.)	(in.)	(in.)	(in.)	(in.)
37	0.75	0.045	0.015	0.014	0.022	0.10	56	-1.25	-0.075	-0.037	-0.029	-0.034	-0.18
38	-0.75	-0.043	-0.014	-0.015	-0.023	-0.10	57	1.25	0.073	0.035	0.024	0.032	0.16
39	1.00	0.060	0.025	0.019	0.027	0.13	58	-1.25	-0.075	-0.037	-0.029	-0.034	-0.18
40	-1.00	-0.065	-0.024	-0.023	-0.029	-0.14	59	1.25	0.073	0.035	0.024	0.032	0.16
41	1.00	0.060	0.025	0.019	0.027	0.13	60	-1.25	-0.075	-0.037	-0.029	-0.033	-0.17
42	-1.00	-0.065	-0.024	-0.023	-0.029	-0.14	61	1.25	0.085	0.043	0.027	0.036	0.19
43	1.00	0.060	0.025	0.019	0.027	0.13	62	-1.25	-0.090	-0.047	-0.035	-0.033	-0.21
44	-1.00	-0.065	-0.024	-0.023	-0.029	-0.14	63	1.50	0.082	0.047	0.027	0.037	0.19
45	1.00	0.060	0.025	0.019	0.027	0.13	64	-1.50	-0.088	-0.043	-0.034	-0.033	-0.20
46	-1.00	-0.065	-0.025	-0.023	-0.029	-0.14	65	1.50	0.082	0.047	0.027	0.037	0.19
47	1.00	0.055	0.025	0.019	0.027	0.13	66	-1.50	-0.086	-0.043	-0.033	-0.033	-0.20
48	-1.00	-0.065	-0.025	-0.023	-0.029	-0.14	67	1.50	0.082	0.047	0.027	0.037	0.19
49	1.00	0.053	0.025	0.019	0.026	0.12	68	-1.50	-0.085	-0.043	-0.032	-0.033	-0.19
50	-1.00	-0.060	-0.025	-0.023	-0.028	-0.14	69	1.50	0.078	0.045	0.026	0.037	0.19
51	1.25	0.073	0.035	0.024	0.032	0.16	70	-1.50	-0.083	-0.042	-0.031	-0.031	-0.19
52	-1.25	-0.075	-0.035	-0.029	-0.034	-0.17	71	1.50	0.075	0.045	0.026	0.034	0.18
53	1.25	0.073	0.035	0.024	0.032	0.16	72	-1.50	-0.080	-0.042	-0.030	-0.030	-0.18
54	-1.25	-0.075	-0.035	-0.029	-0.034	-0.17	73	1.50	0.078	0.045	0.026	0.035	0.18
55	1.25	0.073	0.035	0.024	0.032	0.16	74	-1.50	-0.075	-0.040	-0.025	-0.030	-0.17

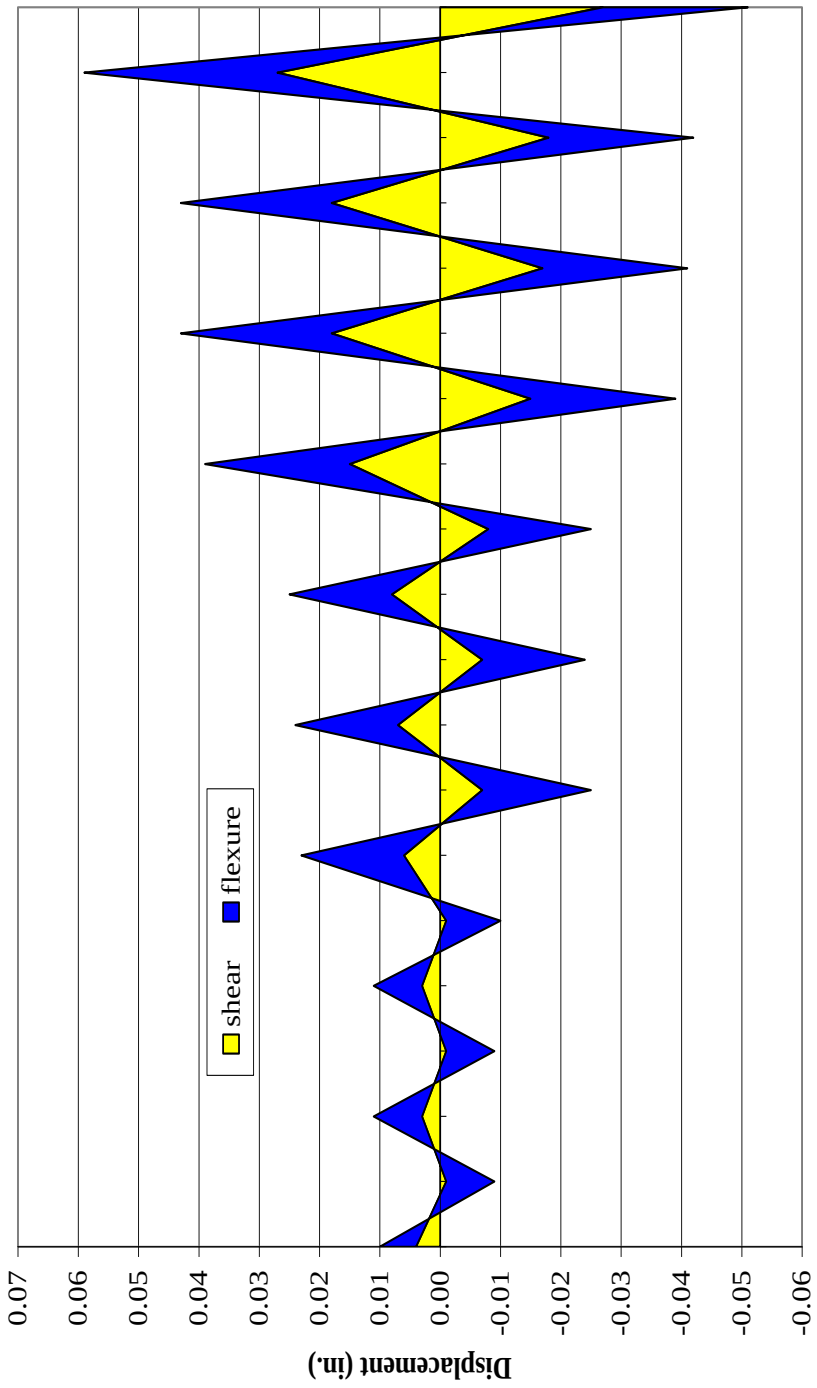

Figure 3.25: Specimen 3 measured deflection components

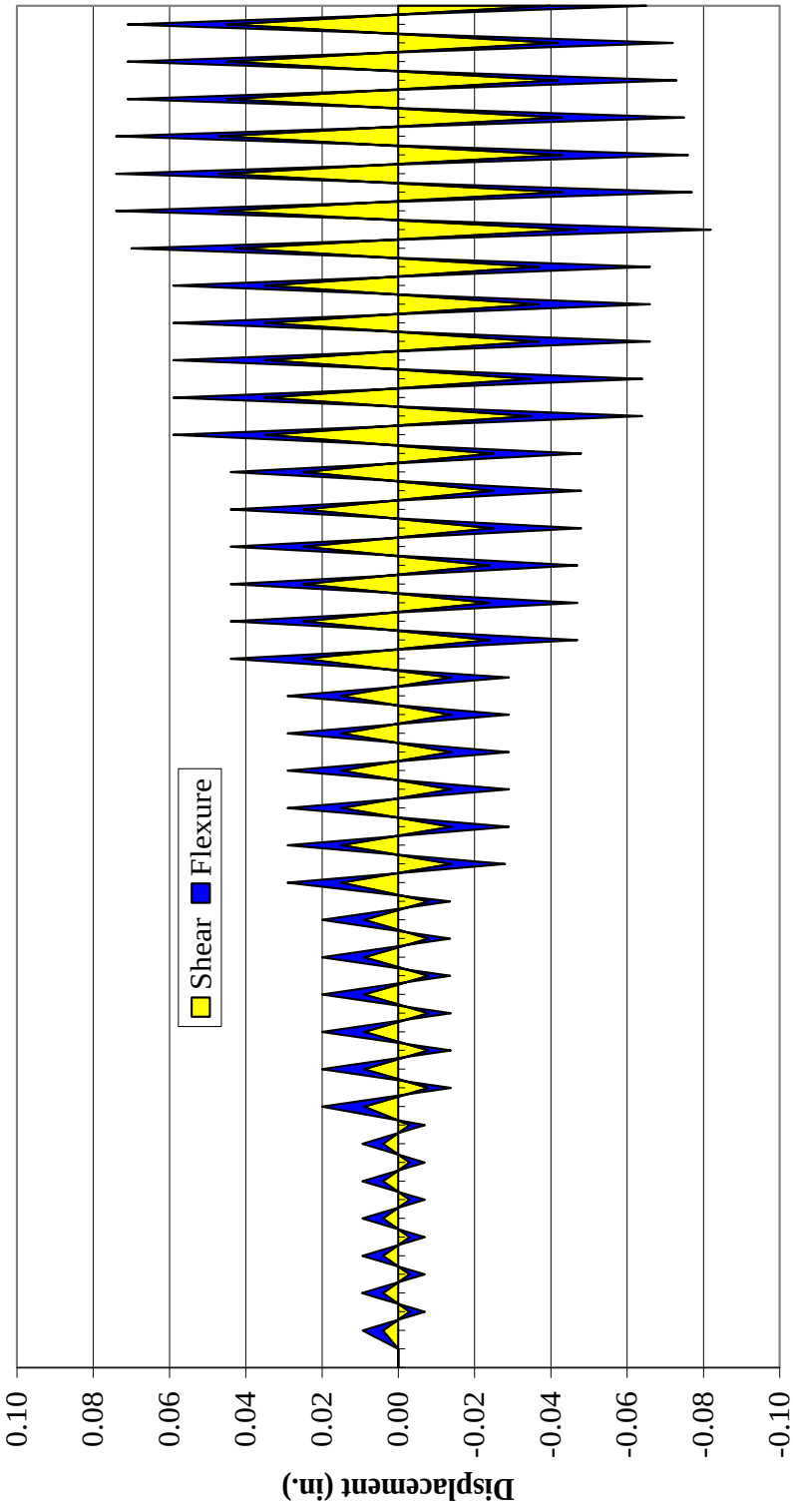

Figure 3.26: Specimen 4 measured deflection components

3.7 Bar Strain Readings

As described in the experimental program, strain gages were attached to both the longitudinal and transverse reinforcing steel. Throughout the following discussion, strain gages are referenced following the designations outlined in the experimental program section (Fig. 2.14). Based on tension tests, the measured yield strains for the longitudinal reinforcement in columns 3 and 4 were 2240 microstrain (#10 longitudinal bars) and 2210 microstrain (#9 longitudinal bars), respectively.

Figure 3.27 shows readings from selected strain gages attached to the longitudinal reinforcement of column 3. Strain gages LM4 and RM4 were located at the top of the column, approximately 6 in. below the interface between the cap beam and the column. Both gages indicate that yielding of the longitudinal reinforcement in tension did not occur prior to axial failure. However, readings show that both of the aforementioned gages as well as RM4 experienced significant compressive strains, indicating that localized buckling likely occurred prior to axial failure. This is consistent with the large expansion of the core that was measured with displacement transducers, which came as a result of yielding of the transverse reinforcement and possibly anchorage failure of the hoops.

Readings from strain gage LF5, located approximately 11 inches down from the interface between the column and the cap beam, are consistent with those of gages LM4 and RM4, although the magnitude of the compressive strains was significantly lower at this location. Measurements from gage LM7, located approximately 6 in. up

from the interface of the bottom beam and the column, suggest that the specimen was just reaching the yield point when axial failure took place.

Figure 3.28 shows transverse strain gage readings for column 3. All three gages show readings taken from the top of the column, at the location of failure. Transverse gage H1LB, located at the first hoop, approximately 12 in. below the cap beam, indicates that yielding occurred during the positive displacement peaks corresponding to 1.00% drift ratio, and all three of the gages indicate that larger strains were reached during the positive displacement cycles. These readings are consistent with the observed column behavior. The column experienced axial failure at the positive displacement cycle likely as a result of yielding and/or anchorage failure of the hoop.

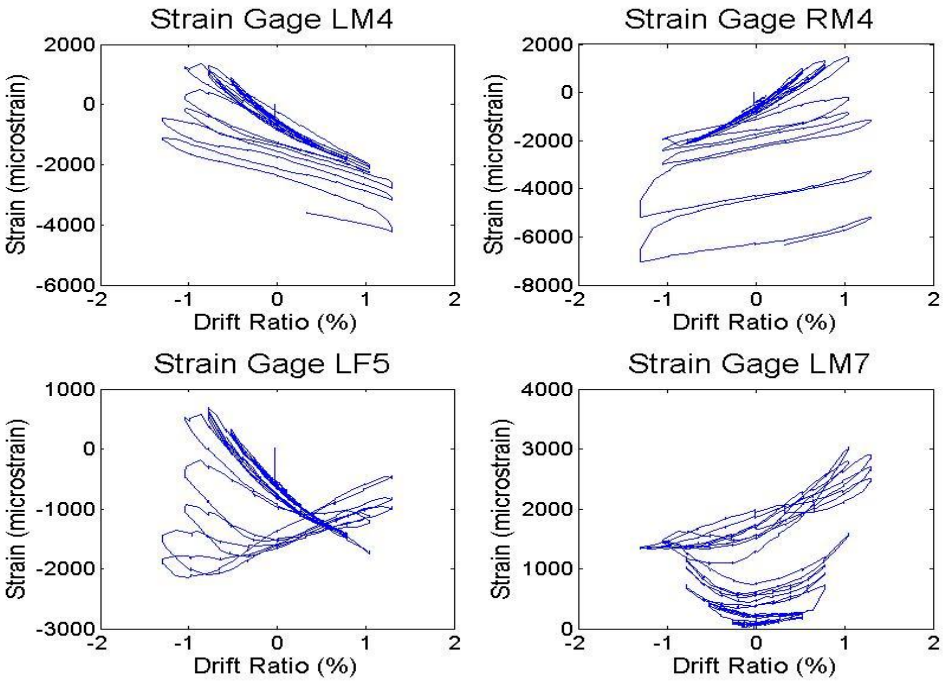

Figure 3.27: Measured longitudinal reinforcement strains for column 3

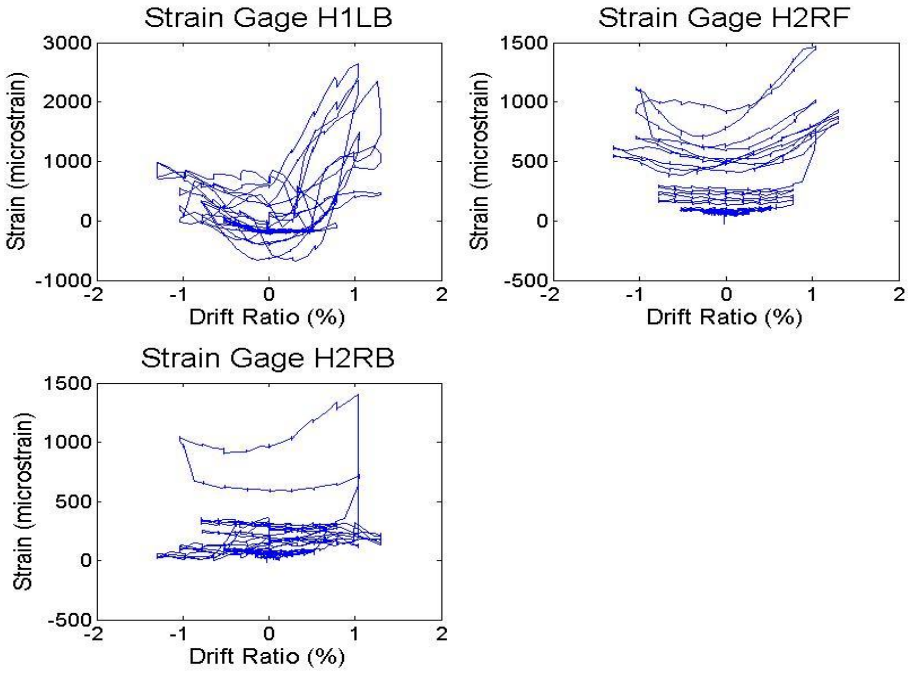

Figure 3.28: Measured transverse reinforcement strains for column 3

Figure 3.29 shows readings from strain gages attached to the longitudinal reinforcement of column 4. Longitudinal gages LM3, located at the interface between the column and the cap beam, and RM5, located approximately 11 in. below the cap beam, clearly show that the longitudinal reinforcement in column 4 experienced significant yielding prior to axial failure. Both strain gages indicate that larger strains were experienced while laterally displacing the column in the negative direction, which is consistent with the location of the bars and the direction of loading. Readings from gages RF7 and LF7 (Fig. 3.29), located approximately 6 in. above the bottom beam, are consistent with those obtained from gages at the top of the column.

Figure 3.30 shows readings from strain gages attached to the transverse reinforcement of column 4. Gages H2LF and H2RB were located at the top of the column, approximately 12 in. below the cap beam. Both gages clearly show that yielding occurred prior to axial failure. All gages shown in Fig. 3.30, including those gages located at the bottom of the column, indicate that larger stresses were occurring during the positive displacement cycles.

Gages H4LF and H3LB, located at the bottom of the column also indicate that yielding occurred.

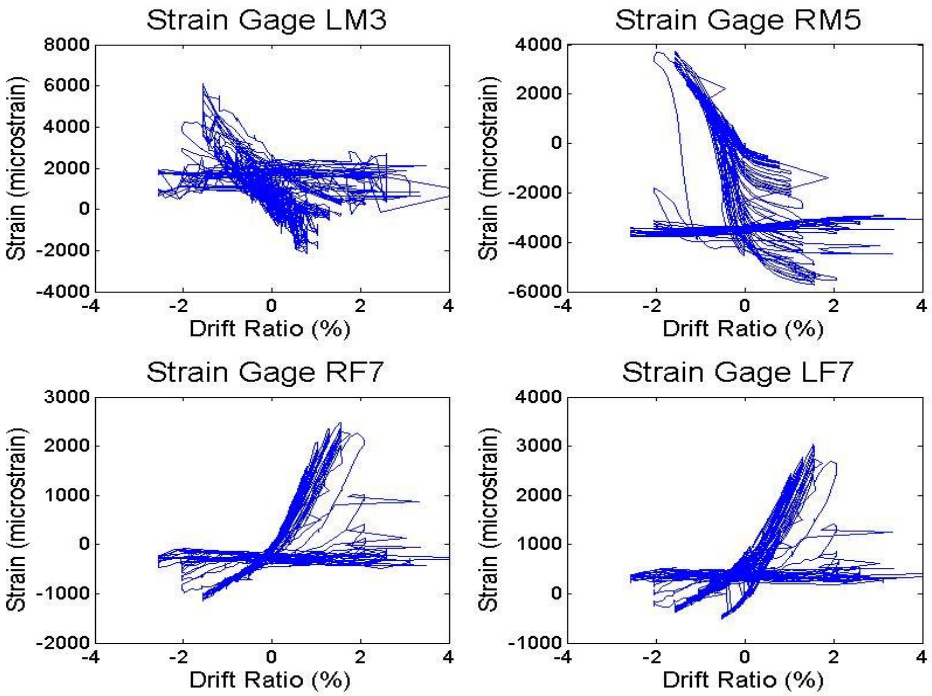

Figure 3.29: Measured longitudinal reinforcement strains for column 4

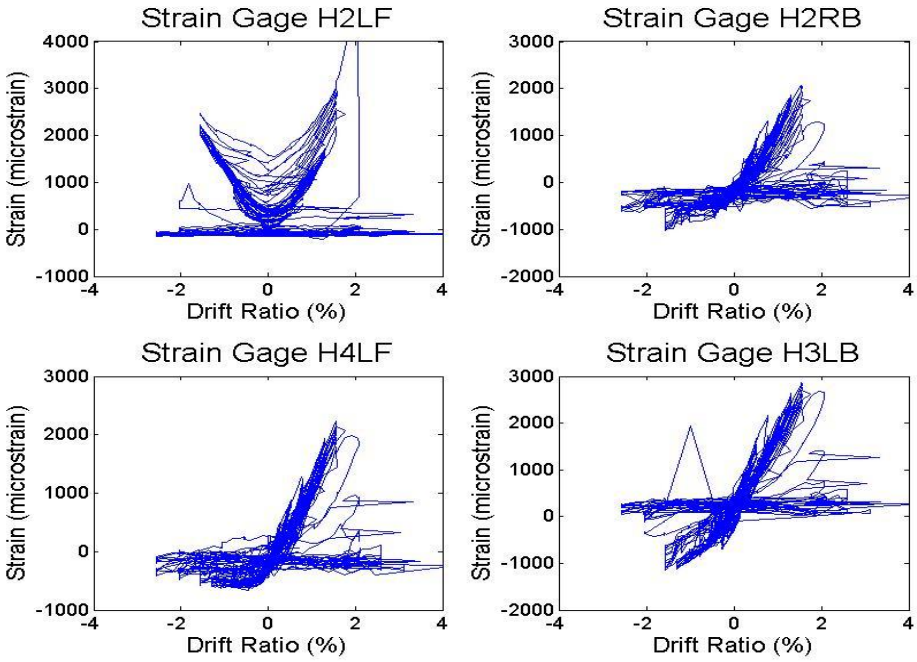

Figure 3.30: Measured transverse reinforcement strains for column 4

3.8 Shear Strength

Shear strength was calculated using design equations in the ACI 318-08 Building Code (2008). The shear force carried by the concrete was calculated using Eq. 11-4 of the ACI 318-08 Building Code (2008), reproduced here as Eq. (3.10). The shear strength was calculated as the sum of the contributions of the concrete and the steel, in accordance with Eq. 11-15 and 11-2 of the ACI Code, shown here as Eq. (3.11) and (3.12), respectively. Table 3.7 shows the maximum shear force measured during both tests, the calculated shear strength based on ACI-318 equations, and the estimated shear force required to cause yielding of the longitudinal reinforcement.

$$V_c = 2 \cdot \left(1 + \frac{P}{2000 A_g} \right) \cdot \sqrt{f'_c} \cdot b \cdot d \tag{3.10}$$

$$V_s = \frac{A_{st} \cdot f_{yt} \cdot d}{s} \tag{3.11}$$

$$V_n = V_c + V_s \tag{3.12}$$

where:

V_c = shear force carried by concrete (lb.)

P = applied axial force (lb.)

A_g = gross cross-sectional area of the column (in^2)

f'_c = concrete compressive strength (psi)

b = column width (in.)

d = effective depth (in.)

V_s = shear force carried by reinforcing steel (lb.)

A_{st} = area of the transverse reinforcement (in^2)

f_{yt} = yield stress of the reinforcement (psi)

s = spacing of transverse reinforcement (in.)

Table 3.7: Calculated and measured shear strength

Column	**Axial Load *(kips)***	***V_{test}* *(kips)***	***V_c* *(kips)***	***V_s* *(kips)***	***V_n* *(kips)***	***V_p* *(kips)***	***V_n/V_p***
3	500	70.3	49.5	10.2	59.7	80	0.75
4	150	70.3	35.6	30.7	66.3	68	0.98

Table 3.7 shows values of maximum measured shear force and computed shear strengths based on measured material properties. For both specimens 3 and 4, the maximum measured shear force was higher than the calculated strength based on measured material properties, indicating that strength values calculated with Eq. 3.10 through 3.12 were conservative. Experimental measurements show that for column 3, the column experienced shear failure prior to yielding of the longitudinal reinforcement due to flexure, so the ratio of V_n to V_p was approximately 1. Test measurements suggest that Eq. 3.10 though 3.12 resulted in estimates of strength that were 12% below observed values.

The maximum shear force in column 4 was also greater than the shear strength calculated using measured material properties and design Eq. 3.10 through 3.12. In the case of column 4, strain gage and moment-curvature measurements

indicate that the longitudinal reinforcement did yield prior to shear failure, so contrary to the calculations in Table 3.7, the specimen was not shear critical.

3.9 Elwood-Moehle Drift Ratio at Axial Failure

The model developed by Elwood and Moehle (2005) was used to calculate the drift ratio at axial failure for both columns. Table 3.1 shows the calculated drift ratio at axial failure for both columns for all failure events. Column 3 experienced the first axial load failure event at the positive peak of the first displacement cycle at a drift ratio of 1.12%. Afterward, Column 3 was able to maintain an axial load of 400 kips for a short period of time as cycling continued down to zero displacement. After the second axial failure event, the column stabilized at zero lateral displacement, and an axial load of 300 kips was maintained through the second cycle at 1.5% drift. The column maintained a final axial load of 150 kips until the first quarter cycle with a maximum drift ratio of 2%, after which the test was terminated. Figure 3.31(a) shows the observed drift ratios at axial failure for column 3. The failure envelope provided by the Elwood-Moehle model is presented as a reference.

Column 4 lost its initial axial load carrying capacity while loading to the first negative peak of the displacement cycle with a maximum drift ratio of 3 %. The column was able to sustain a post-failure axial load of 150 kips while attempting to move to the positive peak of the cycle with a maximum drift ratio of 3 %. A sequence of axial failure events ensued while loading at this drift level, until the axial load was reduced to 50 kips. Figure 3.31(b) shows the observed drift ratios at axial failure for

Column 4 and the corresponding calculated values according to the Elwood-Moehle Model (2005).

Observed drift ratios at axial failure did not match accurately those calculated using the Elwood-Moehle model (2005) for either of the two columns. In the case of Column 3, the Elwood-Moehle model resulted in a conservative estimate of drift at axial failure of 0.9%, while the observed value was 1.5%. It is important to note that for the case of Column 1 tested by Matchulat (2009), the observed drift at axial failure was 1.07%, much closer to the estimate provided by the Elwood-Moehle model. The only difference between Columns 1 and 3 was the longitudinal reinforcement ratio, which was approximately 2.5% for Column 1 and 3% for Column 3. Because the Elwood-Moehle model does not take into account the effect of the longitudinal reinforcement ratio, and Column 3 had a larger longitudinal reinforcement ratio than column 1, the increased capacity is very likely a result of the effect of the longitudinal reinforcement.

Column 4 lost initial axial load capacity at a drift ratio of 3 %, well before the calculated value of of 4.89%. For comparison, there were two other specimens tested by Sezen (2000) which were similar to column 4, with the only difference being the loading protocol. Those were specimens 2CLD12, which had three cycles per drift ratio, and specimen 2CLD12M, which underwent 3 cycles with a maximum drift ratio of 0.25%, 3 cycles with a maximum drift ratio of 0.5%, and it was subsequently loaded monotonically until failure. The drift ratios at axial failure were 5.66% and 6.47%, for specimens 2CLD12 and 2CLD12M, respectively. These results suggest

that in flexure-critical specimens, those in which yielding of the longitudinal reinforcement takes place prior to shear failure, there is an inverse relationship between the number of cycles per drift level and the drift ratio at axial failure.

Both columns experienced secondary failure events at drift ratios lower than the values calculated with the Elwood-Moehle model. In fact, all axial failure events that occurred after the initial loss of axial capacity did so without any further increase in the drift ratio. In both cases the column dropped to a residual axial capacity of approximately 150 kips, which was maintained through a final compression test.

Results from these two tests suggest that the best alternative for modeling the behavior of columns after axial failure is not to follow the surface of the failure model, but to assume that the lateral stiffness drops to zero and that the axial load capacity of the column drops to a residual value of approximately 20% of $f'_c A_g$. The Elwood-Moehle failure model does not take into account the damage caused by axial failure, and as a result, is not suited to calculate the drift ratio expected for the later failure events.

Table 3.8: Calculated drift ratios at axial failure according to the Elwood-Moehle model

Specimen	Initial Axial Load (kips)	Calculated Drift Ratio at Axial Failure (%)	Reduced Axial Load (kips)	Calculated Drift Ratio at Axial Failure (%)
3	500	0.90	200	2.00
4	150	4.89	90	6.21

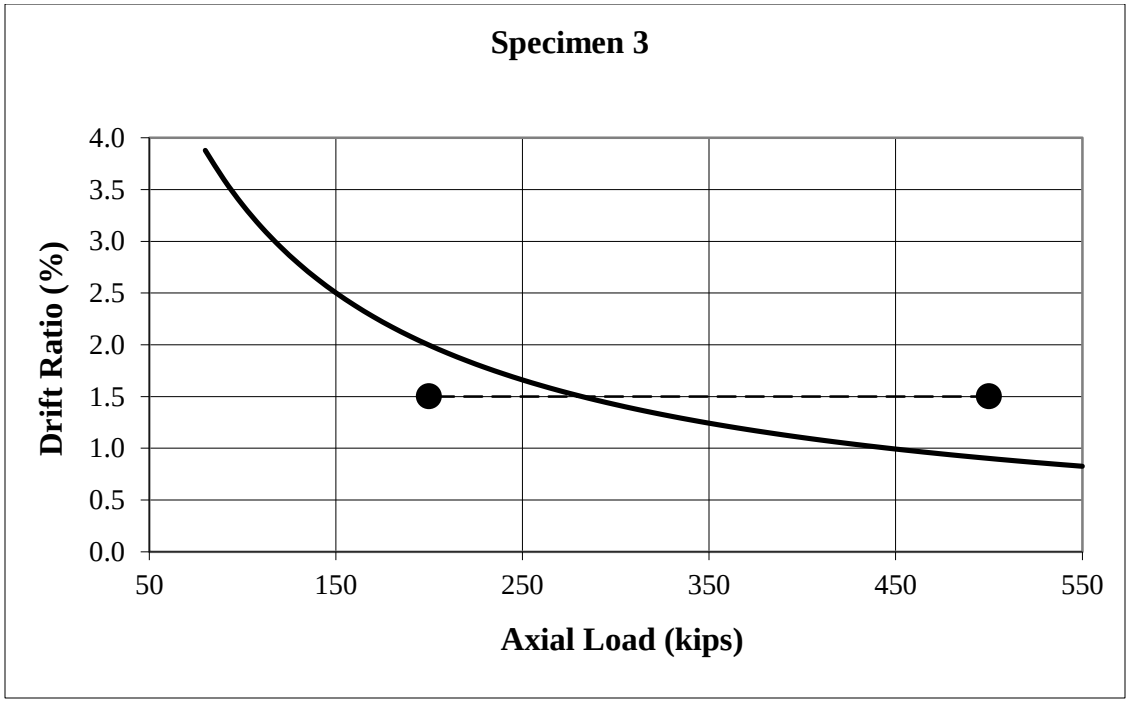

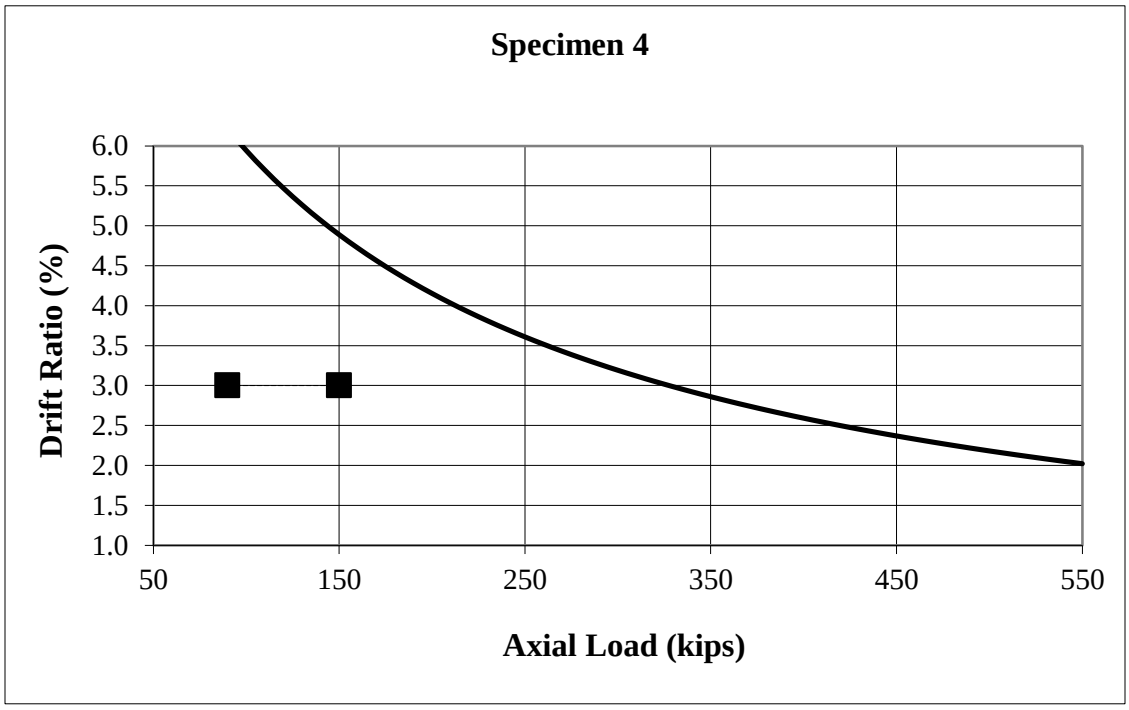

Figure 3.31: Calculated failure envelopes and observed drift ratios at axial failure for (a) specimen 3 (b) specimen 4

3.10 Axial Capacity Longitudinal Reinforcement

Two different failure patterns have been observed with the axial failure of reinforced concrete columns subjected to lateral load reversals (Elwood, 2005). It was suggested by Elwood that the type of failure shape depends on the ratio of the axial capacity of the longitudinal reinforcement to the applied axial load. (Elwood et al., 2005, Matchulat, 2009). Specifically, Elwood observed that columns with axial loads greater than the axial capacity of the longitudinal reinforcement experienced failure shapes that were indicative of buckling, as observed in Fig. 3.9 for column 3. Columns with loads less than the axial capacity of the longitudinal reinforcement have an S-shaped failure pattern, which indicate that the plastic capacity of the bars was exceeded by the combined effects of axial load and bending. Columns 1 and 3 tested by Matchulat (2009) and Woods, respectively, had a mushroom-shape appearance after failure, which is indicative of buckling failure of the reinforcement. Columns 2 and 4 had in an S-shaped failure pattern, indicating that the plastic capacity had been exceeded. The primary difference between the two pairs of aforementioned specimens was the ratio of axial load to axial capacity of the longitudinal reinforcement capacity.

Elwood (2005) developed a set of equations to calculate the axial capacity of the longitudinal reinforcement, $P_{s\text{-}max}$, which are shown in the following Eq. (3-13).

$$\frac{P_s}{A_s f_y} = \frac{\frac{d_b}{L}}{0.75\pi\frac{\Delta}{L} + \frac{d_b}{L}} \qquad \text{If } P<A_s f_y \qquad (3.13)$$

$$= \frac{\frac{d_b}{L}}{0.75\pi\frac{\Delta}{L} + \frac{d_b}{L}} < 0.1\frac{\pi^2 E_t I_{bar} n_{bars}}{s^2 A_s f_y} \qquad \text{If } P \geq A_s f_y$$

Where:

$A_s f_y$ = axial capacity of the longitudinal reinforcement (kips)

d_b = diameter of longitudinal bars (in.)

L = clear height of column (in.)

Δ = column displacement at axial failure (in.)

E_t = tangent modulus of reinforcing steel (ksi)

I_{bar} = moment of inertia of longitudinal bar (in^4)

n_{bars} = number of longitudinal bars

s = spacing of transverse reinforcement (in.)

P_s = axial capacity of the longitudinal bars (kips)

The first Eq. in 3.13 represents the case in which the axial load demand is below the axial capacity of the reinforcement, $P<A_s f_y$, and failure due to yielding of the longitudinal reinforcement under combined bending and axial load is expected to be the controlling factor. For the second case, the capacity is limited by the plastic buckling capacity of the longitudinal reinforcement, $P \geq A_s f_y$. The two columns

referenced in this report, columns 3 and 4, had axial loads less than the axial capacity of the reinforcing bars.

In order to determine the axial capacity of the longitudinal bars, Elwood (2005) suggested the following assumptions. The effective buckling length was assumed to be a function of the spacing of the transverse reinforcement and bounded by support conditions between a fully-fixed and pinned connection. For consistency, an effective length of 0.8*s* was used in this report, the same used in the analyses performed by Elwood (2005) and Matchulat (2009). Results for an effective length of 2*s* have also been calculated and provided in Table 3.9. Also, it was suggested by Elwood (2005) that the tangent modulus be estimated as $0.07E_s$, an assumption that is used in this report.

For Column 3, the results obtained using Eq. (3.13) suggest that buckling capacity was the limiting factor of the two failure modes. The axial load demand was 96% of the yield capacity of the reinforcement, and the axial load carried by the reinforcement at failure was approximately 20% of the axial load. Given the large percentage of the axial load carried by the concrete at failure, it was expected that failure be sudden and brittle, and because the axial load was so close to the yield strength of the reinforcement, it is expected that the reinforcement would buckle soon after shear failure.

Based on the Elwood model (2005), Column 4 was expected to have longitudinal reinforcement failure that was controlled by the plastic capacity of the reinforcement. In this case, the Elwood model suggests that the percentage of the

axial load carried by the reinforcement at axial failure was 33%, and the ratio of axial load to yield strength of the reinforcement was 25%. Table 3.9 shown below provides a comparison between plastic axial and buckling capacities.

Table 3.9: Axial capacity of longitudinal reinforcement for specimens 3 and 4

Specimen	**Axial Load (kips)**	**Gross Axial Capacity, A_sf_y (kips)**	**Plastic Axial Capacity (kips)**	**Buckling Capacity, 0.8s (kips)**	**Buckling Capacity, 2s (kips)**
3	500	660	194	99	16
4	150	512	65	137	22

Table 3.10: Axial Capacity of longitudinal reinforcement

Specimen	Axial Load (kips)	Gross Axial Capacity, $A_s f_y$ (kips)	Plastic Axial Capacity (kips)	Buckling Capacity (kips)
Woods (2010)				
3	500	660	194	99
4	150	512	65	137
Matchulat (2009)				
1	500	512	150	61
2	340	512	127	61
Lynn (2001)				
3CLH18	120	488	59	99
2CLH18	120	303	33	38
3SLH18	120	488	59	99
2SLH18	120	303	27	38
2CMH18	340	303	79	38
3CMH18	340	488	88	99
3CMD12	340	488	88	222
3SMD12	340	488	88	222
Sezen (2000)				
2CLD12	150	512	41	137
2CHD12	600	512	92	137
2CVD12	Variable	512	61	137
2CLD12M	150	512	41	137

CHAPTER 4: SUMMARY AND CONCLUSIONS

4.1 Summary

Two, full-scale reinforced concrete columns subjected to cyclic lateral loads were tested until failure. Column geometry, concrete and steel properties, and loading protocol were set to represent columns found in buildings constructed prior to 1971 earthquake codes. A target concrete compressive strength of 3000 psi as well as reinforcing steel conforming to ASTM A615 for transverse steel and ASTM A706 for longitudinal steel were used in both columns. Both specimens were cast in the horizontal position at the Structural Testing Laboratory at the University of Kansas. Testing and instrumentation was performed at the NEES MAST Laboratory at the University of Minnesota. The two specimens had identical dimensions. The parameters varied between the two specimens were axial load level, longitudinal steel ratio, and transverse steel ratio. Specimen 3 contained No. 10 longitudinal bars with No. 3 hoops spaced at 18-inch centers and a 500 kip axial compressive load. Specimen 4 contained No. 9 longitudinal bars with two No. 3 hoops spaced at 12-inch centers, one standard hoop in addition to a diamond hoop. A 150 kip axial compressive force was applied to specimen 3. String potentiometers, Linear Variable Displacement Transformers (LVDTs), strain gages, and load cells were used to measure column behavior during testing. Further information about test setup and procedures can be found in Chapter 2 of this report.

Specimen 3 referenced in this report and Specimen 1 referenced by Matchulat (2009) were compared to evaluate the effect of longitudinal steel ratio. Both columns

were identical except the longitudinal reinforcement ratio, which was 3% and 2.5% for specimens 3 and 1, respectively. Both columns were subjected to an applied axial compressive force of 500 kips. The calculated drift ratio at axial failure calculated with the Elwood-Moehle model for both columns was 0.90%. Specimen 1 tested by Matchulat (2009) had a simultaneous shear and axial failure after sustaining a drift ratio of 1 %. Specimen 3 experienced shear failure after sustaining a maximum drift ratio of 1.1% and axial failure after a maximum drift ratio of 1.6%. While specimen 1 experienced simultaneous shear and axial failure, specimen 3 failed first in shear, followed by axial failure at a larger drift demand. Unlike specimens 1 and 2 by Matchulat (2009) loss of lateral stiffness in specimen 3 did not immediately result in axial failure. Both specimens 1 and 3 were near yield at the time of axial failure.

Specimen 4 was compared with two specimens previously tested by Sezen (2000) in which different loading protocols were used to study the effect of displacement history on the drift ratio at axial failure. All three specimens had the same cross section, axial load demand, and longitudinal and transverse reinforcement configurations. Specimen 2CLD12M by Sezen (2000) was tested using three displacement cycles per drift level for demands below yield and then monotonic loading until axial failure. Specimen 2CLD12 by Sezen (2000) was tested using three displacement cycles at each drift level. Specimen 4 of this report was tested using six displacement cycles at each drift level.

Specimens 2CLD12M and 2CLD12 reached drift ratios at axial failure of 5.1% and 5.0%, respectively. Specimen 4 of this report reached a maximum drift

ratio of 3.1% before axial failure. Specimens 2CLD12M and 2CLD12 reached drift ratios of 2.8% and 2.6% at shear failure, respectively. Specimen 4 reached a maximum drift ratio of 2% before shear failure. All three specimens experienced yielding of the longitudinal reinforcement prior to axial load failure, and all three experienced shear failure prior to axial failure.

4.2 Conclusions

4.2.1 Specimen 3

1. Longitudinal reinforcement ratio affected drift ratio at axial failure. Larger longitudinal reinforcement ratio resulted in a larger drift ratio at axial failure.
2. Longitudinal reinforcement ratio affected failure occurrences. Specimen 1 experienced simultaneous axial and shear failures, while specimen 3 did not. Specimen 3 was able to withstand axial load through cycling until the next larger drift demand. Lateral load loss did not immediately affect axial load capacity.
3. Neither specimen 1 or 3 can be said to have reached yield prior to axial failure; however, both specimens were just at the point of yield as indicated by instrumentation. The increase in longitudinal reinforcement ratio did not result in yielding.

4. Specimen 1 correlated well with the Elwood-Moehle axial failure model. However, specimen 3 did not, likely as a result of the longitudinal reinforcement ratio.
5. Longitudinal reinforcement ratio affected drift ratio at shear failure. Larger longitudinal reinforcement ratio increased the drift ratio at shear failure.
6. Axial load ratio affected the drift ratio at axial and shear failures. Increased axial load level decreased the drift ratios for axial and shear failures.

6.2.2 Specimen 4

1. Displacement demand affected drift ratio at axial failure. The increased number of cycles at each displacement level resulted in a lower drift ratio at axial failure.
2. Displacement demand affected drift ratio at shear failure. The increased number of cycles at each displacement level resulted in a lower drift ratio at shear failure.
3. Elwood-Moehle drift model does not include number of cycles at each drift level. The model overestimated drift ratio at axial failure.

REFERENCES

ACI Committee 318. (2008). *Building Code Requirements for Structural Concrete and Commentary*. American Concrete Institute, Farmington Hills, MI, 467 pp.

ASTM C 39/C 39M – 05. (2005). "Standard Test Method for Compressive Strength of Cylindrical Concrete Specimens". ASTM International, West Conshohocken, PA, 7 pp.

ASTM C 78 – 08. (2008). "Standard Test Method for Flexural Strength of Concrete (Using Simple Beam with Third-Point Loading)". ASTM International, West Conshohocken, PA, 4 pp.

ASTM C 469 – 02. (2002). "Standard Test Method for Static Modulus of Elasticity and Poisson's Ratio of Concrete in Compression". ASTM International, West Conshohocken, PA, 5 pp.

Southern California Earthquake Center. (2007). *A Comparison of the February 28, 2001, Nisqually, Washington, and January 17, 1994, Northridge, California Earthquakes.* Retrieved from http://www.scec.org/news/01news/feature010313.html

El-Bahy, A., Kunnath, S.K., Stone, W.C. and Taylor, A.W. (1999). Cumulative Seismic Damage of Circular Bridge Columns: Benchmark and Low-Cycle Fatigue Tests. *ACI Structural Journal*, Vol.96, No.4.

El-Bahy, A., Kunnath, S.K., Stone, W.C. and Taylor, A.W. (1999). Cumulative Seismic Damage of Circular Bridge Columns: Variable Amplitude Tests. *ACI Structural Journal*, Vol.96, No.5

Elwood, Kenneth J. and Jack P. Meohle. (2003). "Shake Table Tests and Analytical Studies on the Gravity Load Collapse of Reinforced Concrete Frames". *PEER Report 2003/01*, Pacific Earthquake Engineering Research Center, University of California, Berkeley, 346 pp.

Elwood, Kenneth J. and Jack P. Moehle. (2005). "Axial Capacity Model for Shear-Damaged Columns". *ACI Structural Journal*. Vol. 102, No. 4, July-Aug., pp. 578-587.

Elwood, Kenneth J. and Jack P. Moehle. (2004). "Evaluation of Existing Reinforced Concrete Columns". *13th World Conference on Earthquake Engineering*. Vancouver, BC, Canada, August 1-6, No. 579.

Elwood, Kenneth J., et al. (2007). "Update to ASCE/SEI 41 Concrete Provisions". *Earthquake Spectra*. Vol. 23, No. 3, Aug., pp. 493-523.

Hognestad, E. (1951). “A Study of Combined Bending and Axial Load in Reinforced Concrete Members”. *Bulletin 399*. University of Illinois Engineering Experiment Station, Urbana, IL, 128 pp.

Laplace, Patrick N. et. al. (2005). "Performance of Concrete Bridge Columns Under Shaketable Excitation". *ACI Structural Journal.* Vol. 102, No. 3, May-June, pp. 438-444.

Lynn, Abraham C. (2001). “Seismic Evaluation of Existing Reinforced Concrete Building Columns”. *PhD Dissertation*, University of California, Berkeley.

Lynn, Abraham C. et al. (1996). “Seismic Evaluation of Existing Reinforced Concrete Building Columns”. *Earthquake Spectra*. Vol. 12, No. 4, Nov., pp. 715-739.

Matamoros, Adolfo B., Lisa Matchulat, and Charles Woods. (2008). “Axial Load Failure of Shear Critical Columns Subjected to High Levels of Axial Load”. *14th World Conference on Earthquake Engineering*. Beijing, China, October 12-17, 8 pp.

Matamoros, Adolfo B. (2006). “Degrading Slope for Post-Peak Response of RC Columns Subjected to Load Reversals”. Proceedings, *The Second NEES/E-Defense Workshop on Collapse Simulation of Reinforced Concrete Building Structures*, October 31-November 1, E-Defense, Kobe, Japan, pp. 267-280.

Matamoros, Adolfo B. (1999). “Study of Drift Limits for High-Strength Concrete Columns”. *PhD Dissertation*, University of Illinois at Urbana-Champaign.

Matchulat, Lisa M. (2009). "Mitigation of Collapse Risk in Reinforced Concrete Buildings". *Master's Thesis*, University of Kansas.

Nakamura, Takaya and Manabu Yoshimura. (2002). “Gravity Load Collapse of Reinforced Concrete Columns with Brittle Failure Modes”. *Journal of Asian Architecture and Building Engineering*. Vol. 1, No. 1, March, pp. 21-27.

Pujol, Santiago et al. (2006). "Displacement History Effects on Drift Capacity of Reinforced Concrete Columns". *ACI Structural Journal.* Vol. 103, No. 2, March-April, pp. 253-262.

Saatcioglu, Murat and Guney Ozcebe. (1989). “Response of Reinforced Concrete Columns to Simulated Seismic Loading”. *ACI Structural Journal*. Vol. 86, No. 1, Jan.-Feb., pp. 3-12.

Sezen, Halil. (2000). “Seismic Behavior and Modeling of Reinforced Concrete Building Columns”. *PhD Dissertation*, University of California, Berkeley.

Sezen, Halil and Jack P. Moehle. (2006). “Seismic Tests of Concrete Columns with Light Transverse Reinforcement”. *ACI Structural Journal*. Vol. 103, No. 6, Nov.-Dec., pp. 842-849.

University of Minnesota. (2008). Multi-axial Subassembly Testing Laboratory. http://nees.umn.edu.